Molecular basis of Gerodermia Osteodysplastica, a premature ageing disorder

A Dissertation

Submitted in Partial Fulfilment of the Requirements for the Degree

of Doctor rerum naturalium (Dr. rer. nat.)

to the Department of Biology, Chemistry and Pharmacy

of Freie Universität Berlin

by

CHAN, Wing Lee

Berlin, May 2012

This study was carried out from January 2007 to June 2011 in the Max-Planck-Institut für Molekulare Genetik under the supervision of Prof. Dr. Stefan Mundlos.

1.Supervisor: Prof. Dr. Stefan Mundlos

Max-Planck-Institut für Molekulare Genetik

Ihnestrasse 63- 73, D-14195 Berlin

Tel: 030-84131263

Email: mundlos@molgen.mpg.de

2. Second Examinar : Prof. Dr. Petra Knaus

Freie Universitaet Berlin

Institut für Chemie und Biochemie

Thielallee 63, D-14195 Berlin

Tel: +030 838 52935

Email: knaus@chemie.fu-berlin.de

Date of defence:__12 March 2012_____

Acknowledgement

The experimental works in this study was carried out in three different institutes: the Max-Planck-Institut für Molekulare Genetik, The Department of Biochemistry of The University of Hong Kong, and the Institut für Medizinische Genetik und Humangenetik of Charité Universitätsmedizin. I would like to thank Prof. Stefan Mundlos for giving me this opportunity to work on this project and his superivision and guidance. He is a great role model and I've learnt a lot from him as a scientist. I would also like to thank the Mundlos group members. The Monday morning meetings with them have been truly enlightening and gave me a lot of exposure into different areas and fields of study.

I would like to thank Dr. Danny Chan from the Department of Biochemistry of the University of Hong Kong. Dr. Chan has guided me into the interesting field of developmental biology and bone development. During the time in his laboratory, I have learnt the techniques of generating genetically modified mouse and also techniques necessary for developmental biology. The time in his laboratory was truly enjoyable and fruitful. I am deeply grateful for his guidance and patient. I would also like to thank all the DC lab members for their support and friendship. Special thanks to Dr. Wilson Chan and Ms. Andrea Ng for their help and teaching on homologous recombination, ES cell culturing and blastocyst injection. Also I would like to thank Prof. Kathryn Cheah and all the KC lab members for their suggestions and comments on my project.

I would like to thank Dr. Uwe Kornak of the Institut für Medizinische Genetik

und Humangenetik for taking care of me in Berlin and his endless patient and discussions on the project. His supervision and suggestions guided me through the study. I would also like to thank him for commenting and helping through the writing of my thesis. And also a big THANK YOU to all the members of the Institute for their help and friendship. Special thanks to Dr. Guo Gao and his family, for their friendship.

I would also like to thank Prof. Petra Knaus of the Free University, for taking me up as her external student, and for her suggestions and comments on my study.

Since I've worked in three different institutes, there were so many people who have helped me in one way or the other, e.g. for taking care of the animals, for keeping a nice laboratory environment, for helping me through administrative works, for lending me chemicals or equipment, for cheering me up etc, and I cannot thank them one by one. Therefore I would just "Thank you" from the bottom of my heart to everyone in the three institutes.

Last but not least, I would like to thank my family for their love and support. I would also like to thank my girlfriend Ms. Dorothy Fan for everything she has done for me, for cheering me up when I'm tired or bored, for pushing and scolding me when I got lazy in work, and for her love. It's not easy to maintain a long distance relationship and I'm deeply grateful that she has took up the challenge and gave so much in keeping our relationship.

Abstract

Gerodermia Osteodysplastica (GO) is an autosomal recessive segmental progeroid disorder characterized by wrinkled skin and osteoporosis. The molecular cause are mutations in the gene *GORAB*. The study described here focused on the in vitro and in vivo investigation of the molecular pathophysiology. In *in vitro* approaches, it was shown that GO patient skin fibroblasts suffered from cellular senescence, with decrease in proliferating cell population, increased in senescence associated beta-galactosidase activity and increase in the cyclinD kinase inhibitor, p16Ink4a, expression. GO patient skin fibroblast and knockdown of GORAB by siRNA in both Hela cells and U2OS cells showed increase in DNA double strand breaks, suggesting that genome instability was the cause of cellular senescence. Upon knockdown of GORAB by siRNA in Hela cells, the cells accumulated significantly higher level of Reactive Oxygen Species (ROS) upon CCCP challenge, suggesting that loss of GORAB increased the cells susceptibility to ROS and could be the cause for increased genome instability.

In order to understand the role of Gorab in bone development, a conditional mouse model of Gorab was constructed and crossed with Prx1cre, Col2a1cre, Dmp1cre to inactivate Gorab in the limb bud mesenchyme, cartilage/chondrocyte, and late osetoblast/osteocyte, respectively. The aim was to inactivate the role of Gorab in these tissues to study the contribution of the chondrocytic and osteoblastic lineage to osteoporosis in GO. The Gorab$^{fl/fl}$;Prx1cre mutants showed the strongest phenotype, with decreased numbers of trabeculae, thinning of cortical bone and shortening of long bones. Gorab$^{fl/fl}$;Col2a1cre mutants also showed decrease in trabeculae and shortening of long bones comparable to the Gorab$^{fl/fl}$;Prx1cre mutants, suggesting that

the chondrocytic lineage contributed to these phenotypes. Gorab$^{fl/fl}$Dmp1cre mutant showed no significant changes in cortical bone thickness and length of long bone, but a significant decrease in trabeculae. This suggested that Gorab inactivation in the late osteoblast /osteocyte did not contribute to the abnormal cortical bone thickness and the dysregulation has its origin in earlier stages in osteoblastogenesis.

Analysis of 4 weeks old Gorab$^{fl/fl}$;Prx1cre mutants showed decrease in mineral apposition rate at the endosteal cortical tibia and increase in osteoid volume and thickness in the trabeculae tibia, indicating that osteoblast function was compromised. qPCR analysis of osteocytes showed increase in expression of late osteoblast marker, Osteopontin and Dmp1, but decrease in osteocytes marker Sclerostin expression, suggesting that osteoblast differentiation was delayed/impaired. It was also found that expression of p21, a cyclinD kinase inhibitor, was increased in the osteocytes, suggesting that cellular senescence may also have taken place upon Gorab inactivation in osteoblast lineage. It was also shown that the TGFβ signaling pathway was activated in GO patient fibroblast, upon GORAB knockdown in Hela and U2OS cells by siRNA and in the osteocytes of 4weeks old Gorab$^{fl/fl}$;Prx1cre mutants. Suggesting that the TGFβ pathway may participate in cellular senescence and osteoblastogenesis defects upon Gorab inactivation.

Taken together, this study has shown that induced cellular senescence and impaired chondrocyte and osteoblast function and differentiation underlied the pathomechanism of GO and the TGFβ signaling was a candidate pathway involved in the phenotype manifestation.

Zusammenfassung

Gerodermia osteodysplastica (GO) ist eine autosomal rezessiv vererbte segmental progeroide Erkrankung, die durch Osteoporose und Faltenbildung der Haut gekennzeichnet ist. Die molekulare Ursache sind Mutationen im Gen *GORAB*. Die hier beschriebene Studie befasste sich mit in vitro und in vivo Untersuchungen zur molekulare Pathophysiologie. In vitro Experimente ergaben eine verringerte Proliferationsrate GORAB-defizienter Zellen. Als Ursache stellte sich eine vermehrte zelluläre Seneszenz heraus, die sich in erhöhter Expression der Seneszenz-assoziierten Beta-Galaktosidase und des Zellzyklus-Inhibitors p16Ink4a äußerte. Weitere Untersuchungen zeigten als Ursache für die Seneszenz eine Akkumulation von DNA-Doppelstrangbrüchen und außerdem eine vermehrte Produktion von Reaktiven Sauerstoffspezies (ROS) nach Gabe des Mitochondrien-entkoppelnden Protonophors CCCP.

Für die in vivo Untersuchung der Funktion von Gorab wurde ein konditionelles Mausmodell etabliert. Durch Kreuzung mit den Linien Prx1cre, Col2a1cre, Dmp1cre sollte eine Inaktivierung des Gens im Mesenchym der Extremitätenknospe, im Knorpel und in späten Osteoblasten/Osteozyten erreicht werden, um die Beiträge der verschiedenen Zelltypen zum GO Phänotyp voneinander zu unterscheiden. Gorab$^{fl/fl}$;Prx1cre und Gorab$^{fl/fl}$;Col2a1cre zeigten einen sehr ähnlichen Phänotyp in Röhrenknochen mit einem mild verminderten Wachstum und einer stark verminderten Anzahl von metaphysären Knochentrabekeln. Nur bei Gorab$^{fl/fl}$;Prx1cre Mutanten konnten auch eine Abnahme der Dicke des kortikalen Knochens und eine auffällige Morphologie der Osteozytenlakunen beobachtet werden. Überraschenderweise zeigte sich kein entsprechender Osteozytenphänotyp nach Ausschalten von Gorab in

Osteozyten durch Dmp1cre, sondern lediglich eine leichte Abnahme des trabekulären Knochens.

Die detaillierte Analyse der Gorab$^{fl/fl}$;Prx1cre Mutanten im Alter von 4 Wochen ergab eine verminderte Appositionsrate des Knochens und vermehrtes nicht mineralisiertes Osteoid, was für eine Funktionsstörung der Osteoblasten spricht. Zur näheren Untersuchung dieser Osteoblastenfehlfunktion erfolgte eine Expressionsuntersuchung des kortikalen Knochens, die eine Zunahme der Expression später Osteoblasten-, aber eine Abnahme von Osteozytenmarkern ergab. Zusätzlich zeigte sich eine verstärkte Expression des Zellzyklus-Inhibitors p21 und von TGF-beta 1 und 2. Eine vergleichbare verstärkte TGF-beta Expression fand sich auch in GO Hautfibroblasten und in verschiedenen Zellinien nach GORAB Inaktivierung durch RNA-Interferenz.

Insgesamt scheinen die für die Pathogenese des GO Knochenphänotyps verantwortlichen Zelltypen Chondrozyten und Osteoblasten und/oder ihre mesenchymalen Vorläuferzellen zu sein, während die Osteozyten eine untergeordnete Rolle spielen. Auf zellulärer Ebene begünstigt der Verlust von GORAB – vermutlich durch Anhäufung von DNA-Doppelstrangbrüchen - die zelluläre Seneszenz und die Expression von TGF-beta.

Contents

Chapter 1: Introduction

1.1 Gerodermia Osteodysplastica

Gerodermia Osteodysplastica (GO) is a rare autosomal recessive disorder. GO was first reported in 1950 by Bamatter et al on 5 Swiss sibs. GO Patients have lax and prominent wrinkled skin at birth over the dorsum of the hands and feet ("Gerodermia"). They also have excessive wrinkled abdominal skin when assuming a sitting position (Fig.1.1A). Histologically, the skin showed reduced amount and excessive fragmentation of elastic fiber (Fig.1.1B, Steiner et al 2005), and this was more pronounce in the wrinkled skin than in the “normal-looking” skin from other body parts (Lisker et al 1979). However it was reported that there’s no significant defects in the secretion and electromobility of procollagen I and III from GO patients’ fibroblast (Hunter et al 1988).

GO patients have generalized osteoporosis (hence the name "osteodysplastica"), especially in the vertebral body which often results in compression fractures (Fig.1.1C and D, Hunter et al 1978). Platyspondyly, scoliosis and kyphosis in the vertebral column have also been reported in some cases. There is also low mineral density in the long bones, causing bowing and increased fracture risk (Fig.1.1D and E).

GO patients often show striking craniofacial abnormalities, including drooping eyelids, sagging cheeks, large protruding ears, relative mandibular prognathism and maxillary hypoplasia (Fig. 1.1F and G). These features, combining with the wrinkled and lax skin, give the patients a prematurely aged appearance.

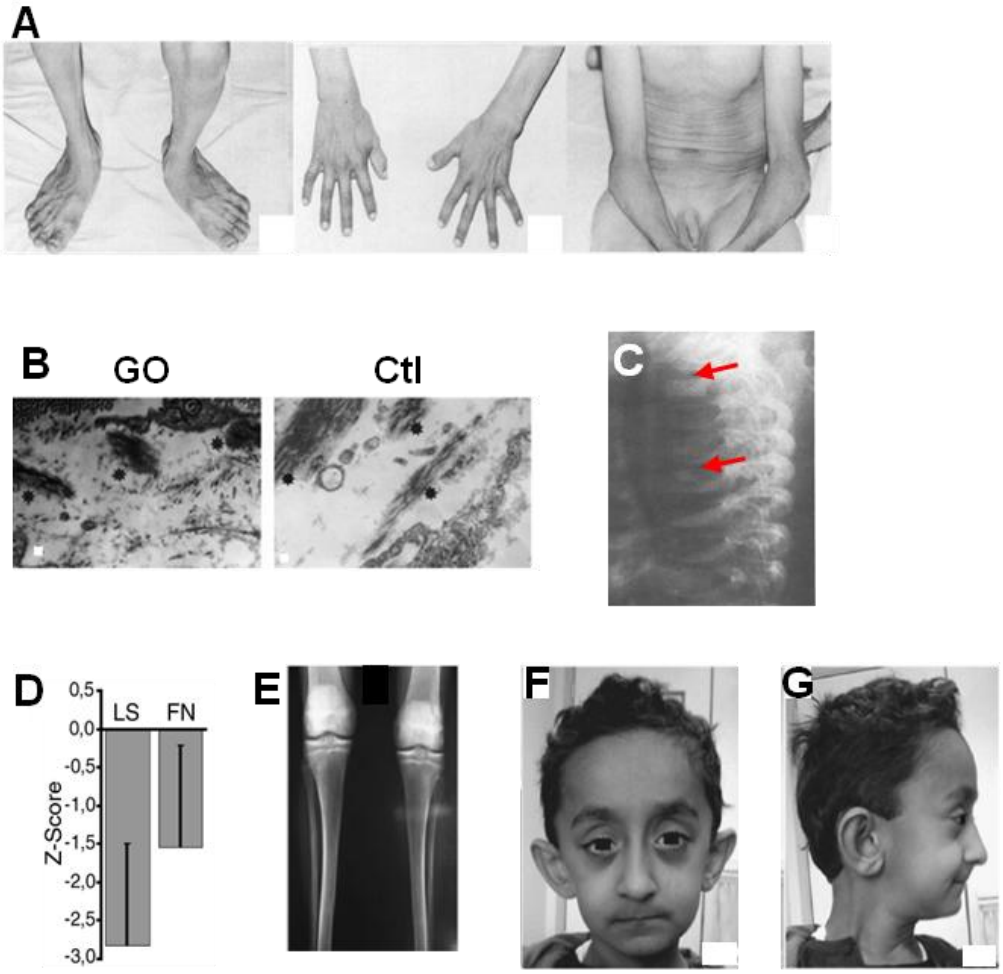

Fig. 1.1 (A) Skin phenotype of GO patient. Lax and wrinkled skin localized on dorsum of feet, hand, and over the abdomen when sitting (Adopted from Lisker et al 1979). (B) Micrograph of skin from GO patient comparing with age-and-sex matched Controls. Elastic fiber in the patient appeared as irregular dark masses and is also reduced in amount (marked by asterisk, picture adopted from Steiner et al 2005). (C) Radiograph showing compression fracture in the thoracic vertebrae of a 10 months old GO patient as indicated by the arrows (Adopted from Hunter et al 1978). (D) Z-score of GO patient showed osteoporosis in the lumbar spine (LS) and osteopenia in femoral neck (FS) (Adopted from Hennies et al 2008). (E) Bowing of tibiae in a 12 years old GO patient. (F) Large ear, sagging cheeks, drooping eyelids of GO patients; (G) Maxillary hypoplasia and mandibular prognathism (E-G adopted from Rajab et al 2008).

There are a lot of intrafamilial and interfamilial variations among patients classified clinically as suffering from GO. There have been many clinical symptoms that were reported in some patients but not found in others. However it is difficult to determine whether that is due to absence of the symptom or if the symptom was simply not noted by the investigator. These include hypotonia, delayed motor milestones, mental retardation etc.

1.2 GO and other cutis laxa disease

Cutis laxa is a group of connective tissue disorders characterized by lax, inelastic skin. There are many subtypes in this family of disorders and only the two that share a lot of common features with GO, autosomal recessive cutis laxa type II, Debré type (also called type IIA; ARCL2A), and PYCR1-related autosomal recessive cutis laxa (also called type IIB; ARCL2B) is discussed here. The clinical difference between type IIA and type IIB is that ARCL2A patients show defect in N- and O- linked glycosylation, while ARCL2B don't (or at least, no detectable glycosylation defect in plasma transferrin and apolipoprotein CIII, Morava et al 2009). Other than that, the symptoms of ARCL2A and ARCL2B are overlapping. These common phenotypes include generalized lax and wrinkled skin, osteopenia, hernias, developmental delay, microcephaly, hypotonia and joint hyperextensibility.

Table 1.1 summarizes the phenotypes of ARCL2A, ARCL2B and GO. It shows that these three disorders share a lot of common symptoms and that differentiation between these three disorders is difficult. However there are still characteristic features for diagnosing the disorders. For example, as mentioned above, ARCL2A shows defective glycosylation but ARCL2B and GO don't; GO patients often suffer

Table 1.1 Comparison of phenotypes in ARCL1, ARCL2 and GO

	ARCL2A	ARCL2B	GO
Generalized cutis laxa	✓	✓	×
Large opened fontanelle	✓	×	×
Progressive skin phenotype	×	×	✓/ ?
Microcephaly	✓/ ?	✓/ ?	×
Mental retardation	✓	✓	×
Delayed motor development	✓	✓	✓/ ?
Hypotonia	✓	✓	✓/ ?
Osteopenia	✓/ ?	✓/ ?	✓
Spontaneous fracture	×	×	✓
Joint Hyperextensibility	✓/ ?	✓/ ?	✓
Abnormal N- and O-glycosylation	✓	×	×
Causative gene(s)	ATP6V0A2	PYCR1	GORAB

✓: features present in majority of cases; ✓/?:features described in some cases; ×: features not reported

from multiple bone fractures while for the other two disorders, although there've been reports of osteoporosis, reports of bone fracture were relatively rare; the lax and wrinkled skin phenotype in ARCL2A and ARCL2B tends to improve with age but in the case of GO, the wrinkled and lax skin phenotype is reported to be rather progressive; Progressive prognathism was only reported in GO but not in the other two disorders; Microcephaly was reported in ARCL2A and ARCL2B patients but not in GO. Mental retardation is usually not observed in GO. These differences implicated that these three disorders, though clinically similar, were distinctive entities and

resulted from different genetic defects. Indeed, it has been reported that the causative genes for ARCL2A included ATP6V0A2 (Kornak et al. 2008), while mutations in Pyrroline-5-carboxylate reductase 1 (PYCR1, Reversade et al 2009) caused ARCL2B and mutation in GORAB caused GO (Hennies et al 2008). ATP6V0A2 is a subunit of the ATPase H+-pump that regulates the acidity of organelles e.g. the Golgi apparatus, endosome etc; PYCR1 is a mitochondrial enzyme that participates in the NAD (P) H-dependent reduction of pyrroline-5-carboxylate to proline; and GORAB is a Rab6 interacting golgin. It is amazing that how mutations in proteins with seemingly different cellular localization and function would results in disorders that share astonishingly high similarity in phenotype manifestations.

Take the skin phenotype as an example. It's easy to understand how mutations in FBLN4 and FBLN5 would cause loss and fragmentation of the elastic fiber since they are components of the fiber. However, ATP6V0A2, PYCR1, GORAB are not components of the elastic fiber. They have diverse functions and yet mutations in them results in similar defects in skin. This suggests that these three proteins could have participated in a common mechanism governing the formation and maintenance of elastic fiber. It has been shown that loss of function mutations in ATP6V0A2 caused expansion and disintegration of the Golgi cisternae; accumulation of lysosomes and autophagosomes; accumulation of tropoelastin in the Golgi and as intracellular and extracellular aggregates; and increased apoptosis (Hucthagowder et al 2009). It would be interesting to investigate whether similar observations could be found in PYCR1 and GORAB mutants. In addition, similar defects in extracellular matrix deposition may also happen in bone and this is likely to be the underlying pathomechanism for the skeletal defects in ARCL2A, ARCL2B and GO and deserves further analysis.

1.3 GORAB as the causative gene of Gerodermia Osteodysplastica

Previously, it was found that the gene GORAB (formerly known as SCYL1BP1) was the causative gene of Gerodermia Osteodysplastica (Hennies et al 2008). In that study, GO patients from 4 Mennonite families were subjected to genome wide scanning and a candidate region of 5.1Mb was identified in chromosome 1q24. Then, through systematic sequencing, a homozygous mutation in the gene SCYL1BP1 was found in all affected individuals from the four Mennonite families. The mutation, 367G>T, results in a premature stop codon (Glu123X). Further analysis identified mutations in SCYL1BP1 in another 9 patients from different families. A total of 9 mutations in SCYL1BP1, including 5 nonsense mutations, 2 frameshift mutations, 1 splice site mutation and 1 mutation in the start codon were reported in that study (Fig. 1.2A). Western Blot analysis of protein lysate from patients' skin fibroblast showed that the protein product of SCYL1BP1 was absent, suggesting that the mutations resulted in loss of function of SCYL1BP1 (Fig.1.2B). Later on, another report described a missense mutation in GORAB gene of GO patients (Al-Dosari et al 2009), in which it was suggested that the alpha helix structure connecting the two coiled-coil domains of the protein was disrupted. These two reports conclude that loss of function mutation in GORAB was the cause of Gerodermia Osteodysplastica.

1.4 Gorab and its' interacting partners

Gorab is a highly conserved gene. According to the Ensembl database, Gorab could be found in a wide variety of species, including human, mouse, dog etc. The human GORAB protein has three coiled-coil domains (56-76aa, 174-194aa and

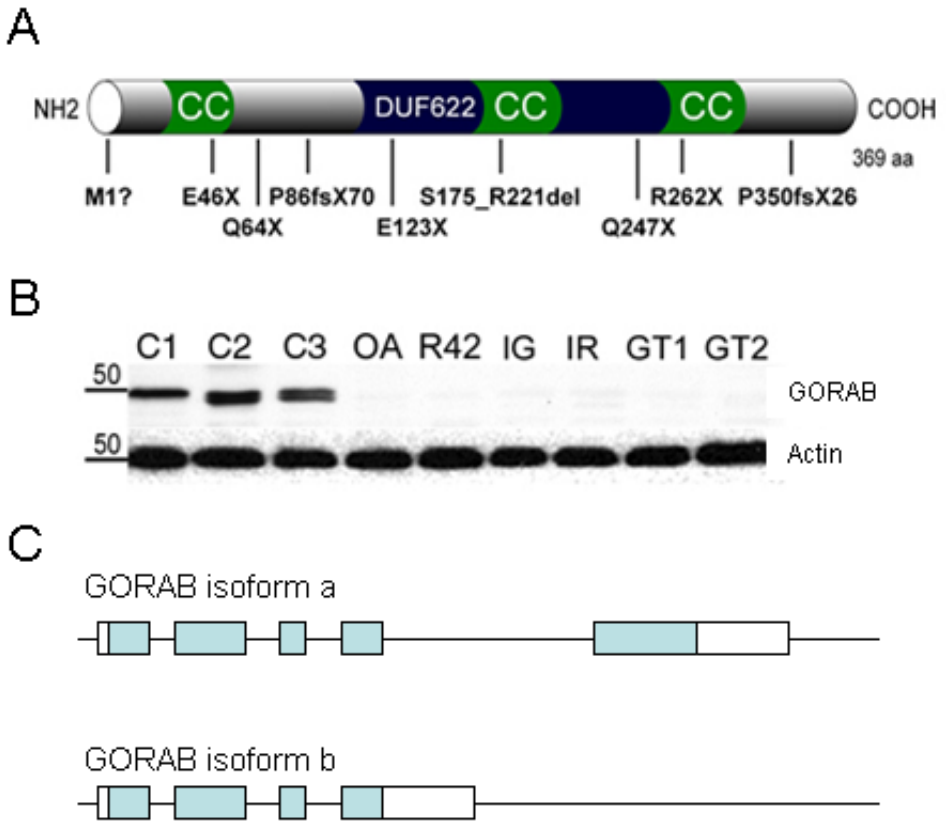

Fig. 1.2 GORAB as the causative gene of GO. A). Schematic diagram showing the position of mutations found in GO patients and the different domains in the Gorab protein. CC- coiled-coil; DUF622-an uncharacterized domain; B). Western Blot analysis showing the loss of GORAB protein in GO patients. C1 to C3 were protein lysate from control fibroblasts; C). The two GORAB isoforms.

282-309aa). The different domains of the protein are depicted in Fig.1.2A. According to the Ensembl database, there have been 2 transcription variants reported in human Fig.1.2C. The major difference in the transcription variants lies in the C-terminal of the protein. The variant GORAB isoform a (Ensembl transcript ID ENST00000367763) is 394aa in size, while the variant GORAB isoform b (Ensembl transcript ID ENST00000367762) is 246aa in size, with only two coiled-coil domain. However, as argued in our previous publication, the isoform a of GORAB is more likely to utilize a later translation start site, resulting in a protein of 369aa (Hennies et

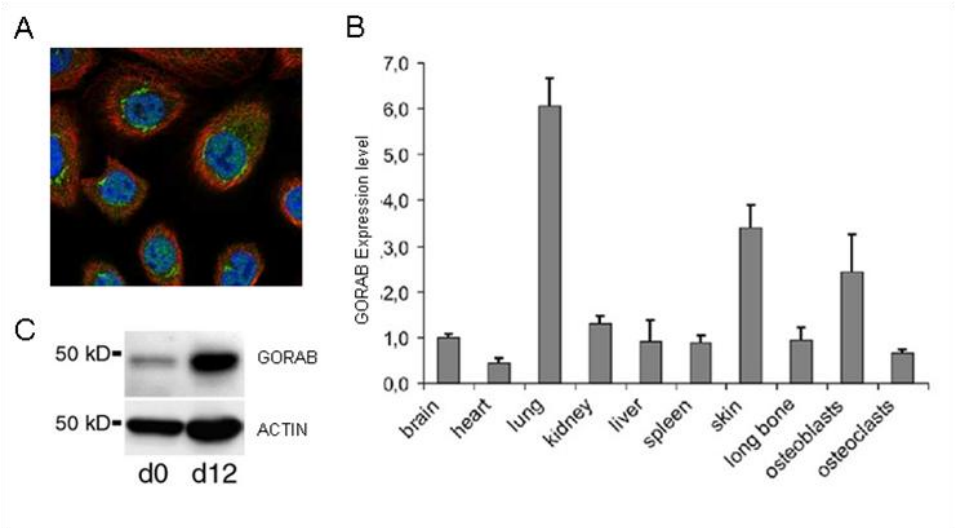

Fig. 1.3 A). Subcellular localization of GORAB in Hela cells. The Green channel is immunofluorescence signal of GORAB, primarily localized at the Golgi-apparatus but also found in nucleus and cytoplasm (www.proteinatlas.org); B). Expression level of Gorab in P5 mouse. The highest expression was found in lung, skin and osteoblasts; C). Western blot showing increase of Gorab expression during differentiation of primary murine calvarial osteoblast culture.

---

al 2008). The functional differences between these two variants remain unknown. In mouse, there has been only one reported transcript of Gorab, encoding a protein of 368aa, which shares 83% homology with the human GORAB isoform a and also is predicted to have 3 coiled-coil domain;

Gorab is ubiquitously expressed and is localized to the Golgi apparatus, while it has also been reported to be found in nucleus and cytoplasm (Fig.1.3A). In P5 mouse, the highest expression level is in lung, skin and bone (Fig. 1.3B, Hennies et al 2008). It has also been found that the protein level of Gorab increased with time in murine osteoblast culture (Fig. 1.3C). The high expression level of Gorab in skin and bone coincided with the two major affected organs in Gerodermia Osteodysplastica,

pointing to a specific role of Gorab in the development and maintenance of these two organs.

Gorab was at first identified as a binding partner to a gene called NTKL, N-terminal kinase-like protein and therefore it was named NTKL binding protein 1. Later, the NTKL protein was renamed into Scyl1 and thus the name changed from NTKLbp1 to Scyl1bp1. More recently, because of the identification of *SCYL1BP1* as the causative gene of Gerodermia Osteodysplastica and the interaction with Rab6, SCYL1BP1 was renamed to GORAB (Golgin, Rab6-interacting) and this name will be used in the following parts of this thesis and the former names would be avoided to minimize confusions.

In order to understand the function of Gorab and its' role in the pathomechanism of GO, it would be essential to identify the interacting partners of Gorab and investigate how the loss of Gorab affects their function. Up till now, there have been four reported interacting partner of Gorab: Scyl-l, Pirh2, Rab6 and MDM2.

Scyl-1

Gorab was originally known as NTKLbp1 because it was identified as a binding protein of NTKL, N-terminal kinase-like protein. NTKL was later renamed into SCYL-1. The identification of SCYL-1 was actually an accident. Liu et al (2000) intended to search for novel binding partners of Protein Kinase B. They have identified a 105kDa protein, which has a kinase like domain at the N-terminal (31-205aa) but was later found not to be interacting with Protein Kinase B. They also found that Scyl-1 was expressed in a variety of tissues including lung, muscle, kidney, heart, brain etc and they found that the protein localized to the cytosol and low density

microsomes (including endosomes, fragmented Golgi and cytoskeletons). Later it was reported that Scyl-1 didn't have kinase activity *in vitro* (Kato et al 2002)

The interaction between Gorab and Scyl-1 was first reported by Di et al 2003. A yeast two hybrid screening using the mouse Scyl-1 protein as a bait against a mouse E10.5 cDNA library was carried out and they identified a novel protein which they named NTKLbp1 (Gorab). They supported their finding by co-immunoprecipitation of Myc-NTKL and HA-Gorab overexpressed in COS7 cells. Kato et al (2002) reported that Scyl-1 has 3 transcription variants and it formed multimer *in vivo*. While two of the variants were localized to the cytosol, one variant showed mitosis specific localization to the centrosome. Kato et al (2002) suggested that this variant specific localization to the centrosome implied functional differences among the isoforms of Scyl-1 and Scyl-1 was involved in centrosome-related functions.

Scyl-1 has also been named TEIF (telomerase transcriptional elements-interacting factor) in the past (Tang et al 2004). It was found that Scyl-1 had DNA binding ability and that it directly bound to the promoter of hTERT (human telomerase reverse transcriptase). Overexpression of Scyl-1 was found to upregulate the expression of hTERT, and thus increased telomerase activity. This implicates that Scyl-1 has a role in the regulation of telomere length and, as a result, the proliferation potential of a cell. Later in 2005, the same group reported further analysis on Scyl-1 and found that Scyl-1 directly bound to the promoter of the DNA polymerase ß and enhanced its transcription. They also showed that stable overexpression of Scyl-1 in Hela cells increased the expression of DNA polymerase ß and thus the tolerance of the cells to H_2O_2. This suggested that overexpression of Scyl-1 may increase cell's resistance to oxidative stress (Zhao et al 2005). In 2009, the same group again

published another paper on the function of Scyl-1 (Gong et al 2009). They showed that a fraction of Scyl-1 localized to the centrosome during mitosis in a variety of cell lines including U2OS, Hela and Saos2 (concurring with the results from Kato et al 2003). They also showed that overexpression of Scyl-1 resulted in centrosome amplification and accumulation of multinucleated cells. On the other hand, knockdown of Scyl-1 didn't reverse the phenotype; instead the number of cells with supernumerary centrosome and multiple nucleus were also increased. This suggested that the level of Scyl-1 must be regulated for proper cell cycle propagation. In addition, DNA damage (induced by H2O2, cisplatin and bleomycin) and telomere dysfunction (induced with synthesized T-oligo or siRNA knockdown of TRF1 and POT1) increased centrosome localization of Scyl-1, the increase in size and number of centrosome and also the number of multinucleated cells. These results suggested that centrosome localization of Scyl-1 and subsequent amplification of centrosome as part of response to DNA damage and telomere dysfunction of a cell.

Loss of function mutation in Scyl-1 has been reported in an autosomal recessive murine neurodegenerative disease "mdf", which stands for 'muscle deficient" (Schmidt et al 2007). An insertion of thymidine in exon 8 of Scyl-1 has been identified in the mdf mice. This one basepair insertion caused a frame shift and generated a premature stop codon, causing a decrease in Scyl-1 mRNA level and complete loss of the protein. Since the yeast orthologue of Scyl-1, Cex1p, has been shown to be a component of the nuclear RNA export machinery, Schmidt et al (2007) proposed that loss of Scyl-1 resulted in a defect in transport of cargos from nuclear to cytosol and caused neurodegeneration. Later, Burman et al (2008) has found that Scyl-1 interacts with COPI (coatomer I) and co-localizes with ßCOP to the cis-Golgi. Knockdown of Scyl-1 expression by siRNA results in defects in COPI mediated

retrograde trafficking from the Golgi to ER but not the anterograde trafficking from ER.

To summarize, loss of function mutation in Scyl-1 caused "mdf" neurodegenerative disease in mice. The detailed pathomechanism has been suggested to be related to impaired nucleocytoplasmic transport (Schmidt et al 2007) or by defective COPI mediated retrograde transport (Burman et al 2008). The 'muscle deficient" phenotype observed in the "mdf" mice is very interesting since hypotonia has also been reported in some of the GO patients (Hunter et al 1978). This suggested that there could be overlapping phenotype between loss of Scyl-1 and loss of Gorab in mice or human and required further verification. Scyl-1 has also been shown to localize to the centrosome during cell cycle and regulates centrosome's function and response to DNA damage and telomere dysfunction. It has been suggested that Scyl-1 has trans-activation activity that it could bind to the promoter of TERT and DNA polymerase ß and activate their transcription. Whether Gorab has any role in the functioning of Scyl-1 or role in any of these cellular processes is unknown, but certainly is a good starting point for further investigation.

Pirh2

In an attempt to identify the binding partners of the human NTKLbp1 (Gorab), the full length Gorab gene was used as bait in a yeast two hybrid screening in a human fetal liver cDNA library (Zhang et al 2005). It was found that Gorab interacted with Pirh2, p53-induced ringH2 protein. The authors also did *in vitro* and *in vivo* binding assays to confirm the interaction. The *in vitro* assay was done by using purified GST-hPirh2 protein and *in vitro* translated protein product of myc-hGorab and the authors showed binding of the myc-hGorab to the GST-hPirh2 but not the

GST alone control. The authors also showed that the hGorab and hPirh2 could be co-immunoprecipitated in SMMC7721 cells co-transfected with vectors overexpressing EGFP-hPirh2 and Myc-hGorab. Based on these results, the authors suggested that hPirh2 and hGorab could interact with each other both *in vitro* and *in vivo*.

Zhang et al (2005) also employed a yeast two-hybrid system to identify the interacting domain of hPirh2 and hGorab. They constructed vectors overexpressing truncated products of hPirh2 or hGorab and co-transformed the vectors into yeast strain AH109. They found that the interaction between the two proteins is mainly mediated by the C-terminal coiled-coil domain of hGorab and the N-terminal zinc finger domain of hPirh2.

Based on these results, Zhang et al (2005) concluded that hGorab interacted with hPirh2. It has been found that Pirh2 had intrinsic E3 ubiquitin ligase activity. It bound to and mediated the ubiquitination and subsequent degradation of p53 independent of Mdm2. The binding of Pirh2 also impairs the transactivation activity of p53 without directing p53 to degradation. Pirh2 also interfered with the role of p53 in cell cycle control. Overexpression of Pirh2 rescued cells from p53 mediated cell death and knock down of Pirh2 with antisense RNA (and as a result, elevated level of p53) increased the number of cells arrested at G1/S phase (Leng et al 2003). Zhang et al (2005) suggested that the hGorab maybe another substrate of hPirh2 or the interaction of hGorab regulates the function of hPirh2. Recently, they published another paper showing that Gorab was indeed a substrate of Pirh2 and that Pirh2 mediated the ubiquitination and subsequent proteasome-dependent degradation of Gorab (Yan et al 2010). The importance of this Pirh2-mediated-ubiquitination on Gorab function

remains to be elucidated.

Rab6

Rab6 belongs to the Rab family of small GTPases. There are three isoforms of Rab6, namely Rab6A, Rab6A' and Rab6B. Rab6 and Rab6A' are splice variants differing in only three amino acid residues, while Rab6B is located on a different locus and has a 91% homology to Rab6A (Opdam et al 2000). Rab6B is mainly expressed in brain while the other two isoforms are ubiquitously expressed in different tissues. The functional differences among the three isoforms are still unclear. However, it's been reported that Rab6A and Rab6A' are key regulators in secretory pathways and also Golgi-ER retrograde trafficking (for review, please refer to Barnekow et al 2009).

Our group has identified the interaction between Gorab and Rab6 by Yeast Two-Hybrid analysis (Fig.1.4A). Gorab was found to specifically interact with the activated (GTP bound) Rab6 but not the inactive form of (GDP bound) Rab6 (Fig.1.4B). Gorab also co-localizes with Rab6 at the trans-Golgi network (Fig.1.4C). The localization of Gorab to the Golgi apparatus, the presence of coiled-coil domain and interaction with Rab6 qualifies Gorab as a golgin. Thus Gorab may play a role in Rab6 mediated endo- and/or exocytosis. In addition, another Gorab interacting protein, Scyl-1 has also been reported to take part in COPI mediated retrograde trafficking (Burman et al 2008). These findings suggest that Gorab has a role in the secretory pathway and could be an important link in the pathogenesis of GO.

Rab6 also has been reported to have a role in cytokinesis. Inactivation of Rab6A' with siRNA in Hela cells blocked the cells in metaphase and activated the

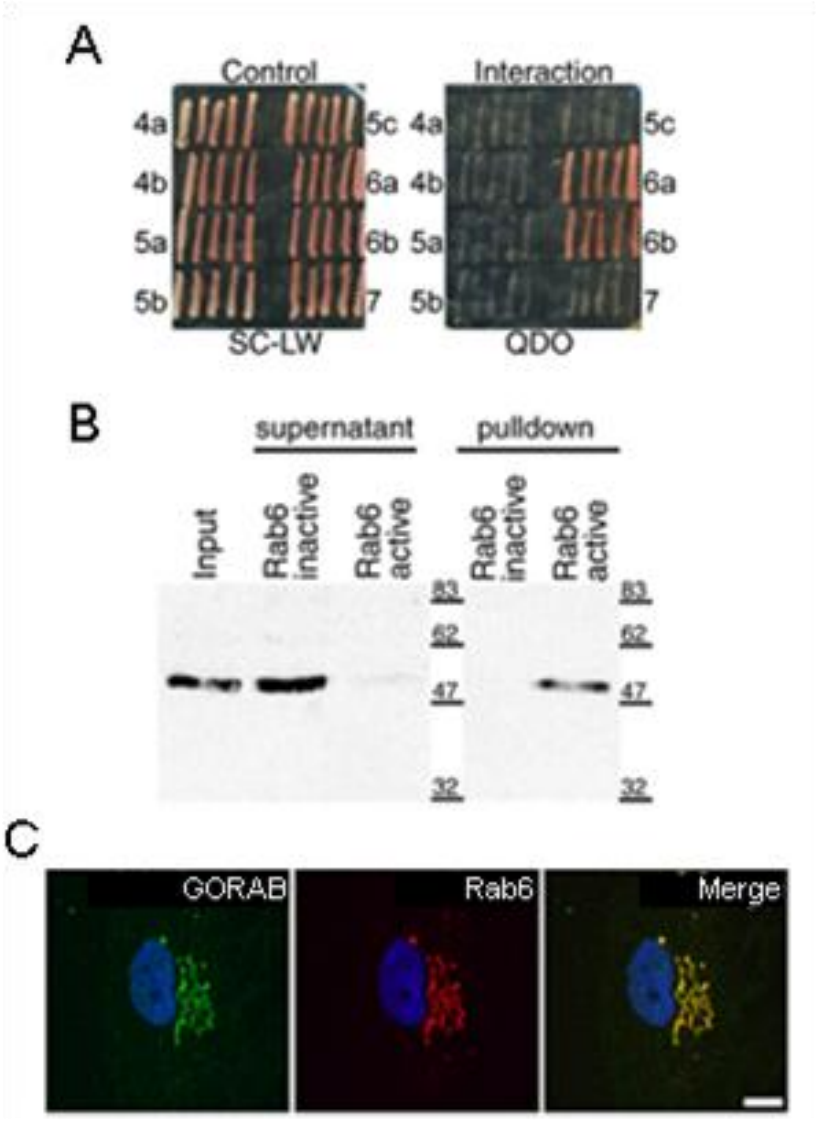

Fig.1.4A). Yeast Two Hybrid assay showing that GORAB interacted with Rab6A and Rab6B; B). Pull down assay showing that GORAB interacted with active (GTP bound) Rab6 but not with inactive (GDP bound) Rab6; C). co-localization of GORAB with Rab6 at the trans-Golgi network. (Adopted from Henneis et al 2008)

Mad2-spindle checkpoint (Miserey-Lenkei et al 2006). The authors also reported strong $p150^{Glued}$ localization at the kinetochore in Rab6A' knockdown cells. $p150^{Glued}$ is a component of the dynein/dynactin complex, which is needed for the removal of various checkpoint proteins, e.g. Mad2, from the kinetochore. The authors suggested that inactivation of Rab6A' disrupted the dynein/dynactin dynamic at the kinetochore.

This disruption activated the Mad2-spindle checkpoint and thus arresting the mitotic cells in the metaphase. This means Rab6A' is another Gorab interacting protein, apart from Scyl-1, that has a role during progression of mitosis. In addition, both Rab6 and Scyl-1 regulated Golgi retrograde trafficking. It is possible that Gorab also plays a role in intracellular trafficking and mitosis progression through influencing the activity of the interacting proteins.

MDM2

MDM2, like Pirh2, is an E3 ligase. It ubiquitinates different proteins and regulates their functions by influencing their subcellular localization or their protein level through proteasome-dependent degradation (for review, please refer to Marine and Lozano 2010). Yan et al (2010a) (the same group that identified the interaction between Pirh2 and Gorab) reported that Gorab physically interacted with MDM2 both *in vitro* and *in vivo*. They also found that MDM2, unlike Pirh2, did not mediate the ubiquitination of Gorab. Instead, overexpression of Gorab induced the ubiquitination and subsequent proteasome-mediated degradation of MDM2. It would be reasonable to hypothesize that this Gorab-induced decrease of MDM2 protein level would lead to accumulation or activation of p53. Indeed, Yan et al (2010b) published another paper addressing this issue. In this report, Yan et al (2010b) showed that overexpression of Gorab increased endogenous p53 protein levels, which could be attenuated by proteasome inhibitor treatment. They went on showing that this Gorab induced stabilization of p53 was cell-type specific and suggested that this specificity was due to the different in p53-ubiquitination mechanism undertaken in different cell types. They further showed that overexpression of Gorab reduced cell proliferation, induced apoptosis and prevented tumorigenicity. They also claimed that overexpression of Gorab formed a complex with p53 and MDM2 *in vitro* and suggested that Gorab

inhibited the MDM2-mediated-ubiquitination of p53 by competing with p53 for binding sites on MDM2. Taken together, they proposed that Gorab regulated the MDM2-p53 feedback loop and could be a novel tumor suppressor. Although their proposed role of Gorab is not yet fully substantiated and required further validation, their results nonetheless showed that Gorab played a role in cell cycle progression, possibly through regulation of MDM2-p53 pathway.

To summarize, among the four reported interacting partners of Gorab, Scyl-1 and Rab6 have been reported to be key regulators of Golgi retrograde transport. These findings, and the localization of Gorab to the Golgi apparatus, suggests that Gorab plays a role in the regulation of protein trafficking. On the other hand, all four interacting proteins have been reported to participate in cell cycle control, either during mitosis and cytokinesis (Scyl-1 and Rab6) or through regulation of master transcription factors of cell cycle (Pirh2 and MDM2). It is therefore also probable that Gorab regulates cell cycle progression through its' interacting partners. Both of these two hypotheses may play a role in the pathomechanism of GO and are good future research directions.

1.5 Preliminary findings on the Genetrap mouse model of Gorab

Previously, our laboratory has acquired a genetrap mouse model of Gorab, in which a genetrap cassette was inserted into the first intron of the gene (Fig.1.5A). Preliminary analysis of the genetrap mouse done by Dr. Haikuo Zhang showed that Gorab expression was strongly knocked down in the Genetrap mouse, indicating that

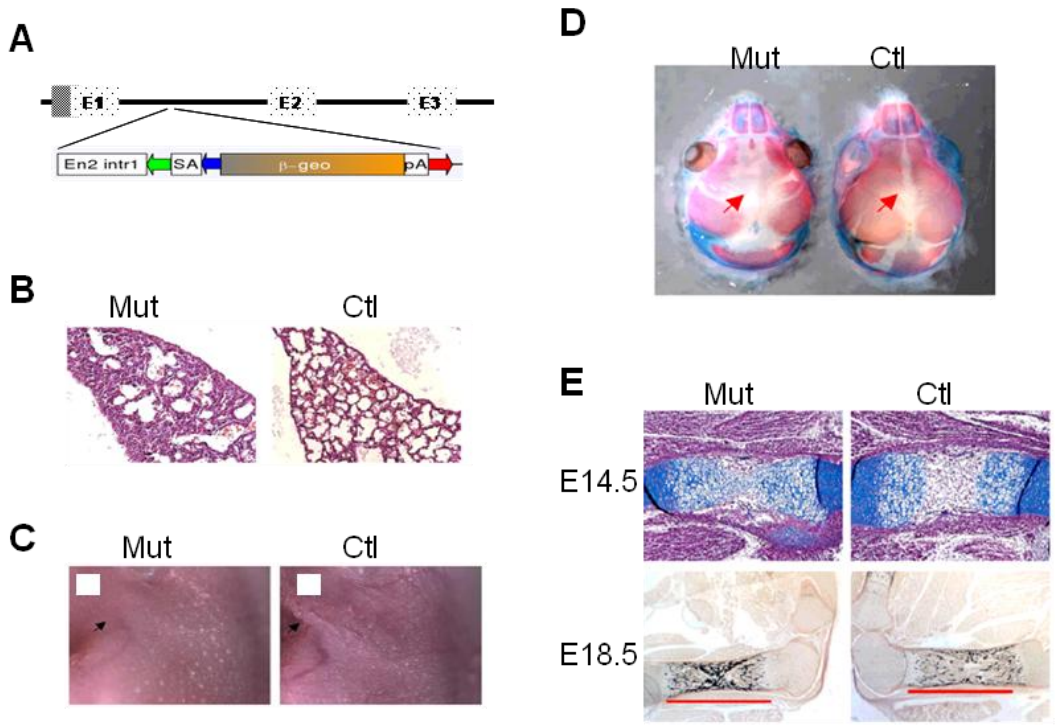

Fig.1.5 Preliminary characterization of the genetrap mouse model of Gorab. A). Schematic diagram showing the insertion of the genetrap cassette into the mouse Gorab locus. B). Histology of the lung from P0 genetrap mutant. Note the decrease in the amount of airspace comparing to the control. C). The mutant mice showed swollen, tightened skin comparing to the control. The arrows point to folded skin that are present in the control animal but not in the mutant. D). The mutant has opened fontanelle. E). At E14.5, the mutant mice showed delay in ossification comparing to the control. However, by E18.5, no significant defect was found in the mutant except a slight shortening in the long bone.

---

the genetrap mouse was a valid Gorab loss-of-function model. Homozygous genetrap mice died shortly after birth, with apparent difficulty in breathing and feeding. The lungs of the dead mutants showed less airspace (Fig.1.5B) and their stomachs were empty. The neonatal infants had tighter skin comparing to the control animals (Fig.1.5C). The mutant mice displayed reduced ossification of the fontanelle and

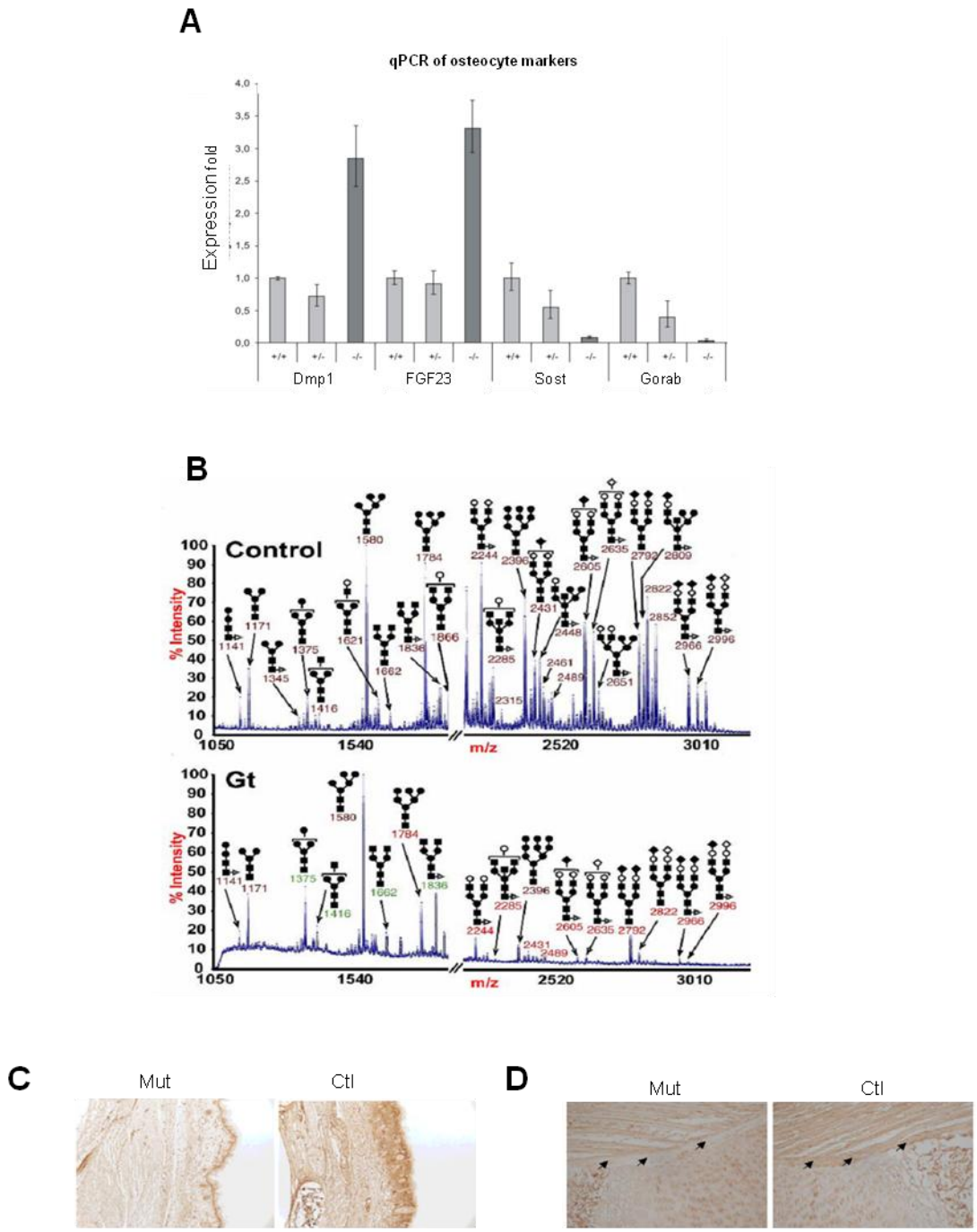

Fig.1.6 A). qPCR analysis of osteocytic markers on the long bones from P0 mutant mice showed 2-3 fold increase in Dmp1 and FGF23 expression but strong reduction in Sost expression. B). MALDI-TOF analysis of skin biopsy from mutant mice showed a decrease in complex N-glycans. ■ = N-acetyl glucosamine, ● = mannose, Δ = fucose, o = galactose, ◆ = sialic acid; C). Reduced E-PHA stain in the mutant mouse skin. D). Reduced E-PHA stain in the perichondrium indicated by the arrows.

mandibular hypoplasia (Fig.1.5D). They also showed delay in ossification in the long bones at E14.5. However, at birth, there were only mild morphological defects found in the long bones (Fig.1.5E), despite the fact that the mutant mice showed altered expression of osteocyte markers comparing to the control mice (Fig.1.6A). The mutant animals also showed defects in glycosylation in skin tissues (Fig.1.6B and C) and in the perichondrium of long bone (Fig.1.6D), as indicated by the MALDI-TOF analysis and reduced E-PHA (a lectin recognizing complex N-glycans) staining. Primary culture of the skin fibroblast from the mutant mice was found to be difficult as the fibroblast grow poorly comparing to the control, which is a phenomenon also found in human patient fibroblast.

The genetrap mice were quite different in phenotype manifestations comparing to the GO patients. Firstly, GO patients have lax skin, while the skin of the genetrap mice was tighter than the control animals; Secondly, the genetrap mice died at birth with lung defects which was not noted in GO patients. These differences required further investigation. However there are also similarities between the genetrap mouse model and GO patients. The mutant mice have an ossification delay, which likely corresponds to the osteopenia in GO cases. The mice also show the jaw hypoplasia which leads to the premature aged appearance of GO patients. These defects point to impaired osteoblast differentiation and function. The causes and effects, if any, of this observation are very important for the study of the bone pathology of the GO patients. Another interesting similarity between the genetrap mouse model and the GO patients is the difficulty of the culturing of their primary skin fibroblast. Both Gorab null mouse and human skin fibroblast grow poorly in culture. The relationship between the low proliferation potential of the Gorab null fibroblast could be an explanation of the lax skin phenotype and required further analysis.

1.6 Research Aims and Approaches

To investigate the role of Gorab in cell cycle progression.

The skin fibroblasts from the genetrap mouse and GO patients showed lower proliferation potential comparing to the controls. This suggests that inactivation of Gorab results in either cell cycle arrest or apoptosis. This is very interesting since all the reported interacting partners of Gorab have been suggested to play a role in cell cycle regulation. For example, Pirh2 and MDM2 are both E3 ligases that regulate p53, a widely studied transcription factor that played major role in cell cycle progression. Scyl-1 and Rab6 has also been reported to play a role in mitosis and cytokinesis, respectively. It is therefore possible that Gorab also plays a role in cell cycle progression by regulating the function of its' interacting partners. Preliminary observations that the cells stop proliferating, have an enlarged size and show very few dead cells suggest that they undergo cell cycle arrest (cellular senescence) instead of apoptosis. In order to test this hypothesis, skin fibroblast from genetrap mice and human patients will be used as the primary model to test for the expression of different cell cycle and apoptotic markers. siRNA targeting Gorab will also be used to study the immediate effects of Gorab knockdown in cancer cell lines e.g. Hela and U2OS cells.

To investigate the effects of Gorab inactivation on bone development.

The genetrap mouse model showed delayed ossification in the long bones at E14.5, indicating delay in the formation of the primary ossification center. This implies defects in chondrocyte function and perhaps a delay in chondrocyte hypertrophy and/or vascular invasion. By E18.5, no significant defect in mineralization and morphology was found in the mutant mouse. Nevertheless, the

mutant mice showed altered expression pattern of osteocyte markers comparing to the control animals and had an unossified fontanelle. These alterations point to defects in chondrocytes and osteoblast differentiation and maturation. The high expression of Dmp1 and FGF23, the two late osteoblast-osteocyte markers, and the decrease in the osteocyte marker Sost expression supported this notion. However, since the genetrap mutant died at birth, it is not possible to use this animal model to further study the effect of defective osteoblast maturation on postnatal bone formation and development. Therefore a conditional mouse model of Gorab will be generated in this project to study the effect of Gorab inactivation on postnatal bone development. This will be accomplished by flanking essential exons of Gorab with loxP sites to generate a conditional mouse model. The subsequent crossing with different mouse lines that express the cre recombinase in different tissues (e.g. chondrocytes, osteoblast and osteocytes) at different stages of bone development will allow the delineation of the spatial and temporal role of Gorab during bone development. In addition, the conditional mouse model also offers the flexibility for studying the role of Gorab in other organs (when in combination with the appropriate cre expression mouse lines).

Chapter 2 Materials and Methods

2.1 Cell culture

Human skin fibroblast from GO patients and controls were cultured in DMEM medium with 10% fetal calf serum and 1% ultraglutamine. Hela cells and U2OS cells were cultured in DMEM with 5% fetal calf serum and 1% ultraglutamine. All cell culture medium and supplements were obtained from Lonza, Switzerland.

2.2 Senescence associated beta galactosidase (SA-betaGal) activity assay

SA-betaGAL activity was done according to Debacq-Chainiaux et al 2009 with modifications. Control and GO patient fibroblast was plated onto glass cover slips at 70% confluence. The cells were then fixed in 2% formaldehyde in PBS at room temperature for 5 minutes followed by washing with PBS twice. The coverslips were then incubated in X-gal staining (1mg/ml X-Gal in 40mM citric acid/sodium phosphate buffer, pH6.0 with 2mM $MgCl_2$, 5mM $K_4[Fe(CN)_6]$ $3H_2O$, 5mM $K_3[Fe(CN)_6]$). solution at 37℃ for 16hours. The stained coverslip were then fixed in 4% paraformaldehyde at 4℃ overnight before imaging.

2.3 siRNA knock down of GORAB in Hela and U2OS

Hela cells and U2OS cells were seeded at 50% confluence in a 6-well plate. Cells were then transfected with siRNA against GORAB (5'-CCAUGAUGGUCACAACAAUTT-3') or control scramble siRNA (Ambion Cat#AM4635)

Table 2.1 Antibodies used in this study.

	Antibody	Manufacturer	Dilution
Primary antibody	Rabbit anti-53BP1	Santa Cruz, Cat#10914	1:200
	rabbit anti-GORAB	Raised in our laboratory	1:200
Secondary antibody	Alexa555 Fluor, donkey anti rabbit IgG	Molecular Probes, Cat#A31572	1:1000

using INTERFERin^{TM} (Polyplus transfection). Briefly, 200nM siRNA was mixed with 2µl interferin in 100µl OptiMEM (Gibco) for 10min before adding to the cell culture. The transfection process was repeated 10 hours later as a secondary transfection to improve transfection efficiency. The cells were then harvested 72hours after the first transfection for immunofluoresence and RNA extraction.

2.4 Immunofluorescence

Control and GO patient fibroblast was plated onto glass cover slips at 70% confluence. The cells were then fixed in 4% paraformaldehyde at 4℃ for 10min. The coverslips were then washed with PBS and permeabilized with 0.1% Triton X-100 in PBS at room temperature for 10min. The cells were than washed twice with PBS and then blocked with 3% bovine serum albumin at 4℃ for 30min. The cells were then incubated with the primary antibody at 4℃ overnight. After that, cells were washed three times with PBS and then stained with secondary antibody at room temperature for 1hour. The cells were then washed three times with PBS and then counterstained with DAPI. A list of antibodies used was listed in Table2.1.

2.5 RNA extraction, cDNA synthesis and quantitative real-time PCR analysis

RNA extraction from cell culture and from tissue samples was done by using TRIzol® reagent (Invitrogen, Germany) following the manufacturer's protocol. 1µg of RNA was then used for cDNA synthesis using the RevertAid kit (Fermentas, Germany) according to manufacturer's protocol. Quantitative real-time PCR was performed with an ABI 7500 real time PCR system (Applied Biosystems) using HOT FIREPol® EvaGreen® qPCR Mix Plus from Solis Biodyne according to manufacturers' protocol. Primers used were listed in Table 2.2.

2.6 Construction of Gorab conditional mouse model

Construction of targeting vector

Targeting vector was constructed following a well established protocol by Liu et al 2003. Fig. 2.1 outlined the construction strategy. Briefly, a BAC clone containing the mouse Gorab locus, BAC clone bMQ-373H11 (129S7Ab2.2) was obtained from Geneservice Ltd. A ~11.1kb region containing Exon2 to Exon4 of Gorab and the flanking introns was extracted into a pBluescript vector by recombination. LoxP sites was then inserted into the targeting vector flanking Exon2 and 3 by homologous recombination.

Gene targeting of mouse ES cell

Gene targeting of mouse ES cells was done with the help from the Transgenic Core Facility of The University of Hong Kong. 20µg of the targeting vector was electroporated into mouse ES cells prepared from mouse strain 129/svev. The cells were screened with G418 antibiotics. Antibiotics resistant clones were isolated and

Table 2.2 Primers used for the Expression profiling in human cell lines by qPCR.

Name	Sequence 5' --> 3'
qhGAPDHF	CAATGGATGCCTATACACATGG
qhGAPDHR	TCAGCTCAGACTCTGTGTTTCC
qhp16/Ink4aF	CAACGCACCGAATAGTTACG
qhp16/Ink4aR	ACCAGCGTGTCCAGGAAG
qhGorabF	GAATTCTCAGGAACCGGATTGAT
qhGorabR	TGCTTCAGCCCTGCAAACC
qhp21/CDKN1A F	CAGACCAGCATGACAGATTTCTACC
qhp21/CDKN1A R	GGCTTCCTGTGGGCGGATTAG
qhTGFb1F	ACC CGC GTG CTA ATG GTG GAA
qhTGFb1R	GTA CCG CTT CTC GGA GCT CT

screened by Southern Blot for correctly targeted clones using external and internal probes from both 5' and 3' ends.

Blastocyst injection for chimeric mice generation

With the help of Dr. Wilson Chan from Department of Biochemistry, The University of Hong Kong, the correctly targeted ES cell clones were injected into the blastocysts from C57BL/6 mice for generating chimeric mice. The coat color of the mice indicated the degree of chimerism. Mice with high degree of chimerism (70-90%, judging from the percentage of agouti coat color) were mated with β-actin/flpper transgenic mice to remove the neo cassette used for antibiotic screening of ES cells. Germline transmitted conditional Gorab mouse was screened by PCR using primers listed in Table 2.3.

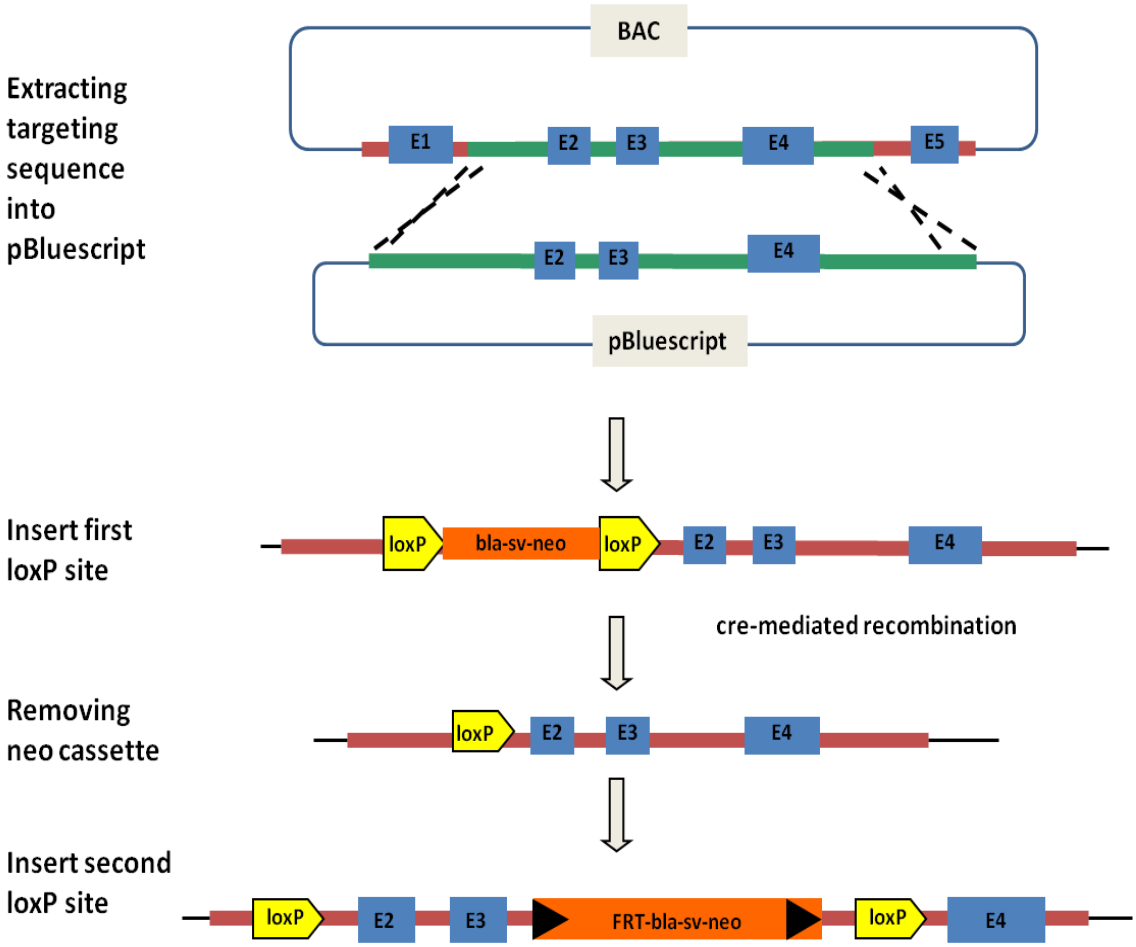

Fig.2.1 Strategy for generating targeting vector. A 11.1kb fragment containing Exon 2 to 4 of Gorab was extracted from BAC clone into pBluescript by homologous recombination, as the back bone of the targeting vector. Then a loxP-bla-sv-neo-loxP cassettes was inserted 5' of Exon2 by homologous recombination. By transforming the vector into an *E.coli* strain, EL350, which overexpresses cre recombinase, the antibiotic resistance will be removed by cre mediated recombination, leaving behind a single loxP site. Then a FRT-bla-sv-neo-FRT-loxP cassette was inserted 3' of Exon3 by homologous recombination. The bla-sv-neo cassette has a dual promoter, which enables antibiotic resistance in both *E.coli* and in ES cells against kanamycin and G418, respectively. The neomycin resistance can be removed by flpper mediated recombination in later steps. The second loxP site was also inserted and thus completing the targeting vector.

Table 2.3 Primers used for genotyping the mouse models.

Name	Sequence 5' --> 3'
Gorab 1F	CGACACAGGACACAATTTTTGA
Gorab 1R	GAAGATAAAACAATCACAGGGAT
Gorab 2F	TCATGTGCTATGCCATACTGC
Gorab 2R	ATCTCCCTCTCACCATTTCTG
Cre A	GGACATGTTCAGGGATCGCCAGGCG
Cre B	GCATAACCAGTGAAACAGCATTGCTG

2.7 Enrichment of osteocytes from mouse long bone for RNA extraction

Osteocytes from the cortical bone of mouse homers were enriched by sequential collagenase digestion modified from the protocol in Kramer et al 2010. Briefly, both mouse homers bones were first cleared of attaching muscles. Then the epiphysis was cut off and the bone marrow was flushed out with PBS. The hollow bone shaft was then digested twice with 0.2% collagenase (Sigma Cat. #C5138) in isolation buffer (70 mM NaCl, 10 mM $NaHCO_3$, 60 mM sorbitol, 30 mM KCl, 3 mM K_2HPO_4, 1 mM $CaCl_2$, 0.1% bovine serum albumin, 0.5% glucose, 25 mM HEPES) at 37℃ for twenty minutes each under vigorous shaking. The cleared bone shaft was then frozen in liquid nitrogen and then homogenized with pestle and mortar. RNA was then extracted from the homogenized tissue with TRIzol® reagent and reverse-transcribed using the RevertAid Kit following manufacturer's protocol for further gene expression analysis. Primers used were listed in Table 2.4.

Table 2.4 Primers used for the expression profiling of mouse osteocytes by qPCR.

Name	Sequence 5' --> 3'
qmGapdhF	GGGAAGCCCATCACCATCTT
qmGapdhR	CGGCCTCACCCCATTTG
qmGorabF	CGGATGGCTCAGGATTGG
qmGorabR	CGAGTTTTCTTCACAGGAATTCG
qmCol1a1F	TGTTCAGCTTTGTGGACCTC
qmCol1a1R	TCAAGCATACCTCGGGTTTC
qmOsxF	GAGGCCTTTCGTCTGCAACT
qmOsxR	TTCTTCTCCCGGGTGTGAGT
qmBglapF	CCTGGCTGCGCTCTGTCT
qmBglapR	TGCTTGGACATGAAGGCTTTG
qmSpp1F	TGGTGCCTGACCCATCTCA
qmSpp1R	TTCATTGGAATTGCTTGGAAGA
qmDmp1F	TGTCATTCTCCTTGTGTTCCTTTG
qmDmp1R	TGTCATTCTCCTTGTGTTCCTTTG
qmSostF	AGACCTCCCCACCATCCCTAT
qmSostR	TGTCAGGAAGCGGGTGTAGTG
qmp16/Ink4a, transcript 1 F	CGCAGGTTCTTGGTCACTG
qmp16/Ink4a, transcript 1 R	TCTGCACCGTAGTTGAGCAG
qmp21F	TGACAGATTTCTATCACTCCAAGCG
qmp21R	CACACAGAGTGAGGGCTAAGGC
qmTGFb1-F	ATACGCCTGAGTGGCTGTCT
qmTGFb1-R	GCTGAATCGAAAGCCCTGTA
qmTGFB2-F	CGAGGAGTACTACGCCAAGG
qmTGFB2-R	CAA TGAGCCAGAGGGTGTTG

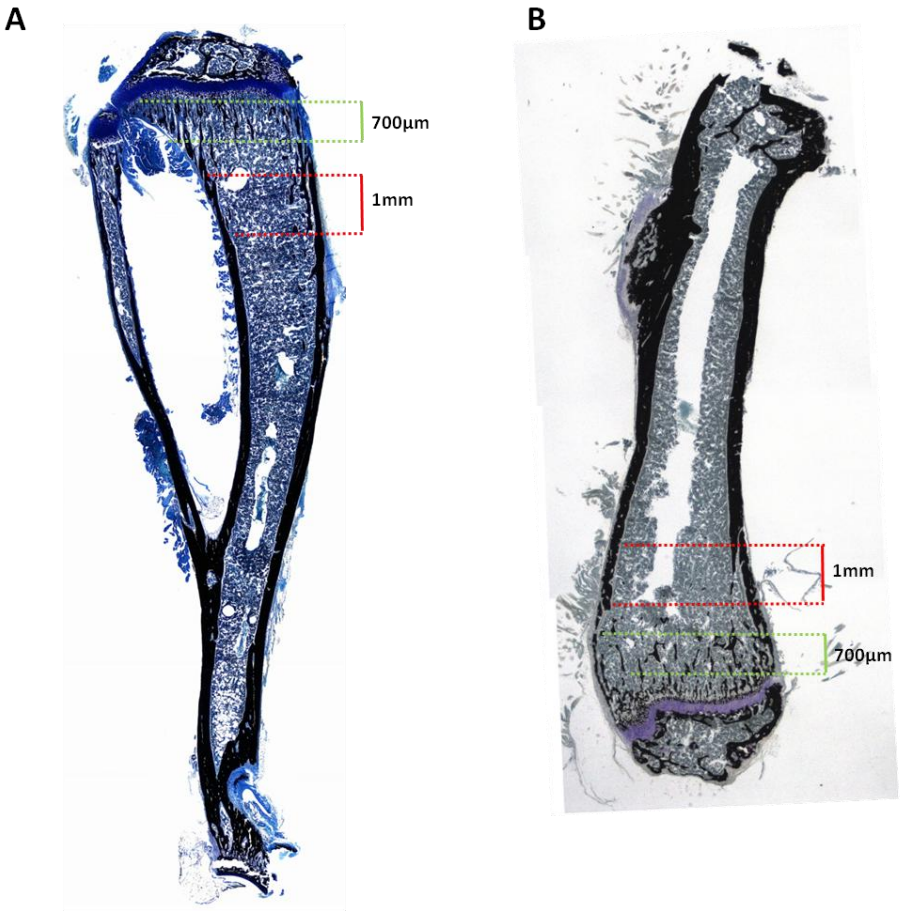

Fig.2.2 The region of interest chosen for microCT measurement of the long bones. (A). 700µm below the proximal growth plate of the tibia was analyzed for trabeculae. 500µm below that region, a 1mm region was analyzed for the cortical bone thickness. (B). 700µm above the distal growth plate of the femur was analyzed for trabeculae. And then, starting from 500µm above the trabeculae, a 1mm region was chosen for cortical bone measurement.

2.8 microCT analysis

microCT analysis was done by using the Scanco uCT40. The trabecular bone measurement was done for a region of 700µm directly under the proximal growth plate of the tibia and above the distal growth plate of the femur. The cortical bone

measurement was done for 1mm, at a region 1200µm below the proximal growth plate of the tibia and above the distal growth plate. Fig.2.2 illustrated the region of interest of the long bones. The trabecular bone of the fifth and sixth lumbar vertebra was done by measuring the trabeculae between the two growth plates of the vertebra.

2.9 Histomorphological analysis

Methylmethacrylate (*MMA*) *embedding and sectioning*

The bone samples were embedded in MMA (Polysciences Cat#00834) and then sectioned for histological study. The bone samples were first fixed in 4% paraformaldehyde for 24 hours at 4℃. Then the samples were dehydrated in 70% ethanol for 24 hours, 80% ethanol for 24 hours, twice in 100% ethanol for 24 hours and twice in xylene for two hours. The samples were then infiltrated with infiltration MMA (10%v/v polyethylene glycerol (Sigma Cat#202398) and 0.33% w/v benzoyl peroxide in MMA) for at least 24hours at 4℃. The polymerization was carried out at 4℃ in polymerization solution (10%v/v polyethylene glycerol, 0.55% w/v benzoyl peroxide, 0.5% v/v *N*,*N*-dimethyl-*p*-toluidine in MMA). The embedded samples were then sectioned using a Leica RM2255 microtome at 5µm thickness for staining and analysis.

Histological stainings

MMA sections were deplasticized by washing in 2-methoxyethylacetate thrice for 10minutes. The sections were then washed in xylene twice for 5 min and then rehydrated through 100%, 70%, 50% ethanol for 1 minute in each step. The sections were then rinsed in water and then used for histology.

Von Kossa and toluidine blue double staining was done for general bone histology. Sections were put into 1% silver nitrate solution for 3 minutes and then washed in water thrice for 2 minutes. The sections were then developed in 5% $NaCO_3$ solution with 10% formaldehyde for 2 minutes. The sections were then washed in running water for 10minutes. The sections were then washed in 5% $Na_2S_2O_7$ solution to remove background staining. The sections were then washed in running water for 10minutes. The sections were then stained with 0.05% toluidine blue solution until attained desired intensity (~2minutes).

Masson Goldner staining was conducted for high quality cellular histology and extracellular matrix staining. The sections were first stained with Weigerts Haematoxylin for 2 minutes. The sections were then washed in running water for 10 minutes. The sections were then stained in Ponceau-Fuchsin solution (Chroma Cat#2C149) for 5 minutes for plasma staining and then rinsed in 1% acetic acid. The sections were then differentiated in Orange G differentiation solution (2%w/v Orange G in 3% phosphomolybdic acid) for 5minutes. The sections were then rinsed in 1% acetic acid and then stained in Light Green solution (0.1% w/v light green in 2% acetic acid) for 5 minutes for collagen fiber staining. The sections were then dehydrated and mounted for imaging.

Von Kossa and Pirko-Fuchsin double staining was done for osteoid staining and measurement. von Kossa staining was done as mentioned above. The sections were then stained in Pikro-Fuchsin solution for 10minutes and then mounted for imaging. Osteoid area, volume and thickness in the metaphysis was determined using the software Osteomeasure^{TM}.

2.10 Mineral Apposition rate

4weeks old Gorab$^{fl/fl}$;Prx1cre mutant and control animals were injected with calcein (10µl per gram body weight) 5 days and 2 days before sacrifice. The tibia of the animals were embedded in MMA and sectioned at 5µm thickness. The calcein labels were analyzed with a fluorescence microscope and the distance between the two lines of calcein labels was measured for mineral apposition rate calculation.

Chapter 3 Results

3.1 Genome instability and cellular senescence in Gerodermia osteodysplastica

The culturing of skin fibroblast from GO patients was difficult since the cells grew much slower than the control fibroblast and stopped proliferating at early passages. The cells were enlarged and flattened in shape comparing to the control fibroblast. Because of these observations, it was hypothesized that GO skin fibroblast suffered from cellular senescence.

Inactivation of Gorab results in cellular senescence and activates TGFβ signaling pathway

In order to test this hypothesis, GO patient skin fibroblasts were treated with BrdU for 24hours to label the proliferating cells in culture (Fig.3.1.1A). It was found that the percentage of proliferating cells in the GO patient fibroblast culture was significantly less than that of the control fibroblast. In addition, GO patient fibroblasts showed increase in senescence associated beta-galactosidase (SAbetaGal) activity (Fig.3.1.1B and C). qPCR analysis of cyclin dependent kinase inhibitors (senescence markers) showed a significant increase in p16/Ink4a message but not in p21 (Fig.3.1.1D). These results indicated that the GO patient fibroblasts suffered from cellular senescence, which was likely to be induced or maintained by the up-regulation of p16/Ink4a. Continuous passage analysis of skin fibroblast from P0 Gorab genetrap mice also showed a decrease in proliferation comparing to their littermates (Fig.3.1.1E). Due to the presence of the LacZ gene in the genetrap cassette SAbetaGal activity could not be tested in these cells. This indicated that the effect of

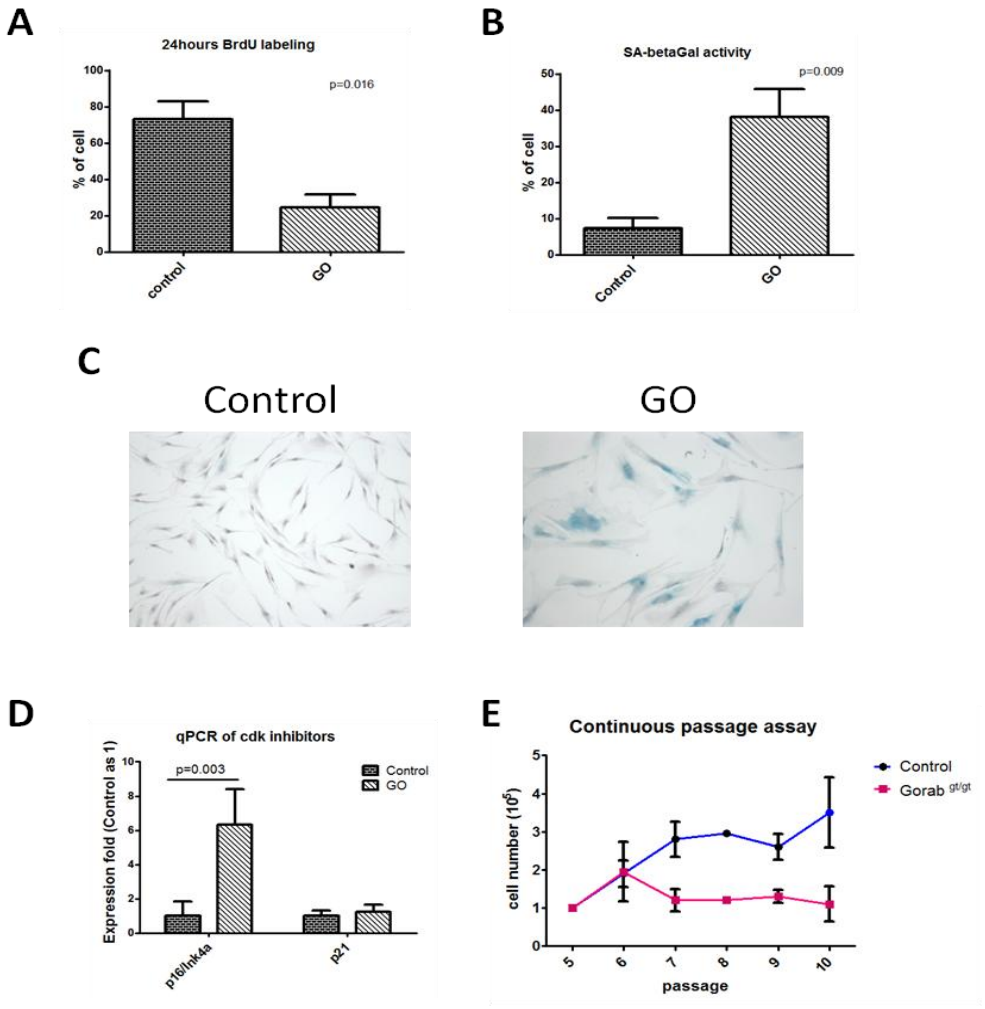

Fig.3.1.1 Loss of GORAB induced cellular senescence. (A). Decrease in proliferating cell population in GO patient skin fibroblast culture, N=3. (B) Increase in Senescence Associated beta-galactosidase activity (SAbetaGal) in GO patient skin fibroblasts, N=3. (C). Senescence Associated beta-galactosidase staining of GO patient fibroblasts. (D). qPCR showing significant Increase in p16/Ink4a, but not p21, expression in GO fibroblasts. (E). Continuous passage assay of skin fibroblasts from Gorab genetrap mutant showed decreased proliferation comparing to control. (N=3, compared with control littermates).

Gorab inactivation on cellular senescence was a common phenomenon in both mouse and human.

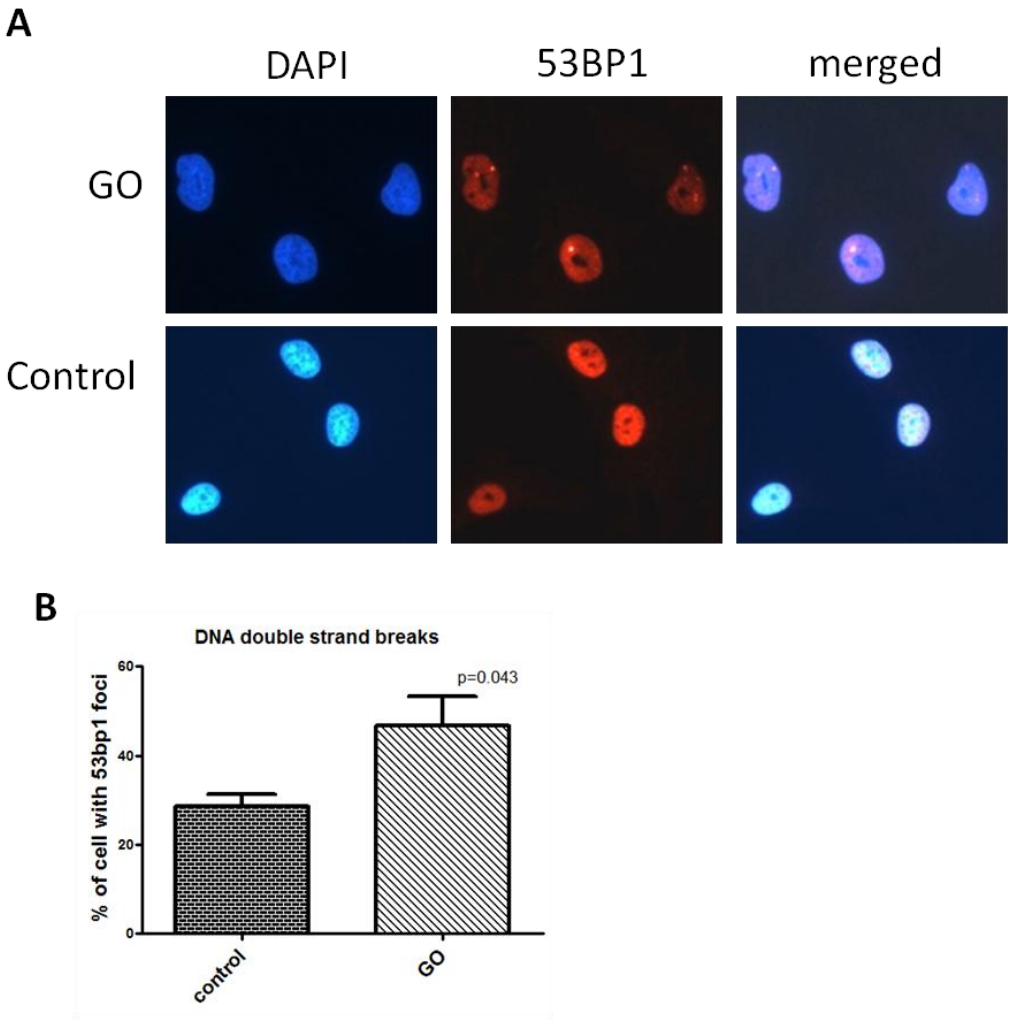

Fig.3.1.2 Accumulation of DNA damage in GO patient. (A). Immunofluorescence staining of a DNA double strand breaks marker, 53BP1, in GO patient skin fibroblasts. (B). GO patient fibroblasts showed significant increase in DNA damage foci, N=3.

Loss of Gorab induces genome instability and increases sensitivity to ionophore

Since genome instability is a known cause of cellular senescence, immunofluorescence of 53BP1, which marked DNA double strand breaks, was undertaken to investigate if there was increased DNA damage in GO patient fibroblasts. Indeed, there was an increase in percentage of GO patient fibroblast cells with 53BP1 foci accumulation in the nucleus (Fig. 3.1.2A and B). In order to investigate whether loss of GORAB directly induces genome instability, siRNA

against GORAB was used to knock down Gorab in Hela and U2OS cells. Fig.3.1.3A and B shows that the siRNA could successfully knockdown the GORAB message and protein, respectively, after 72hours. It was found that knockdown of GORAB by siRNA resulted in a significant increase in the amount of 53BP1 foci in both HeLa and U2OS cells. In addition, there was also an increase in the number of cells with micronuclei, supporting the idea that loss of GORAB induced genome instability (Fi.g3.1.3.C to F).

One of the well established causes of DNA damage is the accumulation of Reactive Oxygen Species (ROS) in cells. It was found that upon siRNA knockdown of GORAB in Hela cells, there was no significant change in the basal level of ROS in the cell. However there was an increase in intracellular ROS upon Carbonyl cyanide m-chlorophenyl hydrazone (CCCP) induced mitochondrial uncoupling (Fig.3.1.3G). This suggested that loss of GORAB impaired the cell scavenging ability of ROS, which may in turn increase the cells' susceptibility towards oxidative stress.

Loss of GORAB activates TGF-beta signaling

In oncogene induced senescence, oncogenic RAS induced cellular senescence through activation of TGFβ signaling pathway (Tremain et al 2000). Therefore, we investigated whether TGFβ signaling was activated in GO. It was found that in our GO fibroblast, there was an increase in the mRNA of TGFβ1 (Fig.3.1.4A). siRNA knockdown of GORAB in Hela cells and U2OS cells for 72 hours also resulted in increase in TGFβ1 message (Fig. 3.1.4B). Western blot analysis of GO fibroblast culture lysates showed an increase in phospho-SMAD2 signal, indicating that the TGF-beta signaling pathway was activated upon GORAB inactivation.

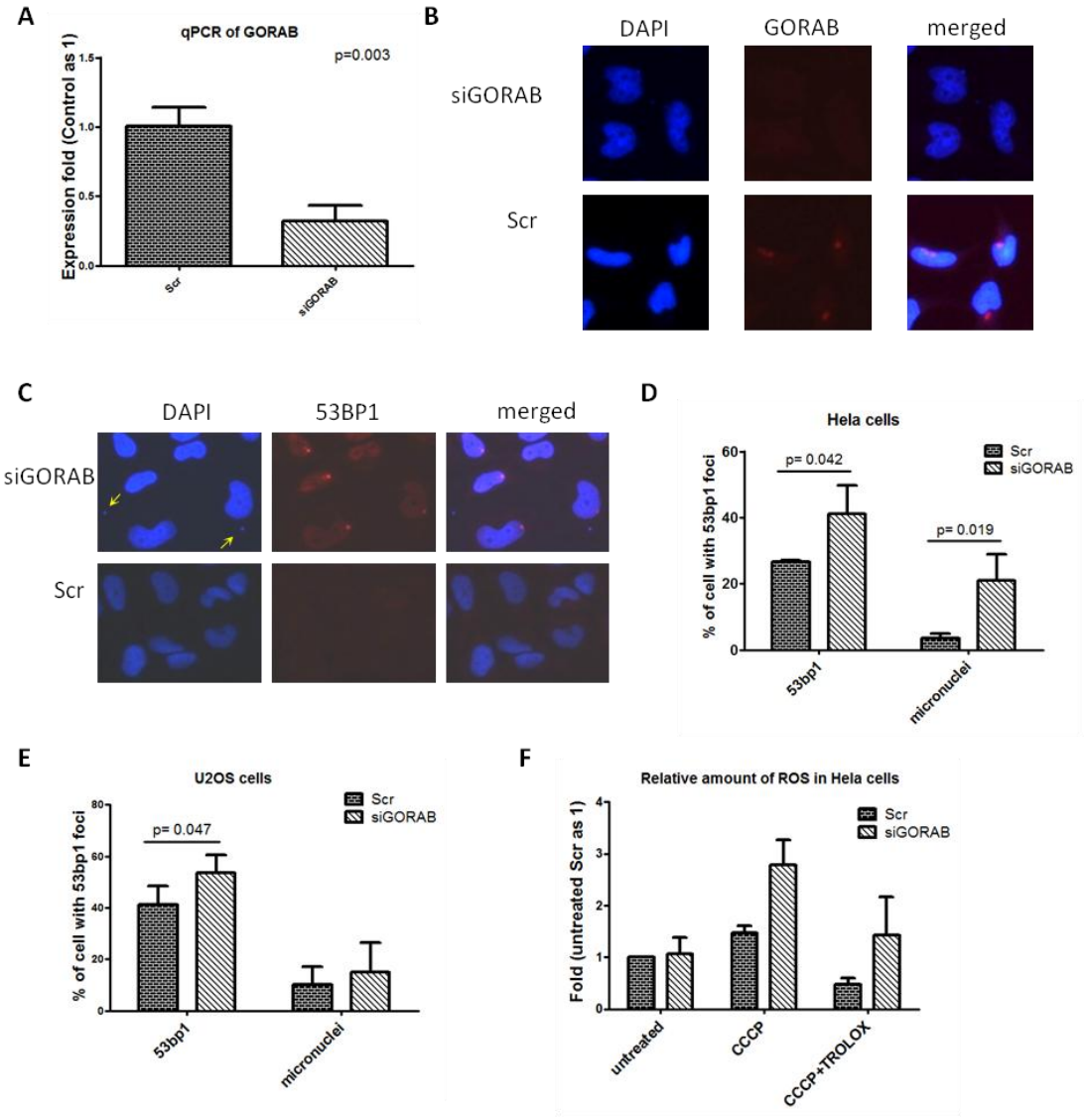

Fig.3.1.3 (A) Reduction in the amount of GORAB protein in Hela upon siRNA knockdown for 72hours. (B). qPCR quantification showed a 70-80% decrease in GORAB message in Hela cells upon siRNA knockdown, (N=3). (C). Increase in DNA damage foci and micronucleus (marked by arrows) in Hela cells upon siRNA knockdown. (D). Knockdown of GORAB by siRNA induced DNA damage and micronuclei formation in Hela cells (N=3). (E). Knockdown of GORAB resulted in significant increase in DNA damage foci, but not in micronuclei, in U2OS cells, N=3. (E). GORAB knockdown in Hela cells had no effect on baseline level of ROS, but resulted in increase in ROS accumulation upon CCCP treatment. Results were averaged from two independent experiment.

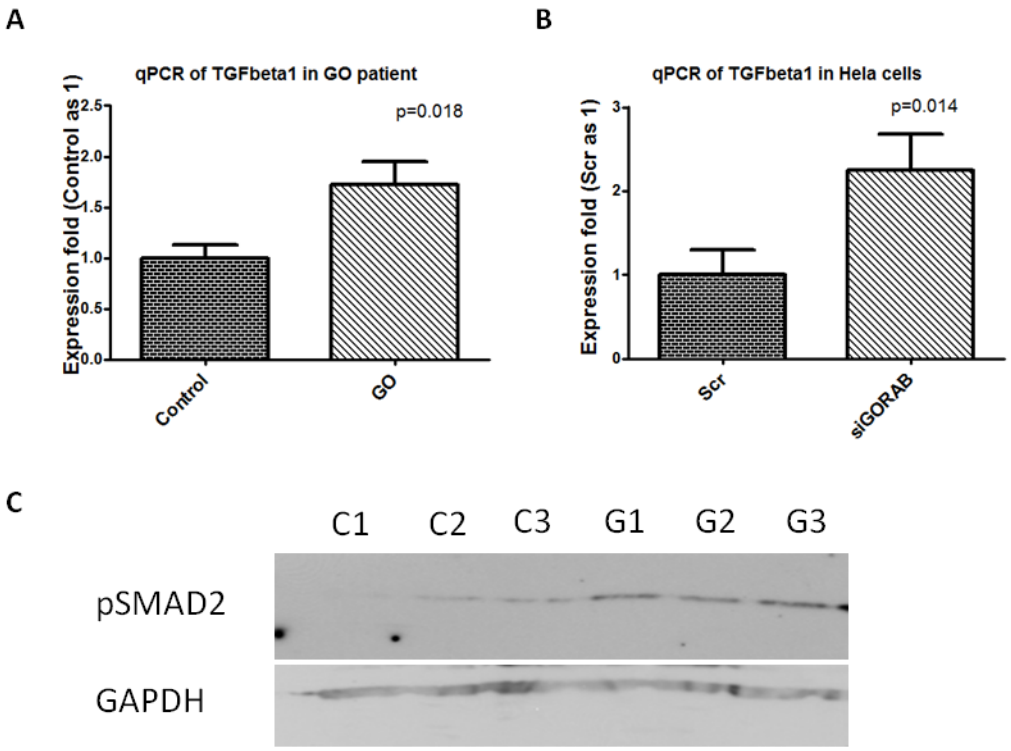

Fig.3.1.4 Loss of GORAB induced TGFβ signaling. (A). qPCR showed significant increase in TGFβ1 message in GO fibroblast, N=3. (B) qPCR showed significant increase in TGFβ1 message in both HeLa and U2OS cells upon siRNA knockdown of GORAB, N=3. (C). Increase in phospho-SMAD2 in GO fibroblast lysates as determined by Western blot. C1-3 were controls and G1-3 were GO patients.

3.2 Construction of conditional Gorab mouse model

Although a genetrap mouse model was available, the mutant mouse died in a few hours after birth, with apparent difficulty in breathing. The exact cause of death of the mutant mouse remained elusive. However, since the mutant died shortly after birth, the genetrap mouse thus was not suitable to study the postnatal effects of Gorab inactivation. Therefore it was essential to develop a conditional Gorab mouse model for studying the effect of Gorab inactivation in different tissues, especially bone development, postnatally.

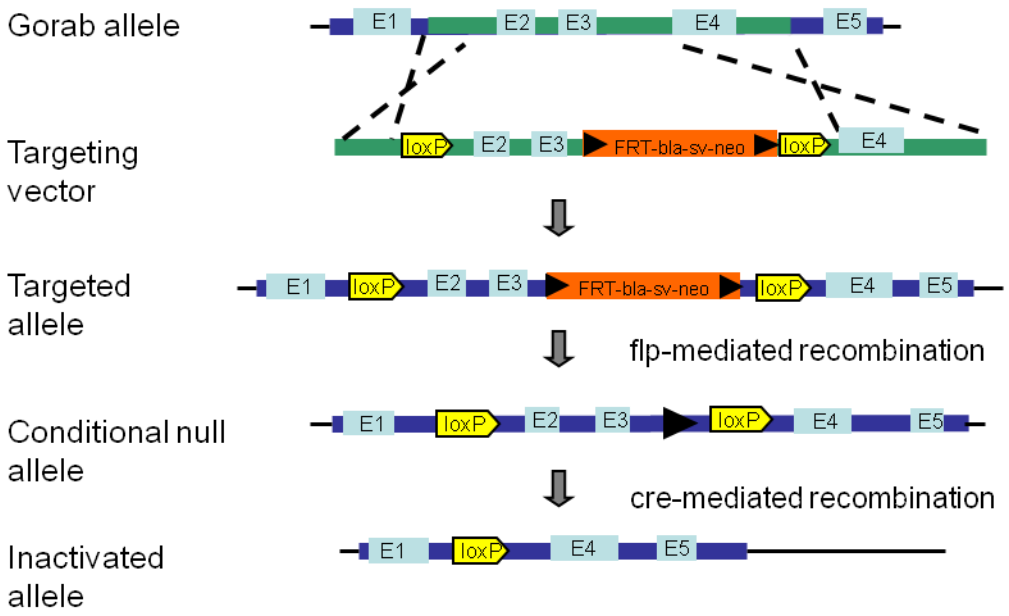

Fig.3.2.1 Schematic diagram showing the generation of conditional Gorab mouse. The targeting vector was used for homologous recombination into the Gorab allele of ES cells. The correctly targeted ES cells were then used for blastocyst injection to generate chimeric mice. The chimeric mice were then crossed with a ß-actin flpper transgenic mice to remove the neo cassette in it and thus generating mice with the conditional null allele, which was used for the subsequent experiment. By crossing the conditional Gorab mice with Cre transgenic mice, Exon2 and 3 will be deleted by cre-mediated recombination and generate an inactivated allele in the cre-expressing cells.

Choosing the region for loxP site insertion

A conditional mouse model of Gorab was constructed by flanking essential exons of the Gorab allele with loxP sites. Upon cre mediated recombination, the exons flanked by the loxP sites would be deleted and thus no functional Gorab protein would be expressed. Exons 2 and 3 of the Gorab allele, which corresponded to 20-173aa of the protein were chosen to be the target exons for deletion for three reasons. Firstly, these two exons represented a relatively small genomic region

(~2.6kb) and were easy to manipulate. Secondly, they encoded the majority of the first coiled-coil domain of the protein. This meant that deleting this region would have removed an essential domain of the protein. Thirdly, deleting these two exons would generate a non-sense mutation and thus premature stop in the translation of the remaining peptide. In other words, deleting these two exons would result in the total loss of Gorab protein instead of generating a truncated protein.

Generating and screening for targeted ES cell

The strategy for the construction of targeting vector was adopted and modified from Liu et al 2003. The BAC clone bMQ-373H11 (129S7Ab2.2) from Geneservice Ltd. was used and the targeting vector was shown in Fig3.2.1. With the help from the Transgenic Core Facility of Department of Biochemistry, The University of Hong Kong, the targeting vector was electroporated into mouse embryonic stem cells and successfully targeted ES cell was screened by Southern blot. Fig.3.2.2 depicted the screening scheme (A). Two positive ES cell clones were obtained for the generation of conditional Gorab mouse (B).

Validating the conditional Gorab allele

The conditional Gorab mouse was crossed with two transgenic mouse lines that express the cre recombinase in the germline tissue in order to generate a total null Gorab mouse. The two transgenic mouse lines used were the Protamine cre mouse (O'Gorman et al 1997) and ZP3 cre mouse (Lewandoski et al 1997). The Protamine cre mouse express the cre recombinase specifically in the male germline, while the ZP3 cre mouse express the cre recombinase in the oocyte. The mating of a Gorab$^{fl/+}$; Protamine cre male mouse with a Gorab$^{fl/+}$;Zp3cre female mouse generated a Gorab-/-;Protamine cre; ZP3cre triple mutant that was essentially a Gorab total null

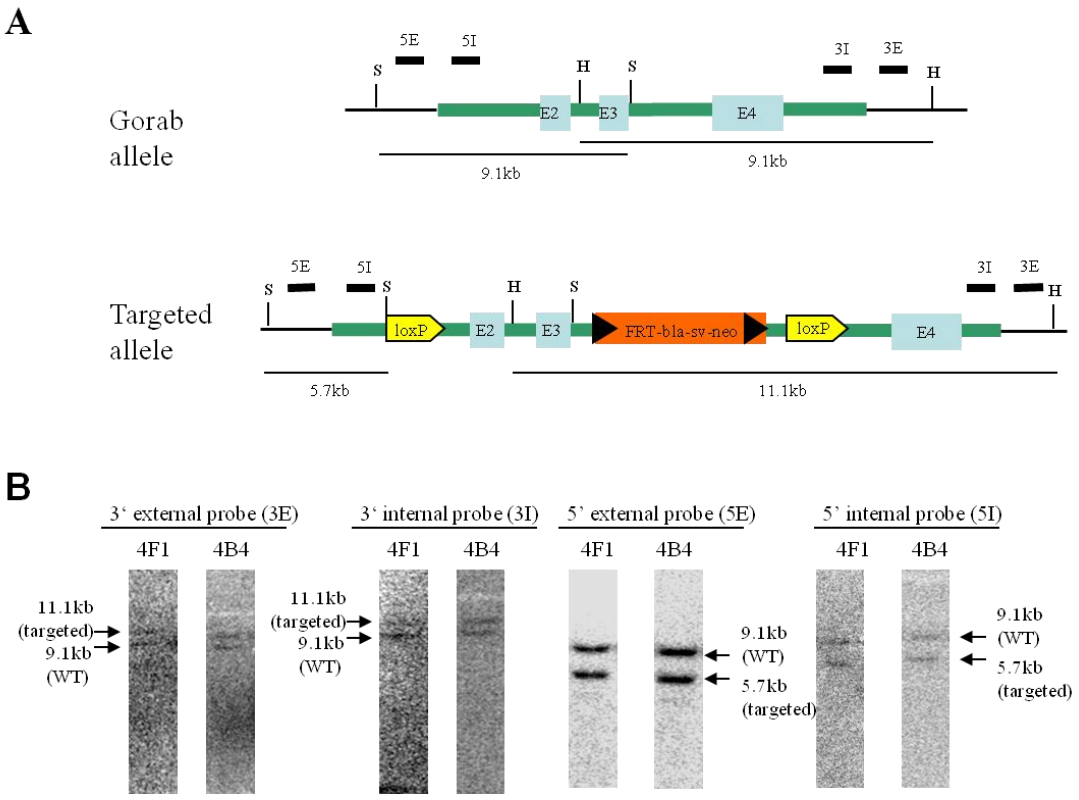

Fig.3.2.2 Southern Blot screening for correctly targeted ES cell clones. (A). Strategy for Southern Blot screening. The green bar was the homologous region between the targeting vector and the Gorab allele. The genome DNA of targeted ES cells was digested with StuI for 5' external and internal probe screening, while HindIII was used for 3' external and internal probe screening. S=StuI, H=HindIII. (B) Southern Blot of the two successfully targeted ES cell clones.

---

mouse. Fig.3.2.3A showed one such mutant, which died shortly after birth and had an appearance similar to the Gorab genetrap mouse mutant, with tight and swollen skin and shortened snort. Genotyping by PCR showed that the mouse had only the excised allele of Gorab, indicating that it was a total null mutant of Gorab (Fig.3.2.3B). RT-PCR showed no Gorab mRNA in the skin of the mouse (Fig.3.2.3C). This showed that the conditional allele was functional and could successfully inactivate Gorab by cre-mediated recombination.

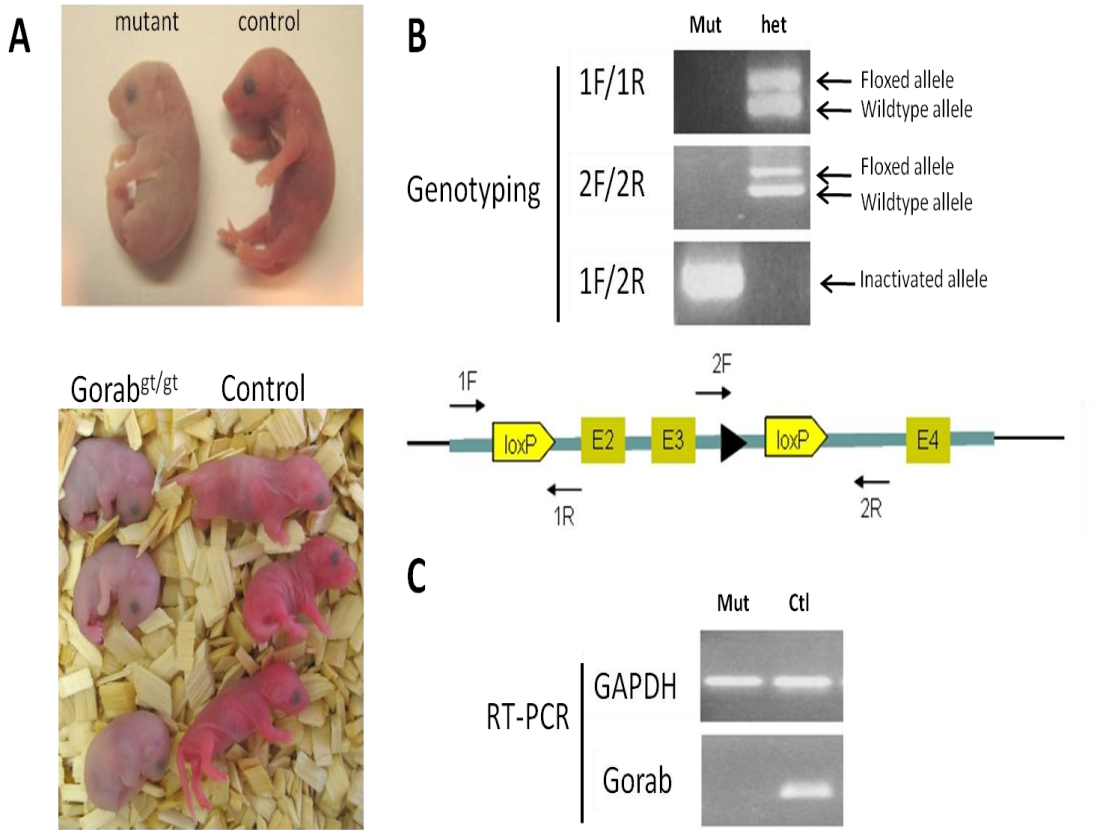

Fig.3.2.3 Functional analysis of the Gorab conditional mouse. (A). The total null mutant generated from the Gorab conditional mouse died shortly after birth, with an appearance similar to the Gorab genetrap mouse mutants. (B). Schematic diagram showing the design of primers for PCR genotyping. The heterozygous control showed two bands with both primer sets flanking the loxP sites but none was shown in the total null mutant, which was only positive for the inactivated allele (1F/2R). (C). RT-PCR showing the loss of Gorab message in the cDNA prepared from the P0 mutant skin biopsy.

3.3 Role of Gorab in bone development

Expression pattern of Gorab

The currently available antibodies against Gorab did not show the necessary specificity in immunohistological stainings and *in situ* hybridization was hampered by

low mRNA expression levels. The genetrap mouse model had a beta-geo cassette inserted into the first intron. This allowed the beta-geo protein (a fusion protein of beta-galactosidase and neomycin) to be expressed under the control of the Gorab promoter. In other words, the beta-geo cassette could be used to study the expression pattern of Gorab by beta-galactosidase activity staining. Sectioning through the tibia at E16.5 showed that Gorab was highly expressed at the articular cartilage, perichondrium, the resting and proliferating chondrocytes, the periosteum and the osteoblast (Fig.3.3.1). There was also signal from the prehypertrophic and hypertrophic chondrocyte, but the signal was much weaker and could be remnant from previous developmental stage and requires further investigation. Targeting these tissues with high Gorab expression, transgenic mouse lines expressing cre recombinase under Prx1 (Logan et al 2002), Col2a1 (Ovchinnikov et al 2000) or Dmp1 (Lu et al 2007) promoter were employed to inactivate Gorab in different tissues at different developmental stages. Prx1cre is expressed at the limb bud mesenchyme and inactivated Gorab from both chondrocytic and osteoblastic lineage. Col2a1cre is expressed in cartilage and chondrocytes and Dmp1cre is expressed in the late osteoblast and osteocyte. By utilizing these three tissue specific cre lines, the spatial and temporal role of Gorab during bone development was dissected.

Phenotypic analysis of Gorabfl/fl; Prx1cre animals

By crossing the conditional mouse with the Prx1cre mouse, Gorab was inactivated in both the chondrocytic and osteoblastic lineage starting from the limb bud mesenchyme, and also in endothelial cells. The mutant mouse, in contrast to the genetrap mouse model, was viable. Mutant mice of 4 weeks (juvenile) and 12 weeks old (adult) were analyzed for phenotypic abnormality.

A

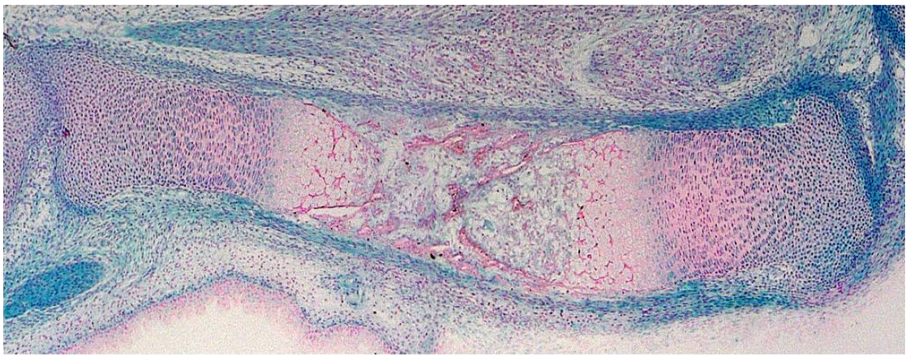

B

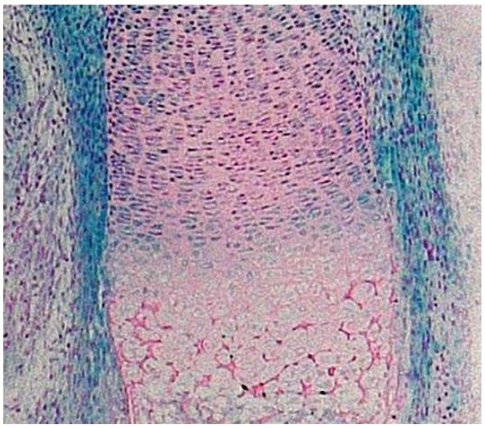

Fig.3.3.1 LacZ staining of Gorab genetrap mouse. Sagittal section of LacZ stained tibia from E16.5 genetrap Gorab mouse embryo. The strongest LacZ staining was found at the articular cartilage, perichondrium, resting chondrocytes, proliferating chondrocytes, prehypertrophic chondrocyte, periosteum and osteoblasts.

Inactivation of Gorab results in defects in bone structure

The X-ray photos of 12 weeks old Gorab$^{fl/fl}$; Prx1cre mutants showed that the mutant animals were smaller comparing to the control animals (Fig. 3.3.2A and B). The long bones of the mutant were undermineralized. Both femur and tibia were shorter than that of the control animals (Fig 3.3.2C). The pelvis was malformed, showing a triangular obturator foramen, short and thin pubis and severe flaring of the ilium and ischium (Fig. 3.3.2D). The vertebra appeared to be shorter, flatter and narrower in size and had smaller processes (Fig.3.3.2D).

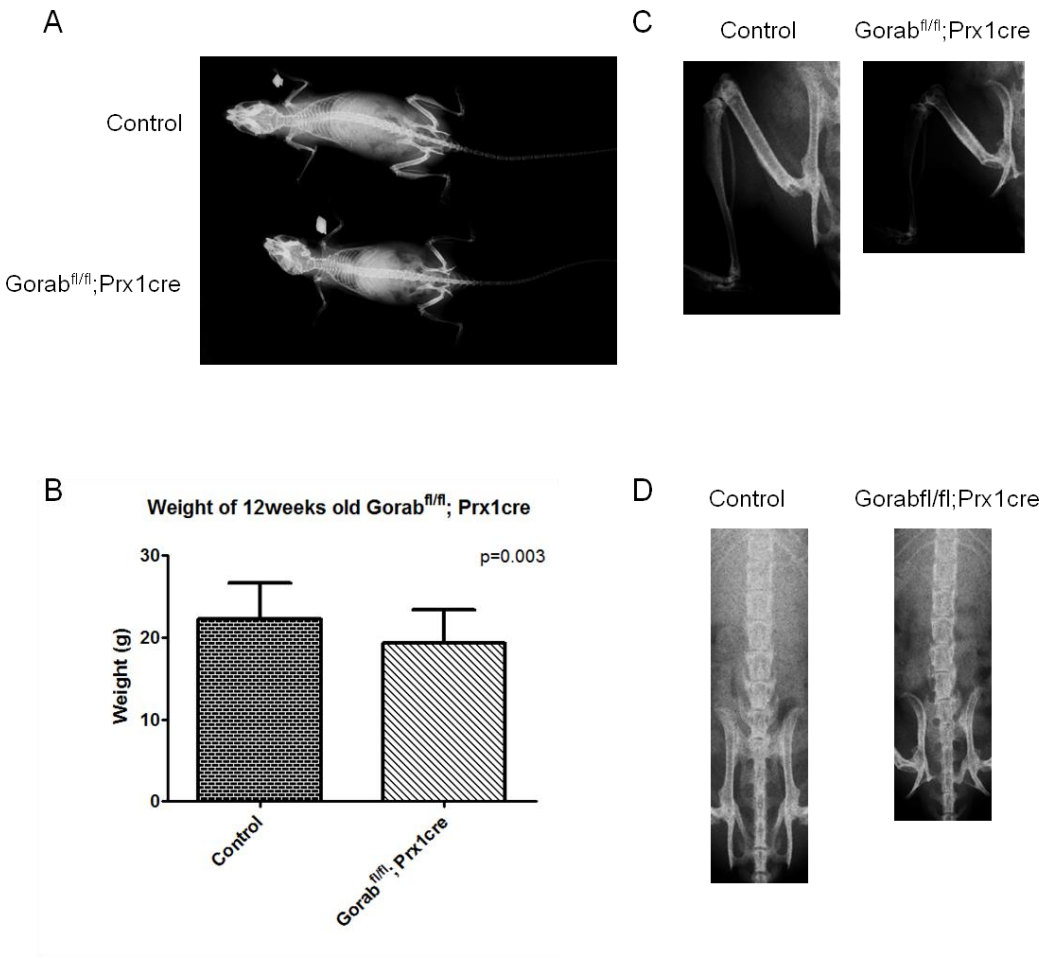

Fig.3.3.2 (A) X-ray radiography of 12weeks old Gorab$^{fl/fl}$;Prx1cre mutant, showing general decrease in size and osteoporosis.. (B) Gorabfl/fl;Prx1cre mutants were smaller in size compared to their littermates. N=5, statistical analysis by two tailed paired t-test. (C) Undermineralization and shortened femur and tibia in the mutant comparing to the control. (D). Decrease in size of the vertebra and malformed pelvis in the mutant.

In order to quantify the bone quality of the mutant mice, microCT analysis was conducted for volumetric analysis of bone structure of the distal femur, proximal tibia and lumbar vertebra of Gorab$^{fl/fl}$; Prx1cre mutants (Table 3.3.1). It was found that at 4weeks the femur of the mutant mice was shorter and narrower than the control animal, as indicated by the decrease in total volume of the cortical bone. The cortical

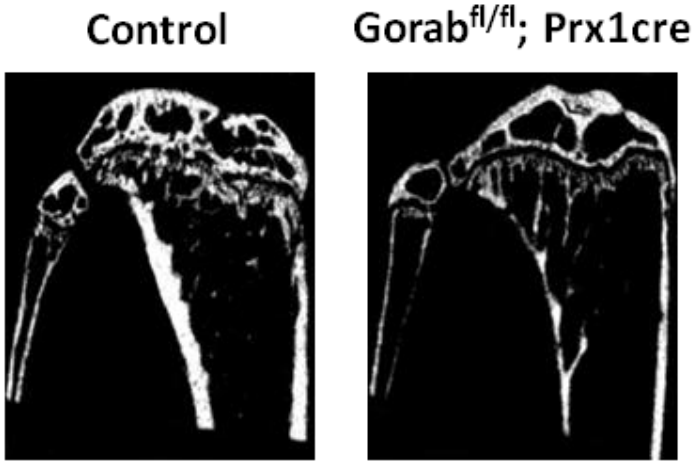

Fig.3.3.3 microCT image showing the proximal tibia of 12weeks old Gorab$^{fl/fl}$;Prx1cre mutant.

bone was also thinner comparing to the control. There was a decrease in the trabecular bone volume, which probably resulted from a decrease in the trabecular number since the trabecular thickness was similar to that of the control. The same phenomenon was found in femora of 12weeks old mutants but not statistically significant. The tibia of the Gorab$^{fl/fl}$; Prx1cre mutants showed no significant difference in trabecular bone volume or trabecular number at 4weeks. However, it showed shortening, narrowing and thinning of the cortical bone as in the case of the femur. At 12weeks, there were not only defects in the cortical bone, but also a decrease in the amount of trabecular bone. The decrease in trabecular bone volume was, as in the case of the femur, due to a decrease in trabecular number but not trabecular thickness. Fig.3.3.3 shows a microCT image of the proximal tibia of a 12 weeks old mutant, illustrating the thinning of the cortical bone and decrease in trabeculae. The fifth and sixth lumbar vertebra of the Gorab$^{fl/fl}$;Prx1cre mutant was similar in the trabecular bone volume at 4weeks. At 12 weeks, there was a trend towards a decrease in the trabecular bone volume, which was not statistically significant.

Table 3.3.1: microCT scanning of the hindlimb and vertebral column of Gorab$^{fl/fl}$; Prx1cre mutant at 4 weeks (N=6) and 12 weeks of age (N=5). mean value ± S.D. * = p<0.05. **=p<0.01. Statistical analysis was done by two-tailed, unpaired t-test.

			4 weeks		12 weeks	
			Control	Gorab$^{fl/fl}$; Prx1cre	Control	Gorab$^{fl/fl}$; Prx1cre
Femur	Trabeculae	BV/TV (%)	4.6 ± 1.9	***1.6 ± 1.6 ****	8.3 ± 2.3	***3.0 ± 2.4 ****
		Tb. N (1/mm)	2.122 ± 0.853	***0.762 ± 0.674 ****	2.375 ± 1.486	***0.998 ± 0.757 ****
		Tb. Th (mm)	0.022 ± 0.003	0.02 ± 0.002	0.033 ± 0.005	0.03 ± 0.001
		Tb. Sp (mm)	0.617 ± 0.533	***2.412 ± 1.993 ****	0.400 ± 0.081	***1.321 ± 0.641 ****
	Cortical bone	TV (mm^3)	0.599 ± 0.094	***0.393 ± 0.134 ****	1.144 ± 0.232	0.760 ± 0.158
		BV/TV (%)	76.8 ± 2.6	***64.9 ± 11.0 ****	86.2 ± 4.8	84.8 ± 4.1
		Length (mm)	12.234 ± 0.516	***10.318 ± 0.931 *****	15.265 ± 0.244	***12.564 ± 1.592 ****
Tibia	Trabeculae	BV/TV (%)	1.7 ± 0.9	1.7 ± 0.9	7.8 ± 1.9	***3.2 ± 1.2 *****
		Tb. N (1/mm)	0.948 ± 0.469	0.728 ± 0.334	2.433 ± 0.326	***1.123 ± 0.429 *****
		Tb. Th (mm)	0.017 ± 0.002	0.022 ± 0.006	0.032 ± 0.005	0.028 ± 0.003
		Tb. Sp (mm)	1.616 ± 1.535	1.827 ± 1.413	0.385 ± 0.057	***0.947 ± 0.289 ****
	Cortical bone	TV (mm^3)	0.693 ± 0.124	***0.378 ± 0.171 ****	0.940 ± 0.093	***0.569 ± 0.203 *****
		BV/TV (%)	70.8 ± 4.9	***58.1 ± 11.5 ****	88.8 ± 1.0	75.0 ± 12.3
		Length (mm)	14.865 ± 0.632	***12.201 ± 1.553 ****	17.284 ± 0.698	***14.844 ± 1.291 *****
Vertebral column	5th Lumbar	BV/TV (%)	3.8 ± 1.6	3.3 ± 1.2	15.3 ± 4	11.7 ± 3.9
	6th Lumbar	BV/TV (%)	3.8 ± 1.4	3.7 ± 1.6	15.8 ± 4.7	12.8 ± 3.9

Histology of Gorabfl/fl; Prx1cre reveals accumulation of lacunae and osteocytes in cortical bone, but no significant defects in growth plate morphology

The femora and tibiae of 4 weeks old Gorab$^{fl/fl}$; Prx1cre mutant were embedded in MMA and sectioned at 5um thickness for von Kossa and toluidine blue staining (Fig.3.3.4A and Fig.3.3.5A). The cortical bone of the femur near the distal metaphysis and that near the proximal metaphysis of the tibia was thinner comparing to the control. This was consistent with the microCT measurement. However the cortical bone at the proximal femur and distal tibia appears to be similar in thickness as the control. This could be due to difference in mechanical loading at different ends of the long bones and required further investigation. The growth plate of the mutant appeared normal (Fig.3.3.4B and Fig.3.3.5B). The femur showed no obvious defect at both lateral and medial cortical bone (Fig. 3.3.4C). The anterior tibia of the mutant also showed no significant difference comparing to the control. However the posterior tibia of the mutant showed accumulation of non-mineralized lacunae (from below the proximal metaphysis to the mid-bone shaft in tibia. Fig.3.3.5C). These lacunae could be blood vessels or osteocytes. Massa-Goldner staining of the tibiae revealed that these lacunae were osteocytes (Fig.3.3.5D). There were more osteocytes in a given area in the mutant comparing to the control. The same accumulation of osteocytes was also found in anterior tibia and in the femur, even though no accumulation of unmineralized lacunae was found (Fig.3.3.5D and Fig. 3.3.4D).

MMA sections from 12 weeks old Gorab$^{fl/fl}$; Prx1cre mutant revealed a similar phenotype as the 4 weeks old mutants. There were thin cortices in both the femur and tibia of the mutant (Fig.3.3.6A and Fig.3.3.7A). The thinning of cortical bone was observed over the entire long bone, but more prominent near the distal metaphysis of

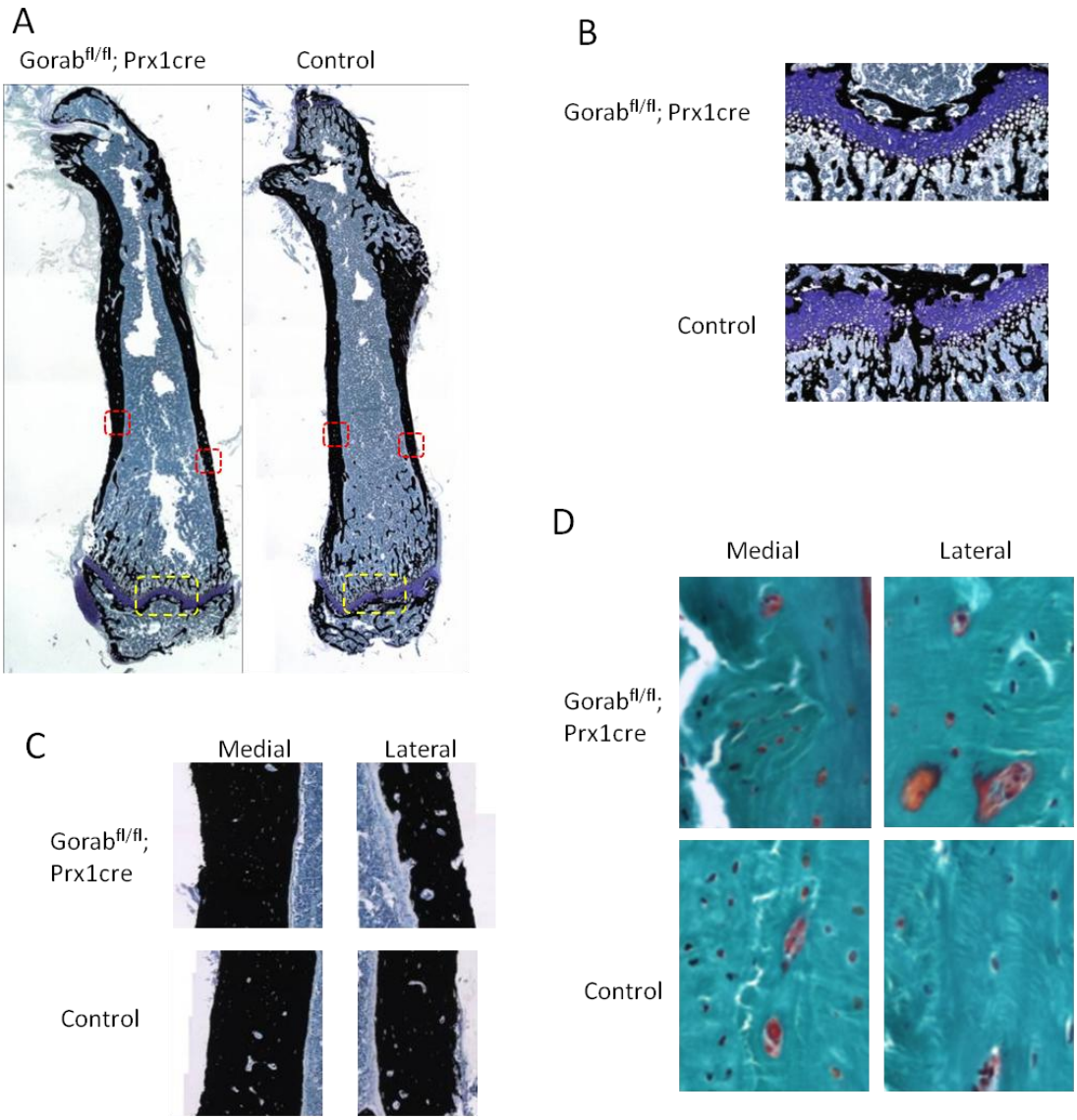

Fig.3.3.4 Histology of the femur of 4weeks old Gorab$^{fl/fl}$;Prx1cre mutant. (A) von Kossa and toluidine blue staining of femur. (B). Higher magnification of the growth plate of the mutant, showing no significant defect comparing to the control. (C). Higher magnification of the cortical bone. (D). Masson-Goldner staining of the cortical bone, showing accumulation of osteocytes.

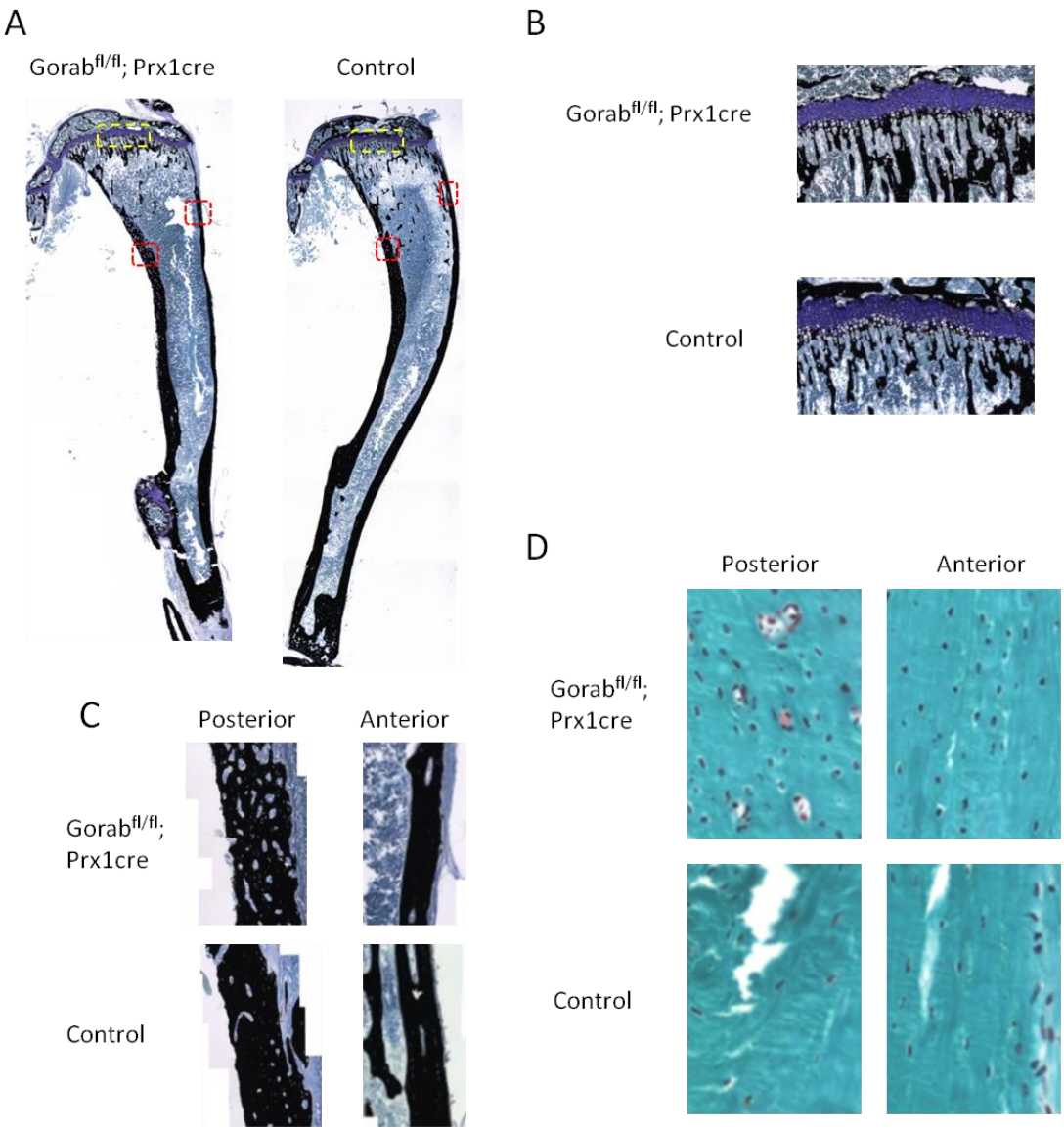

Fig.3.3.5 Histology of the tibia of 4weeks old Gorab$^{fl/fl}$;Prx1cre mutant. (A) von Kossa and toluidine blue staining of tibia. (B). Higher magnification of the growth plate of the mutant, showing no significant defect comparing to the control. (C). Accumulation of unmineralized lacunae in the posterior cortical bone. (D). Masson-Goldner staining of the cortical bone, showing accumulation of osteocytes.

the femur and near the proximal metaphysis of the tibia. There was severe loss of trabecular bone but morphologically normal growth plate (Fig.3.3.6B and Fig.3.3.7B). Accumulation of non-mineralized lacunae was found in the medial femur and posterior tibia (Fig.3.3.6C and Fig.3.3.7C). There was also an accumulation of large round shaped osteocytes in the mutant comparing to the control (Fig. 3.3.6D and Fig.3.3.7D). Back-scattered SEM showed that even the anterior tibia showed no unmineralized lacunae as in the posterior tibia, the osteocyte lacunae were actually larger and rounder in shape comparing to the control (Fig.3.3.8).

Loss of Gorab results in decreased mineral apposition rate and altered osteoblast markers expression

In order to investigate the cause of the thin cortical bone in the Gorab$^{fl/fl}$; Prx1cre mutant, 4 weeks old mutant was double labeled with calcein (3 days between the two labeling) and analyzed for the mineral apposition rate. Since the mineral apposition rate is different at different part of the tibia, the endosteal surface near the mid-bone shaft was chosen as the region for comparison (Fig.3.3.9A). It was found that the mineral apposition rate of the Gorab$^{fl/fl}$; Prx1cre was significantly lower than the control animals, indicating that there was defect in bone formation (Fig.3.3.9B and C). Histological analysis also revealed increased osteoid thickness (Fig.3.3.10A), osteoid surface to bone surface ratio (Fig.3.3.10B) and ratio of osteoid volume (Fig.3.3.10C), suggesting defect in osteoid mineralization.

The decreased mineral apposition rate, accumulation of unmineralized lacunae in the cortical bone and large round shaped osteocytes suggested defects in osteoblast function and differentiation. In order to verify this hypothesis, RNA was extracted

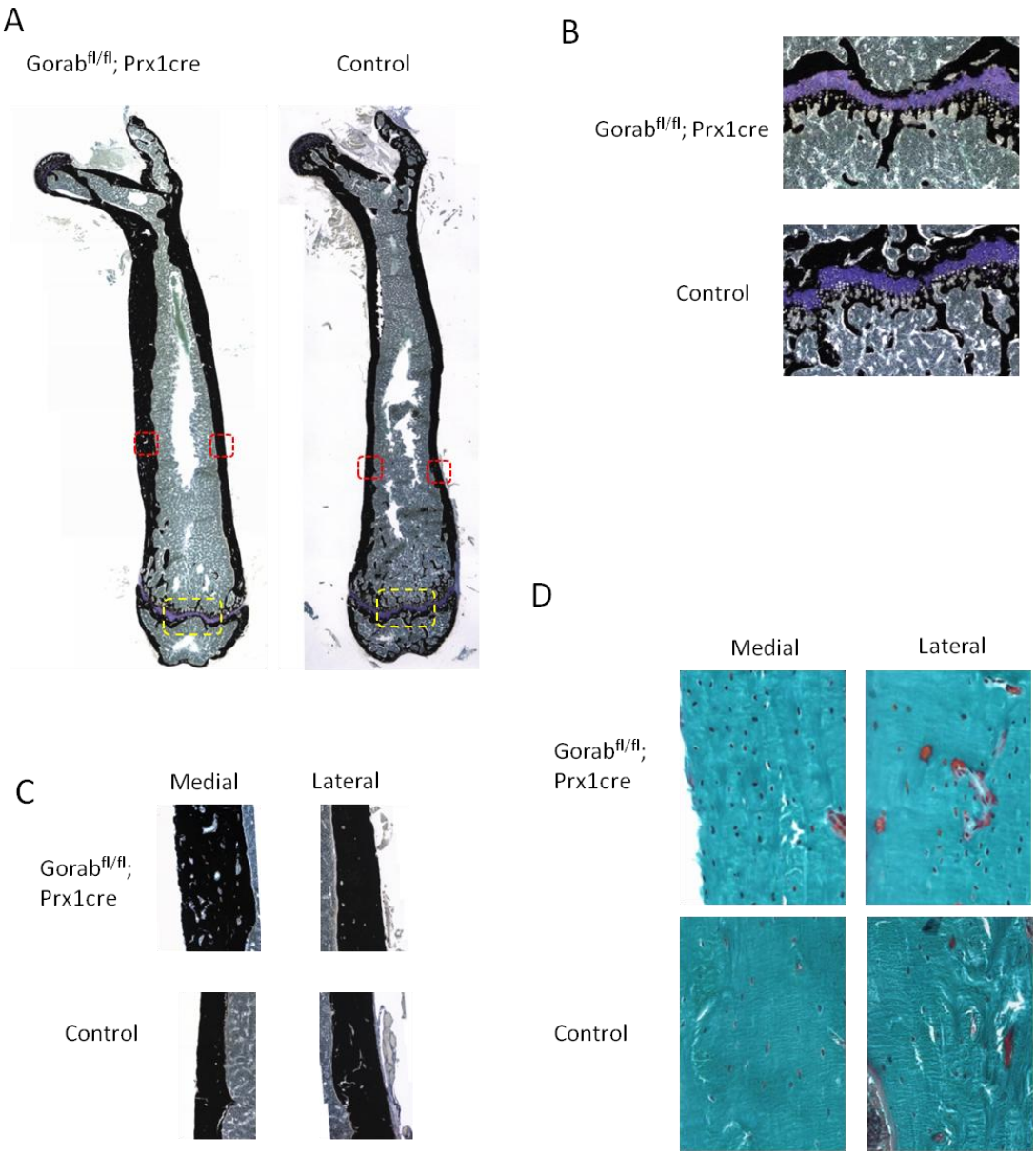

Fig.3.3.6 Histology of the femur of 12weeks old Gorab$^{fl/fl}$;Prx1cre mutant. (A) von kossa and toluidine blue staining of femur. (B). No significant difference in growth plate morphology comparing to control (C). Accumulation of unmineralized lacunae in the medial cortical bone. (D). Masson-Goldner staining of the cortical bone, showing accumulation of round shaped osteocytes.

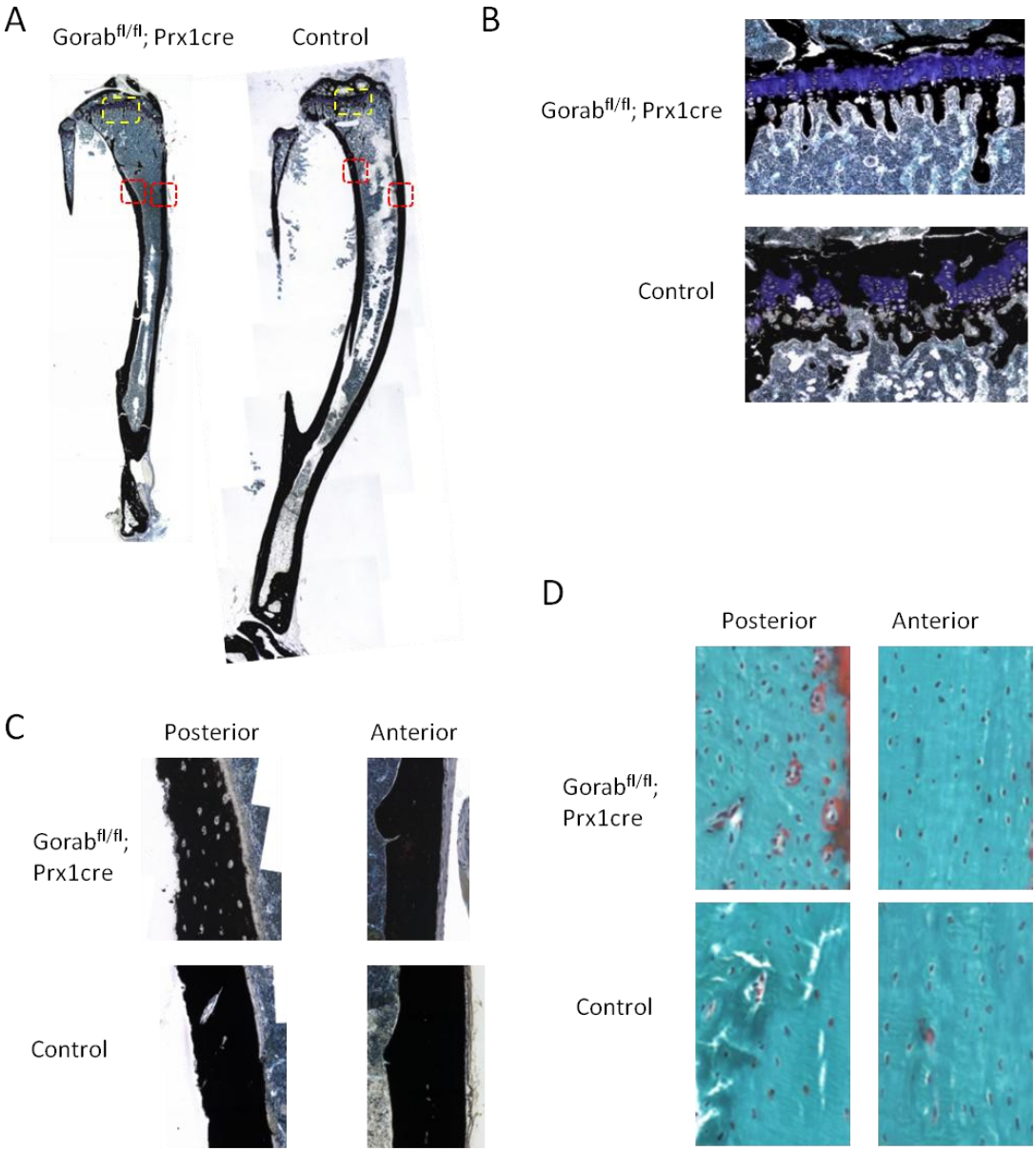

Fig.3.3.7 Histology of the tibia of 12weeks old Gorab$^{fl/fl}$;Prx1cre mutant. (A) von kossa and toluidine blue staining of tibia. (B). No significant difference in growth plate morphology comparing to control (C). Accumulation of unmineralized lacunae in the posterior cortical bone. (D). Masson-Goldner staining of the cortical bone, showing accumulation of round shaped osteocytes.

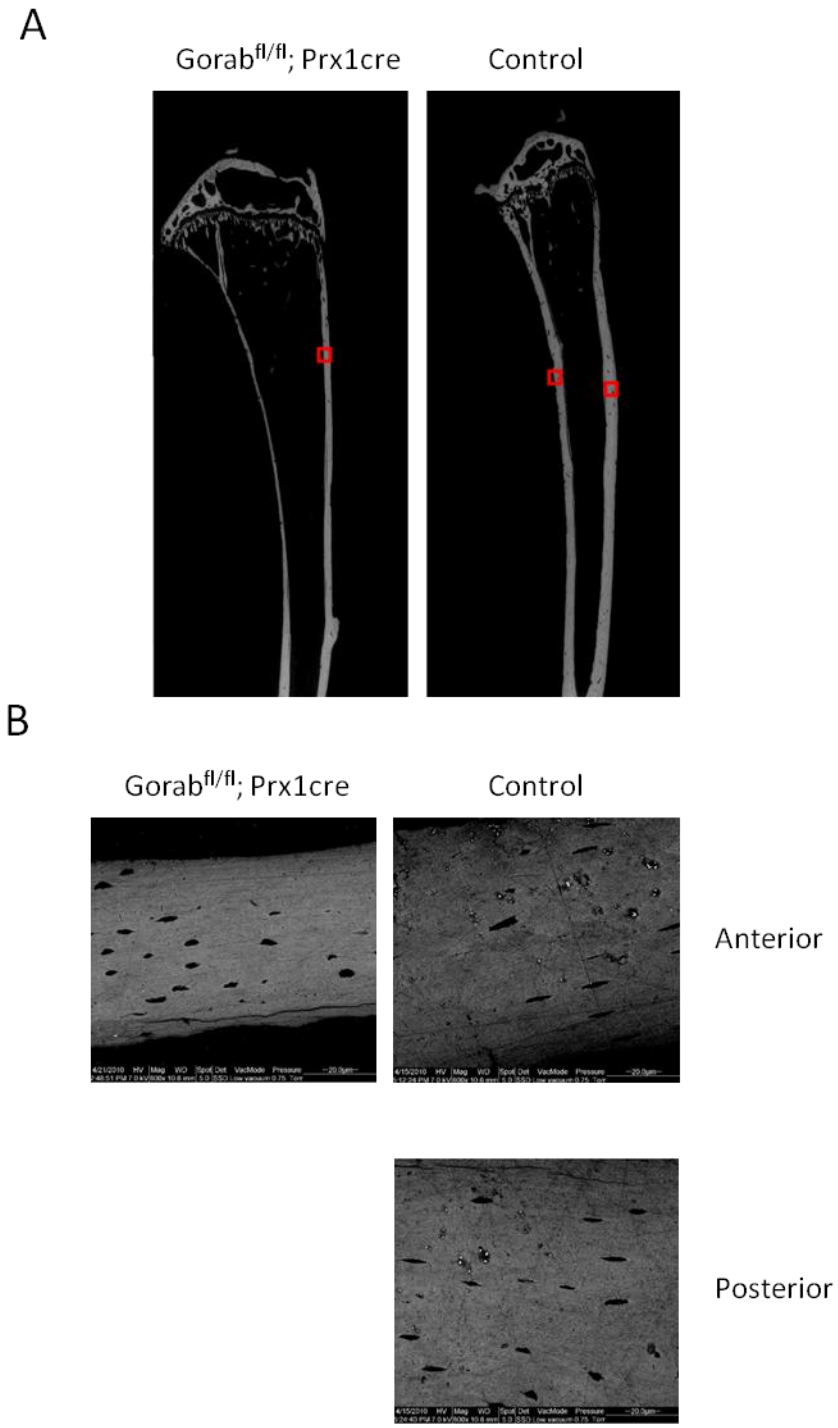

Fig.3.3.8 Back-scattered Electron Microscopy of the tibia of 12weeks old Gorab$^{fl/fl}$;Prx1cre mutant. (A). Overview of the tibia showing the region taken for analysis. (B). Higher magnification of the image showing the increase in size and round shape of the osteocyte lacunae in the mutant comparing to the controls. (Courtesy of Claudia Lange)

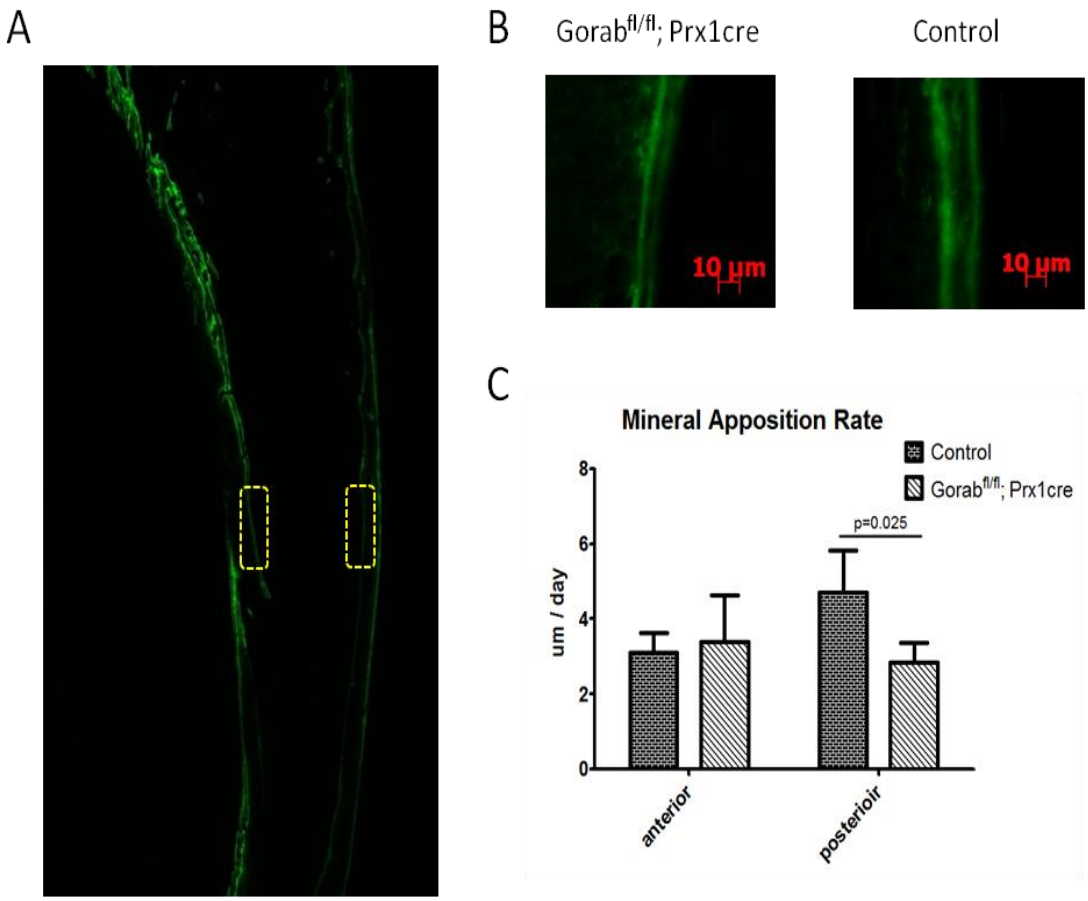

Fig.3.3.9 Decrease in mineral apposition rate in Gorab$^{fl/fl}$; Prx1cre mutant. (A). The endosteal surface near the mid-bone shaft was chosen as the region of interest. (B). The mice were injected two times with calcein, 5 days and 2 days before sacrifice. The shortened distance between the double calcein labels indicated a decrease in mineral apposition rate in the mutant. (C). Significant decrease in mineral apposition rate at the posterior endosteal surface of the Gorab$^{fl/fl}$; Prx1cre mutant. N=4, analyzed by two tailed, unpaired t-test.

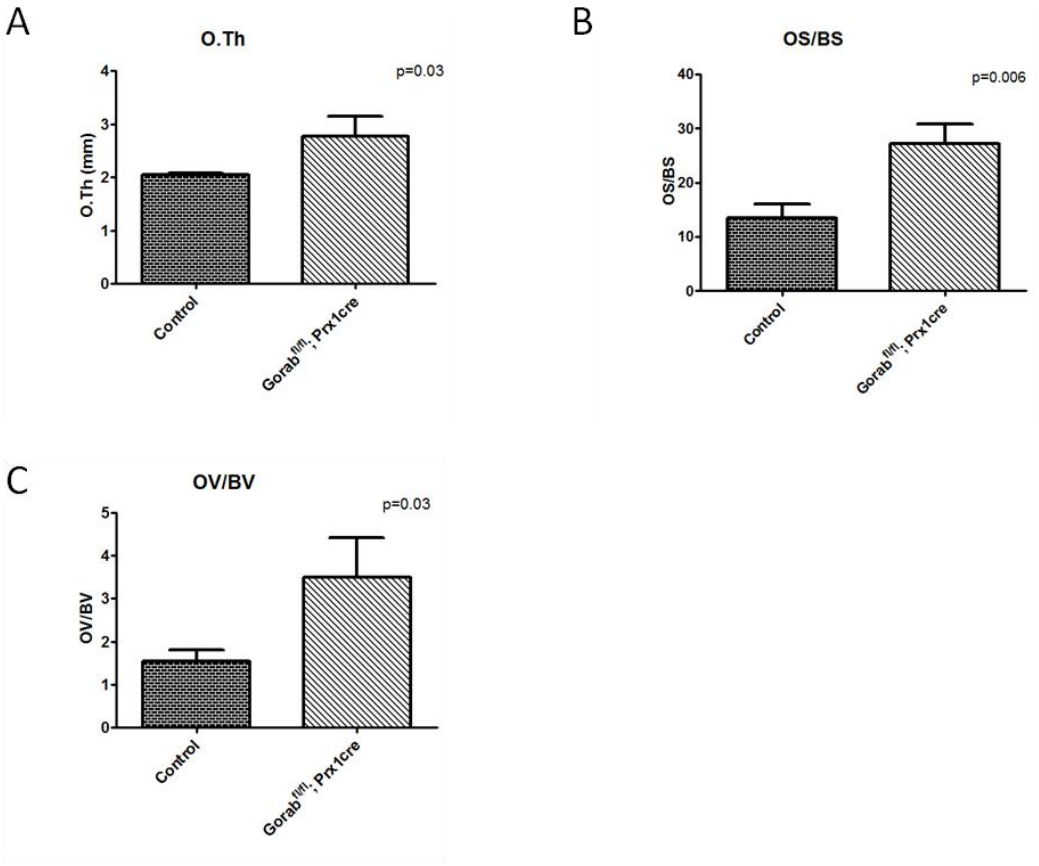

Fig.3.3.10 Histological analysis of the trabecular bone in 4 weeks old Gorab$^{fl/fl}$; Prx1cre mutants. Significant increase in osteoid thickness, O.Th (A), relative osteoid surface area, OS/BS (B) and relative Osteoid volume, OV/BV (C) was found in the mutants. N=3, statistical analysis by two tailed, unpaired t-test.

---

from the cortical bone of the diaphysis of 4 weeks old Gorab$^{fl/fl}$; Prx1cre and qPCR was performed to compare the expression pattern of different osteoblast markers (Fig.3.3.11A). Firstly, it showed that Gorab mRNA expression levels in the cortical bone were 20-40% of wildtype levels. This could be due to incomplete cre-mediated recombination or mRNA from blood vessels and nerves in the cortical bone, where the cre-recombinase was not expressed. Secondly, the expression level of osteoblast differentiation markers was investigated. There was an increase in the expression of Osterix (early osteoblast marker), Osteopontin and Dmp1 (late osteoblast marker), but

A

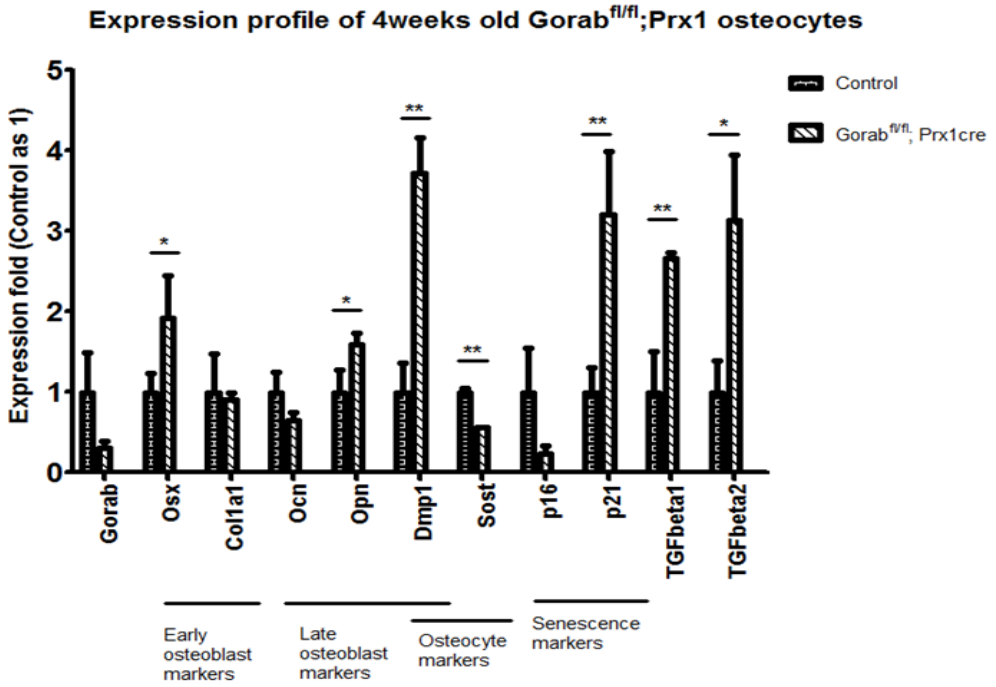

B

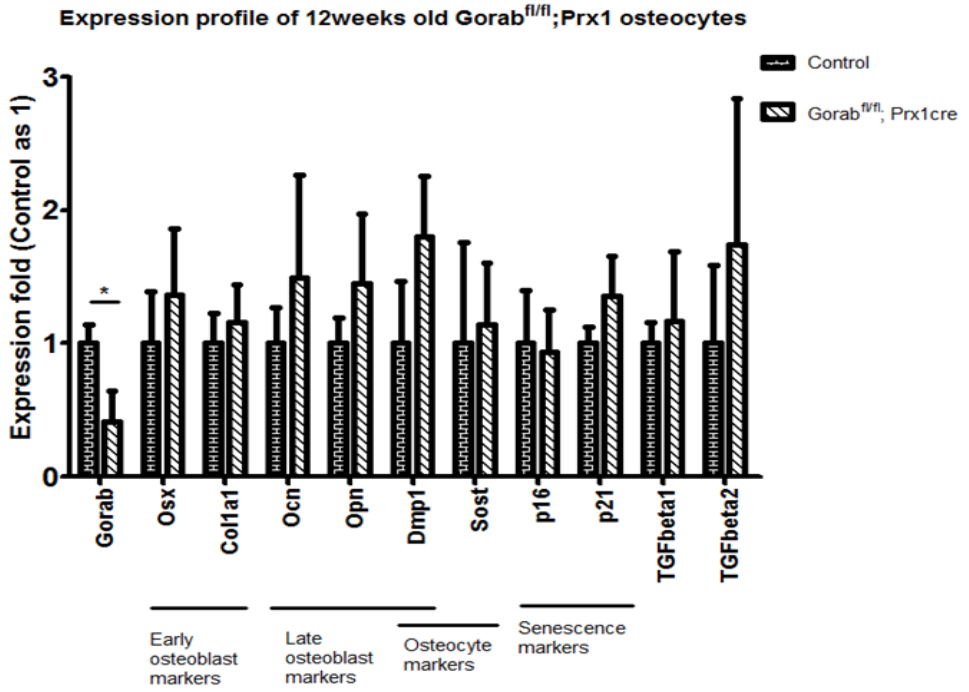

Fig.3.3.11 Expression profiling of osteocyte from humerus of 4weeks old (A) and 12weeks old (B) Gorab$^{fl/fl}$; Prx1cre mutant. N=3, *=p<0.05, **=p<0.01. Statistic analysis done by two tailed, unpaired t-test.

a decrease in the expression of Sclerostin (osteocyte marker). This not only showed altered gene expression pattern in the osteocytes, but also suggested that there were defects in the maturation of osteoblasts into osteocytes. In other words, the large round shaped osteocytes found in the cortical bone of 4 weeks old Gorab$^{fl/fl}$; Prx1cre had an expression profile more similar to that of late osteoblast than osteocyte.

Thirdly, there was an increase in the expression of the cyclin-dependent kinase inhibitor p21 but not p16. This suggested that the osteocytes underwent cell cycle arrest as in the case of the human patient fibroblast, though the contributing factor was p21 instead of p16 as in the case of fibroblast. Lastly, similar to the human fibroblast, there was an increase in the expression of TGFβ1, suggesting there could be an activation of TGFβ signaling in the osteocytes as in the fibroblast. There was also an increase in the expression of TGFβ2 expression in the mutants. Interestingly, all these changes in gene expression disappeared in the 12weeks old mutants and the gene expression level of all the tested markers were comparable between the mutants and control animals (Fig.3.3.11B).

To summarize, there were less trabeculae and thinner cortical bone in the long bones of Gorab$^{fl/fl}$; Prx1cre mutants at both 4weeks and 12weeks of age. The thinning of cortical bone was possibly due to a decrease in mineral apposition rate. The long bones were slightly shortened with accumulation of unmineralized lacunae in the cortical bone. There was accumulation of large round shaped osteocytes which showed a gene expression pattern similar to late osteoblast instead of osteocytes. The osteocytes also had an elevated expression of p21, TGFβ1 and TGFβ2, suggesting cellular senescence and activation of TGFβ signaling pathway in the osteocytes.

Phenotypic analysis of Gorab$^{fl/fl}$; Col2a1cre mutants

Conditional mouse models allow the inactivation of target genes in specific tissues at specific developmental stage, and thus the detailed dissection of how different tissues contribute to the phenotype. The Prx1cre inactivated Gorab in both the chondrocytic and osteoblastic lineage at early stage of development and resulted in severe decrease in trabeculae, shortening and thinning of cortical bone in the long bones. In the next part of the experiment, the role of individual tissue was investigated. The Gorab conditional mouse was crossed with mouse expressing cre recombinase under the Col2a1 promoter in order to inactivate Gorab specifically in cartilage and chondrocytes. In this way, the role of Gorab in chondrocyte and the role of chondrocyte in the bone phenotype of GO could be studied.

X-ray radiography showed that the 12 weeks old Gorab$^{fl/fl}$; Col2a1cre mutant was smaller in size and suffered from generalized osteoporosis (Fig.3.3.12). microCT analysis of 12 weeks old Gorab$^{fl/fl}$; Col2a1cre mutants revealed similar but yet different phenotype comparing to the Gorab$^{fl/fl}$; Prx1cre mutants (Table 3.3.2). Firstly, the Gorab$^{fl/fl}$; Col2a1cre showed mild but significant decrease in the length of the femur comparing to the controls. There was also a trend, though statistically insignificant, of decrease in the total volume of the femur but no significant changes in relative cortical bone volume. In the case of the tibia, there was a trend of decrease in length and total volume of the cortical bone but no changes in relative cortical bone volume, which was similar to the femur . The 12 weeks old Gorab$^{fl/fl}$; Col2a1cre mutants showed significant loss of trabeculae in the femur and tibia, which was similar to the findings in the Gorab$^{fl/fl}$; Prx1cre mutants. The decrease in trabeculae resulted from a loss of trabecular number instead of trabecular thickness. The

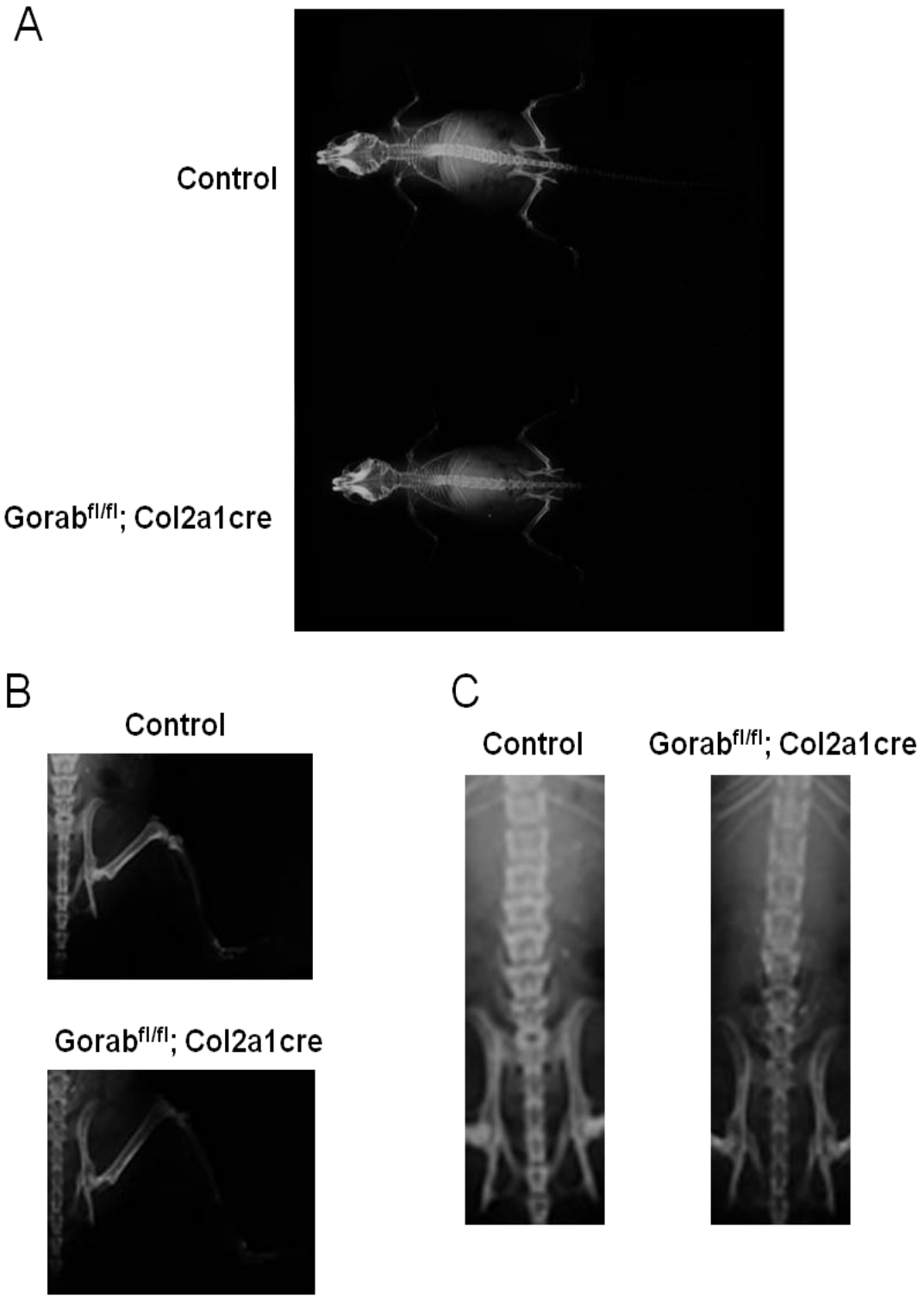

Fig3.3.12 X-ray radiography of 12weeks old Gorab$^{fl/fl}$; Col2a1cre mutant. (A). Generalized osteoporosis in the mutant mouse comparing to the control. (B). Undermineralization of the femur and tibia in the mutant. (C). Undermineralization in the vertebral column. The vertebral bodies were smaller with short processes.

Table 3.3.2: microCT scanning of the hindlimb and vertebral column of Gorab$^{fl/fl}$;Col2a1cre mutant at weeks of age (N=5). mean value ± S.D.* = p<0.05. **=p<0.01. Statistical analysis was done by two-tailed, unpaired t-test.

			12 weeks	
			Control	Gorab$^{fl/fl}$; Col2a1cre
Femur	Trabeculae	BV/TV (%)	8.1 ± 3.3	***2.9 ± 1.3 ****
		Tb. N (1/mm)	2.431 ± 0.710	***0.875 ± 0.353 *****
		Tb. Th (mm)	0.032 ± 0.005	0.033 ± 0.004
		Tb. Sp (mm)	0.423 ± 0.197	***1.247 ± 0.455 *****
	Cortical bone	TV (mm^3)	1.232 ± 0.215	***0.879 ± 0.200 ****
		BV/TV (%)	0.892 ± 0.008	***0.839 ± 0.025 *****
		Length (mm)	14.510 ± 0.625	13.660 ± 0.624
Tibia	Trabeculae	BV/TV (%)	7.2 ± 1.3	***4.9 ± 1.9 *****
		Tb. N (1/mm)	2.338 ± 0.335	***1.518 ± 0.509 ****
		Tb. Th (mm)	0.031 ± 0.001	0.032 ± 0.002
		Tb. Sp (mm)	0.405 ± 0.068	***0.692 ± 0.252 ****
	Cortical bone	TV (mm^3)	1.191 ± 0.256	1.088 ± 0.133
		BV/TV (%)	88.9 ± 1.4	87.2 ± 2.1
		Length (mm)	16.982 ± 0.719	***16.007 ± 0.399 ****
Vertebral column	5th Lumbar	BV/TV (%)	16.8 ± 6.5	***8.0 ± 2.6 ****
	6th Lumbar	BV/TV (%)	17.6 ± 7.2	***7.6 ± 3.3 ****

Gorab$^{fl/fl}$; Col2a1cre mutants also showed a decrease in trabeculae in the sixth and fifth vertebra, which was not found in the Gorab$^{fl/fl}$; Prx1cre mutants.

Histological analysis of the tibia of 12 weeks old Gorab$^{fl/fl}$; Col2a1cre mutants revealed no accumulation of unmineralized lacunae in the cortical bone (Fig.3.3.13A), nor changes in osteocyte number and morphology (Fig.3.3.13C and D). There was also no defect in the growth plate at this age (Fig.3.3.13B). To summarize, Gorab$^{fl/fl}$;Col2a1cre mutants were found to have fewer trabecular bone in the long bones and vertebrae than the control at 12 weeks of age. The growth plate was morphologically normal at this age. The long bones tended to be shorter and narrower.

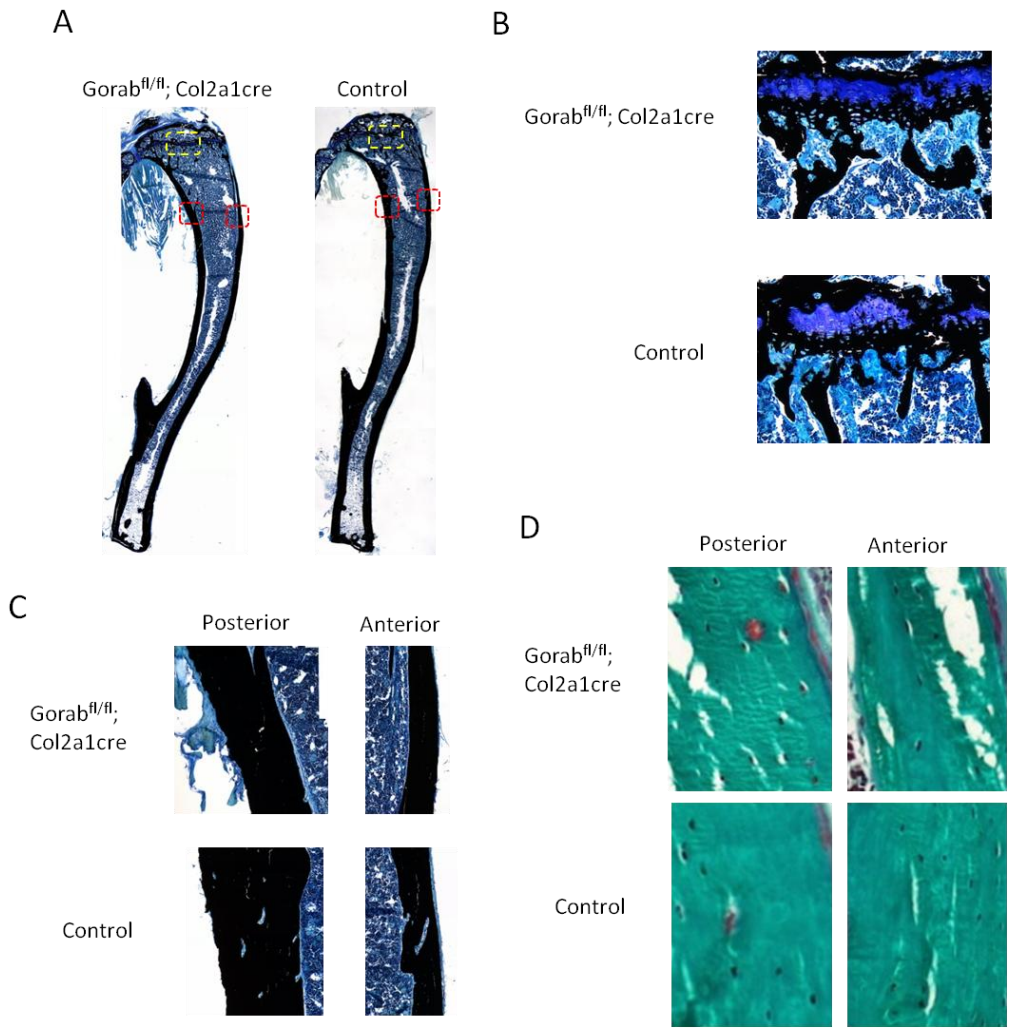

Fig.3.3.13 Histology of tibia of 12 weeks old Gorab$^{fl/fl}$; Col2a1cre mutants. (A) von Kossa-toluidine blue staining of the tibia. (B) Higher magnification of the growth plate showed no abnormality. (C). No accumulation of unmineralized lacunae in the cortical bone. (D). Masson Goldner staining revealed no increase in density or change in morphology of osteocytes.

Other than that, there was no defect found in the cortical bone of the long bones.

Phenotypic analysis of Gorab$^{fl/fl}$; Dmp1cre mutants

In order to study the role of Gorab in osteoblast function and differentiation, the conditional Gorab mouse was crossed with transgenic mice that expressed the cre

Fig.3.3.14 Expression pattern of Dmp1cre. LacZ staining of the femur of E18.5 DMP1cre::Rosa26LacZ embryo showed that the expression of the cre recombinase was low at the osteoblast along cortical bone region. However the cre expression was very strong in the osteoblast in the trabecular bone region and just below the growth plate. Section was stained by von-Kossa silver stain for bone and counterstained with haematoxylin.

---

recombinase under the Dmp1 promoter. Under the Dmp1 promoter, the cre recombinase was expressed in the late osteoblast and osteocytes. Interestingly, the number of LacZ positive cells was higher in the trabecular bone than in the cortical bone, suggesting a different in the expression of the cre recombinase in osteoblast in the trabeculae and the cortical bone (Fig.3.3.14)

microCT analysis revealed no significant defect in both the trabecular bone and cortical bone in 4 weeks old mutant at both femur and tibia. However, there was a significant decrease in trabecular bone volume in the fifth and sixth lumbar vertebra, The decrease in trabecular bone volume in lumbar vertebra was also observed in 12 weeks old mutants. In addition, there was also decrease in trabecular bone volume observed in the long bones of the mutants but no significant changes were found in the cortical bone comparing to the control animals. No change in the length of the long bones was observed in the mutants at both time points (Table 3.3.3). Histology of the tibia from both 4 weeks and 12 weeks old mutant showed no accumulation of unmineralized lacunae in the cortical bone; nor changes in the morphology of the osteocytes (Fig.3.3.15 and Fig.3.3.16). qPCR study showed that Gorab expression in the mutant cortical bone was not decreased at 4 weeks of age. By 12 weeks there was a significant decrease in Gorab expression but there were no significant changes in the expression of osteoblast markers or senescence marker at both time points (Fig.3.3.17).

Table 3.3.3: microCT scanning of hindlimb and vertebral column of Gorab$^{fl/fl}$; Dmp1cre mutant at 4 weeks (N=6) and 12 weeks of age (N=4). mean value ± S.D. * = p<0.05. **=p<0.01. Statistical analysis was done by two-tailed, unpaired t-test.

			4 weeks		12 weeks	
			Control	Gorab$^{fl/fl}$; Dmp1cre	Control	Gorab$^{fl/fl}$; Dmp1cre
Femur	Trabeculae	BV/TV (%)	4.3 ± 2.8	3.9 ± 2.0	11.4 ± 1.1	***4.8 ± 1.8 *****
		Tb. N (1/mm)	1.931 ± 0.983	1.736 ± 0.762	3.601 ± 0.335	***1.543 ± 0.490 *****
		Tb. Th (mm)	0.021 ± 0.004	0.022 ± 0.002	0.032 ± 0.002	0.030 ± 0.007
		Tb. Sp (mm)	0.635 ± 0.334	0.650 ± 0.278	0.248 ± 0.024	***0.667 ± 0.215 *****
	Cortical bone	TV (mm^3)	0.654 ± 0.078	0.663 ± 0.029	1.041 ± 0.104	0.912 ± 0.109
		BV/TV (%)	78.5 ± 2.7	78.8 ± 1.9	87.7 ± 1.4	85.9 ± 2.5
		Length (mm)	12.982 ± 0.512	12.956 ± 0.153	15.376 ± 0.303	15.428 ± 0.294
Tibia	Trabeculae	BV/TV (%)	1.5 ± 1.0	1.2 ± 0.4	10.9 ± 0.8	***5.3 ± 2.1 *****
		Tb. N (1/mm)	0.842 ± 0.513	0.740 ± 0.268	3.469 ± 0.334	***1.633 ± 0.350 *****
		Tb. Th (mm)	0.017 ± 0.002	0.017 ± 0.001	0.031 ± 0.001	0.032 ± 0.006
		Tb. Sp (mm)	1.626 ± 1.136	1.562 ± 0.802	0.259 ± 0.026	***0.602 ± 0.143 *****
	Cortical bone	TV (mm^3)	0.771 ± 0.079	0.763 ± 0.053	1.077 ± 0.083	***0.927 ± 0.075 ****
		BV/TV (%)	72.0 ± 5.5	71.7 ± 4.2	86.7 ± 1.7	86.1 ± 2.2
		Length (mm)	15.340 ± 0.425	15.515 ± 0.349	17.690 ± 0.347	17.584 ± 0.519
Vertebral column	5th Lumbar	BV/TV (%)	4.5 ± 1.7	***1.8 ± 1.1 *****	15.6 ± 1.2	***7.1 ± 1.3****
	6th Lumbar	BV/TV (%)	5.3 ± 2.1	***2.3 ± 1.3 ****	16.0 ± 0.9	***8.0 ± 1.5****

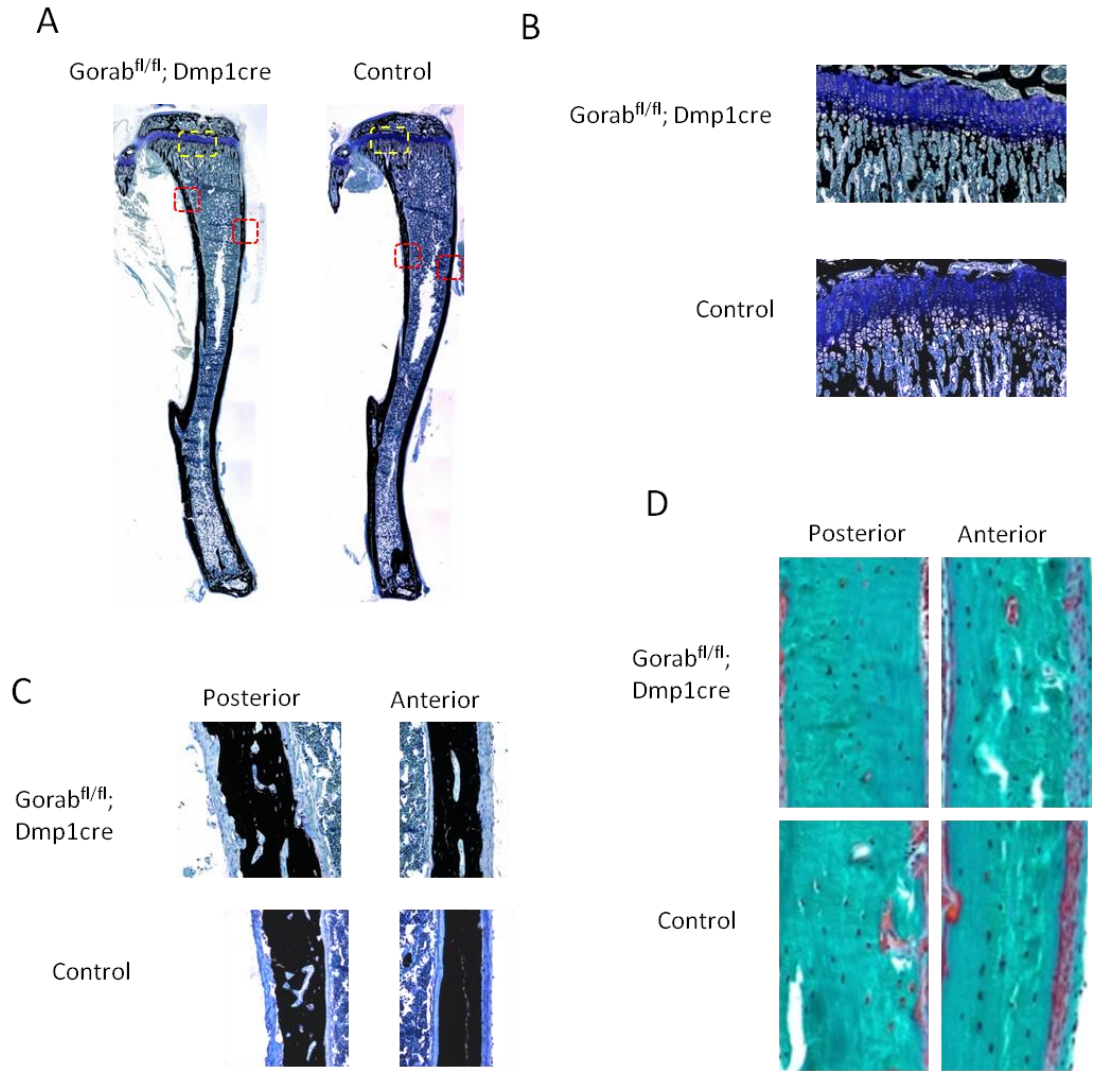

Fig.3.3.15 Histology of tibia of 4weeks old Gorab$^{fl/fl}$; Dmp1cre mutants. (A) von Kossa-toluidine blue staining of the tibia. (B) Higher magnification of the growth plate showed no abnormality. (C). No accumulation of unmineralized lacunae in the cortical bone. (D). Masson Goldner staining revealed no increase in density or change in morphology of osteocytes.

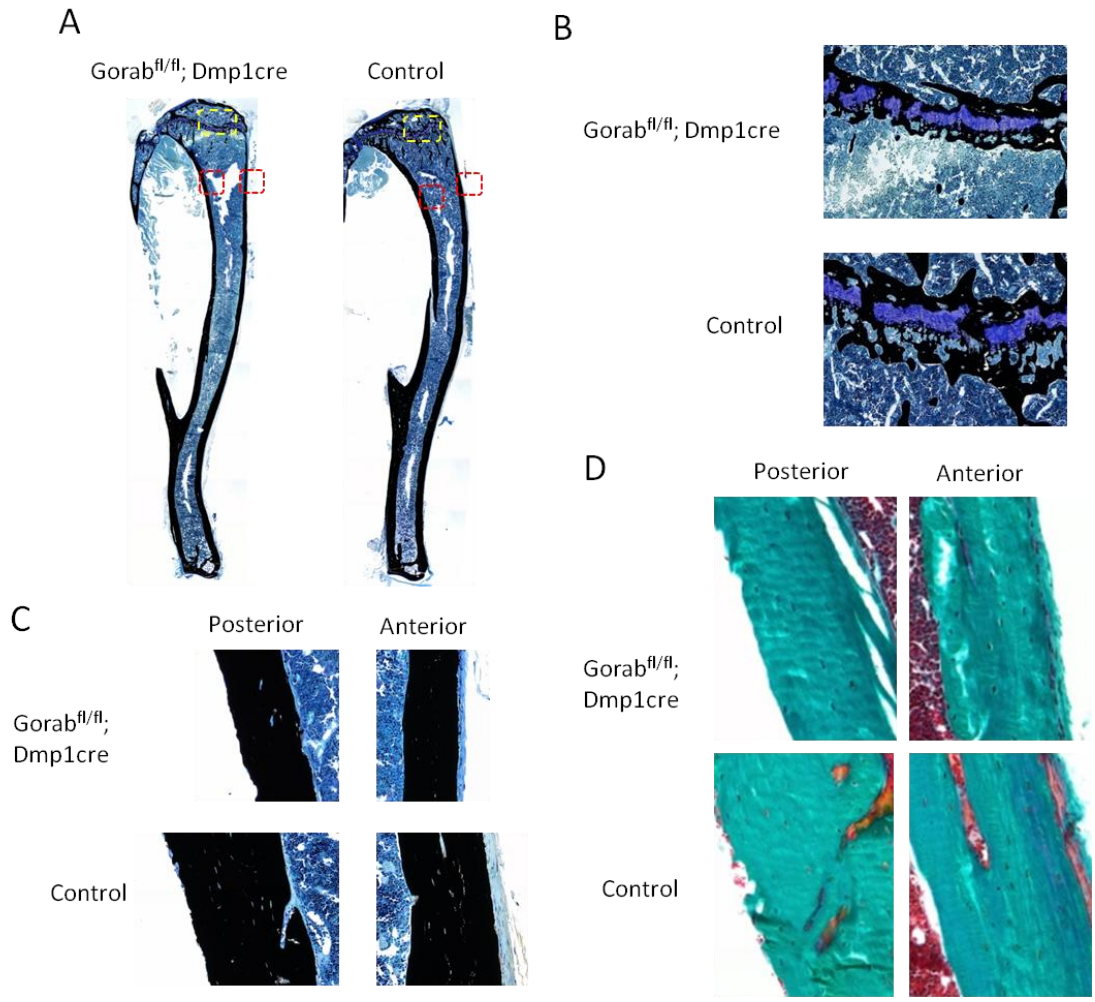

Fig.3.3.16 Histology of tibia of 12weeks old Gorab$^{fl/fl}$; Dmp1cre mutants. (A) von Kossa-toluidine blue staining of the tibia showing significant decrease in trabeculae. (B) Higher magnification of the growth plate showed no abnormality. (C). No accumulation of unmineralized lacunae in the cortical bone. (D). Masson Goldner staining revealed no increase in density or change in morphology of osteocytes.

A

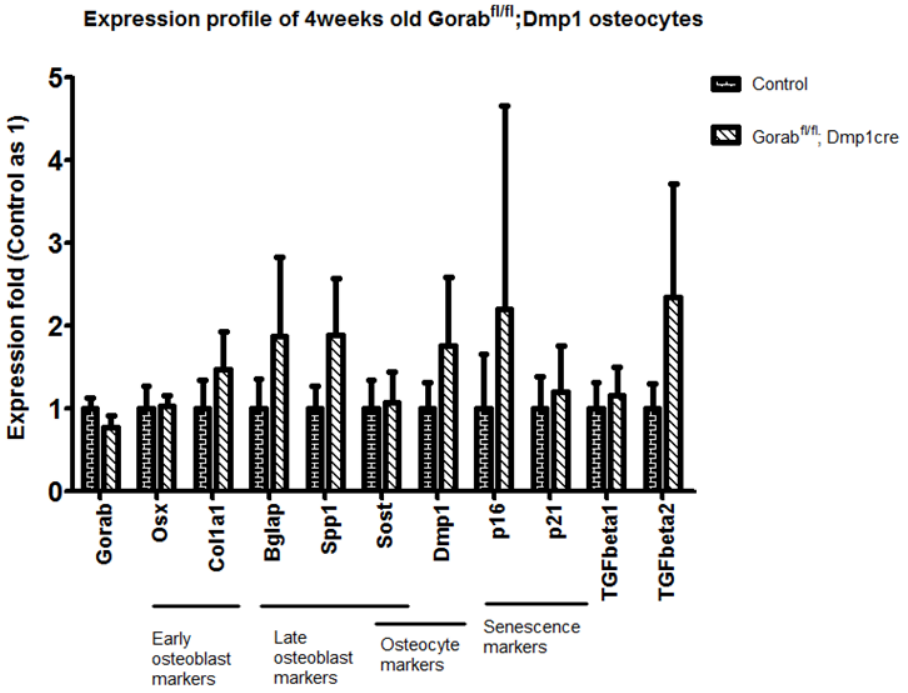

B

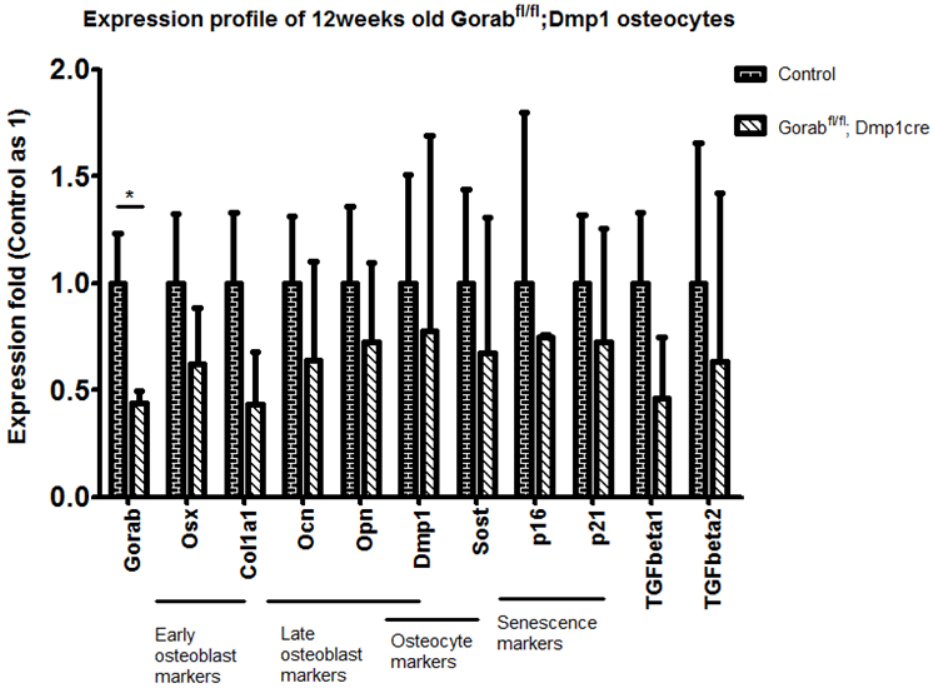

Fig.3.3.17. Expression profiling of Gorab$^{fl/fl}$;Dmp1cre mutants. (A) At 4weeks of age, there was no significant decrease in Gorab expression or significant changes in markers tested. (B). At 12weeks of age, there was significant decrease in Gorab expression but not in other markers.

Chapter 4 Discussion

4.1 The role of Gorab in bone development

The role of the different cre lines in endochondral ossification

One major aspect of Gerodermia Osteodysplastica was that the patients suffer from osteoporosis and high fracture risk beginning at birth. This suggested that the osteoporosis phenotype is a developmental defect. In order to investigate the role of Gorab in bone development, a conditional Gorab mouse model was generated to study the effect of Gorab inactivation in different bone tissues during development.

Bone formation starts with condensation of mesenchymal cells. Then the mesenchymal cells both differentiate directly into osteoblast and lay down matrix for bone formation (intramembranous ossification); or the mesenchymal cells differentiate into chondrocyte to produce a cartilage anlage that is later replaced by bone matrix (endochondral ossification). Apart from a few exceptions, e.g. the flat bones of the skull that are formed by intramembranous ossification, the majority of bones are formed by endochondral ossification. This study focused on investigating the effect of Gorab inactivation in the long bones and the vertebral column, which are both formed by endochondral ossification.

Kronenberg 2003 reviewed the process and regulation of endochondral ossification. Fig.4.1 summarizes the major events taking place in endochondral ossification. Firstly the mesenchymal cells condense and differentiate into chondrocytes, while the outer layer of mesenchymal cells develop into the perichondrium. Then the chondrocytes in the centre increase in size and differentiate

into hypertrophic chondrocytes. The hypertrophic chondroctyes have multiple roles in endochondral ossification. Firstly, they lay down and mineralize their surrounding cartilage matrix. Secondly, they induce the adjacent cells in the perichondrium to differentiate into osteoblasts which later form the bone collar. Thirdly, the hypertrophic chondrocytes secrete vascular endothelial growth factors (VEGF) and other factors to attract blood vessel invasion, which bring along chondroclasts, osteoblasts and osteoblast precursors. The hypertrophic chondrocytes then undergo apoptosis. The chondroclasts degrade the mineralized matrix formed by the hypertrophic chondroctyes and the osteoblasts utilize the remaining cartilage scaffold to build a true bone matrix which is called the primary spongiosa. The location where the primary spongiosa is formed is called primary ossification centre.

As the chondrocytes at the centre of the cartilage mould undergo hypertrophy, the chondrocytes at the ends of the mould proliferate. A portion of these chondrocytes acquire a flattened shape and form columns of cells. They proliferate faster than the rest of the chondrocytes, forming a proliferating zone. The rapid proliferation of chondrocytes in the proliferating zone keeps a supply of hypertrophic chondrocytes and directs the elongation of the bone. As the bone enlarges, the chondrocytes at the epiphysis undergo hypertrophy, attract blood vessel invasion and osteoblasts and form a secondary ossification centre. The proliferating zone sandwiched between the primary and secondary ossification center becomes the future growth plate.

In order to study the role of Gorab in different stages of endochondroal ossification, the conditional mouse was crossed with different Cre transgenic mouse. In this way Gorab was inactivated in different tissues at different developmental stages. Since Gorab was strongly expressed in the chondrocytic and osteoblastic

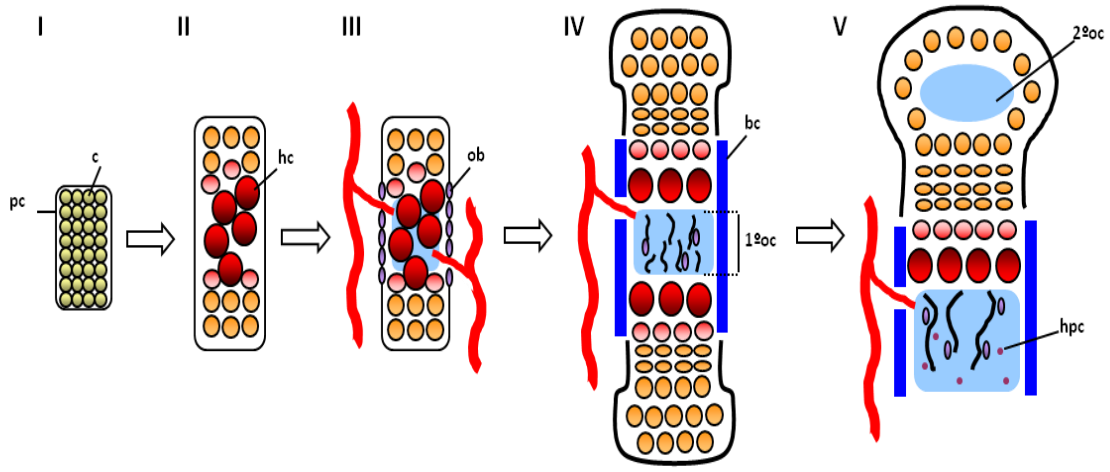

Fig.4.1 (A) Schematic diagram showing different stages of endochondral ossification. Stage I--Mesenchymal cells condense and differentiate into chondrocytes (c), with the outer cells turning into the perichondrium (pc). Stage II--Chondrocytes at the center of the cartilage anlage differentiate into hypertrophic chondrocytes (hc) and start mineralization of the surrounding matrix. Stage III--Hypertrophic chondrocytes direct the differentiation of the adjacent cells in the perichondrium into osteoblasts (ob) and attract blood vessels invasion. Stage IV--A bone collar (bc) is formed by osteoblasts. Osteoblast also follows the invading blood vessels into the center of the cartilage and form the primary ossification center (1ºoc). Stage V--Hematopoietic cells (hpc) expand in the bone marrow cavity. Secondary ossification center is formed at the epiphysis.

---

lineage, Prx1cre, Col2a1cre and Dmp1cre were used for this study. Fig.4.2 showed the different stages of mesenchymal cell differentiation at which the cre recombinase was expressed in the three transgenic cre animals. By comparing the phenotype in these three different mutants, the role of the chondrocytic and osteoblastic lineage in the bone phenotype of Gerodermia Osteodysplastica could be elucidated.

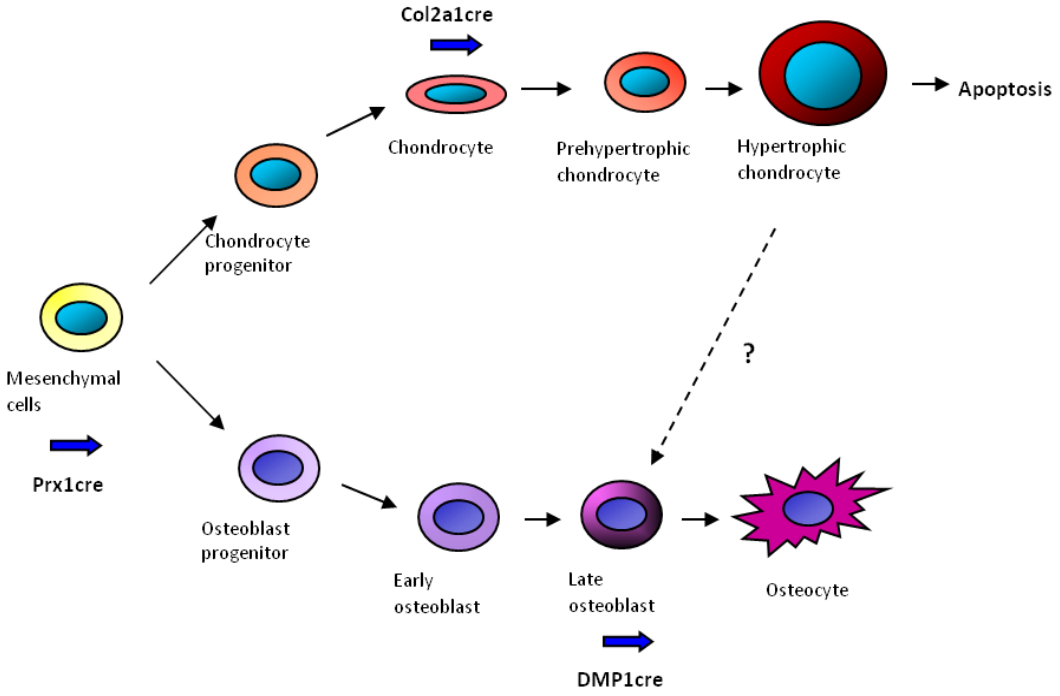

Fig.4.2 Schematic diagram showing the differentiation of mesenchymal cells into the chondrocyte and osteoblast lineage. The Prx1 promoter drives the cre expression in the mesenchymal cells, resulting in the inactivation of Gorab in both chondrocyte and osteoblast lineage. The Col2a1 promoter starts expressing cre from the proliferating chondrocyte onward and inactivated Gorab in all the chondrocytes. Dmp1 promoter expresses cre in the late osteoblast and osteocyte.in the cortical bone

---

Role of the chondrocytic and osteoblastic cell lineage in bone phenotype manifestation in different Gorab mutants.

Fig. 4.3 shows a comparison of the bone phenotype in long bones and vertebra of the three mutants at 12weeks of age (adult stage). In this comparison, instead of analyzing the different mutant with the control animals from their individual cohort, the data from all the animals in this study was taken together for comparison and analyzed by two-tailed unpaired t-test. The Prx1 promoter drives the expression of cre

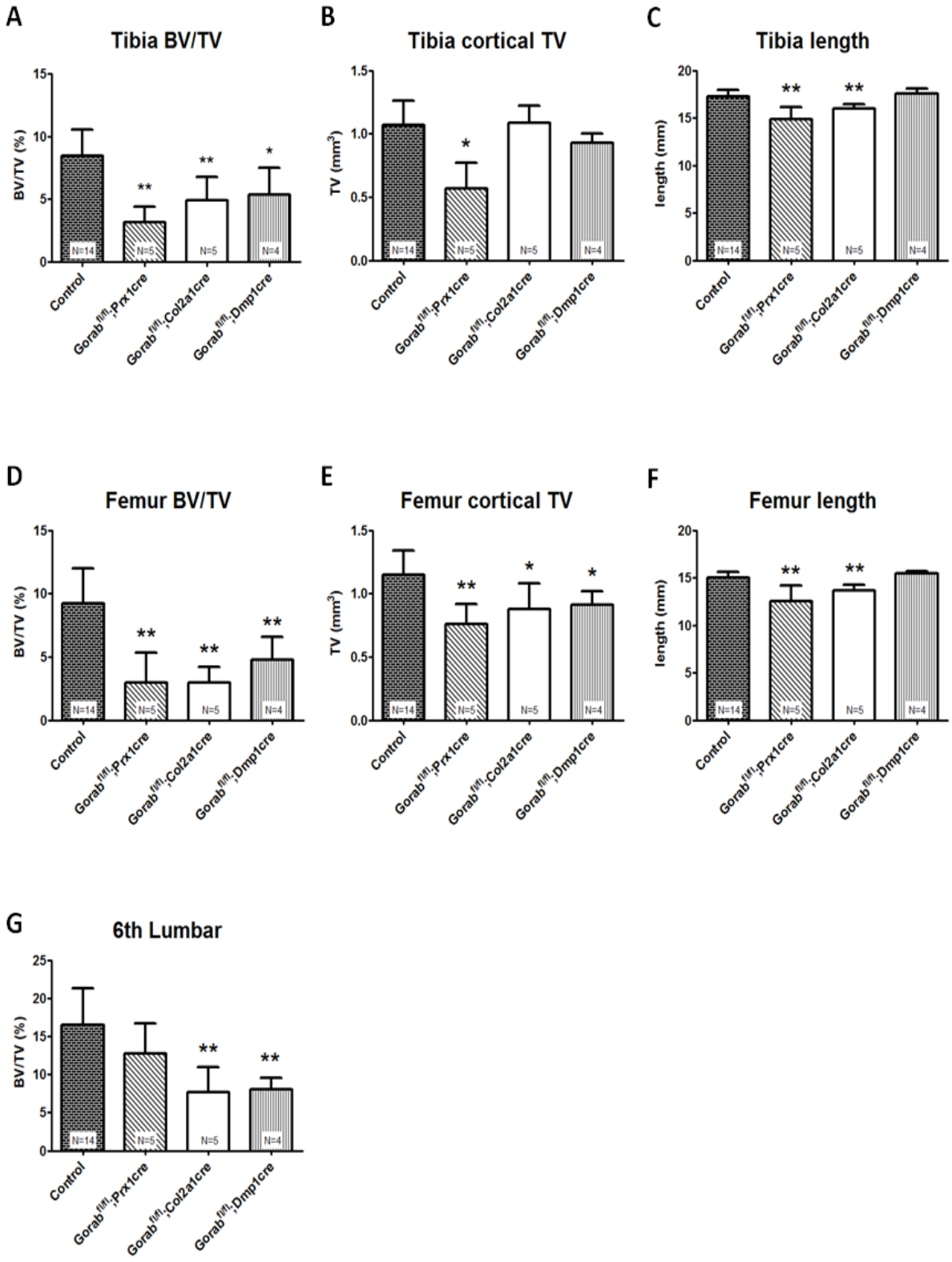

Fig.4.3 Summary of microCT analysis from 12 weeks old mutants. *=p<0.05, **=p<0.01. Statistical analysis was done by unpaired, two tailed t-test comparing each group to the control.

recombinase starting from E10.5 at the limb bud mesenchyme (Logan et al 2002). Therefore Gorab was inactivated early in limb development in both chondrocytic and osteoblastic lineage in the Gorab$^{fl/fl}$;Prx1cre mutant. This was the mutant that gave the strongest phenotype in the long bones, with loss of trabeculae (Fig.4.3A and D), thinning of cortical bone (Fig.4.3B and E) and shortening of the long bones (Fig.4.3C and F). The Gorab$^{fl/fl}$;Col2a1cre mutant showed comparable decrease in trabeculae and shortening in the long bones as the Gorab$^{fl/fl}$;Prx1cre mutant. These results suggested that loss of Gorab in the chondrocytes contributed, at least partly, to the loss of trabeculae and bone shortening observed in the Gorab$^{fl/fl}$;Prx1cre mutant.

The role of chondrocytes in longitudinal bone growth was well documented. The proliferation and hypertrophy of chondrocyte are the major driving force of bone elongation (reviewed in Kronenberg et al 2003). Inactivation of Gorab in the chondrocyte may have impacted on the proliferation and/or differentiation of chondrocytes and thus resulted in shortened bone. The growth plate of the Gorab genetrap mutants at P0 showed no significant morphological difference comparing to the control. This suggested that the effect of Gorab inactivation on chondrocytes was subtle and detailed analysis on chondrocyte differentiation markers and proliferation was needed to further investigate the role of Gorab in chondrocyte function and differentiation.

All three mutants showed similar severity in trabeculae reduction at 12weeks. Before this phenotype was compared and discussed, there was one aspect of the Dmp1cre animal that should be addressed first. The Dmp1cre transgenic showed very low staining in the osteoblast or osteocytes in the cortical bone during embryonic stages. However the expression of the cre recombinase was very strong in the

osteoblasts at the trabecular bone (Fig.3.3.14). This suggested that there was a differential expression pattern of the Dmp1cre in the osteoblast derived from the periosteum and that from the bone marrow cavity. Indeed, it has been shown that cortical osteoblast and the trabecular osteoblast are from different origin and have different role in bone development and fracture healing (Maes et al 2010). This could be the reason why the Dmp1cre has different expression pattern in the cortical bone and the trabecular bone. However it was difficult to conclude the developmental stage at which the recombinase was active. Detailed analysis on the expression pattern of cre recombinase in the Dmp1cre transgenic mouse is needed to delineate the stage of osteoblast differentiation at which Gorab becomes inactivated in the $Gorab^{fl/fl}$;Dmp1cre mutants. On the other hand it should be noted that the expression pattern of the reporter, in this case the beta-galactosidase, does not necessarily translate into inactivation of Gorab. Hebert et al 2000 has reported an interesting finding, in which they crossed a Foxg1-cre mice with either a R26R (LacZ) or Z/AP reporter mice and observed differences in the temporal and spatial pattern of reporter activity. They suggested that the differences were because the loxP-targeted locus may influence the recombination pattern obtained with the cre mice. This could be due to epigenetic regulation of different loci, in which some loci are more susceptible to recombination (or accessible to cre recombinase) while some are not. The cre recombinase activity was also susceptible to transgene silencing, mosaic activity pattern and mouse strain variation (Smith L 2011). Therefore immunohistochemistry (IHG) or *in situ* hybridization (ISH) are needed to verify the inactivation of Gorab in the different mutants. However there is no suitable antibody at the moment for IHC analysis of Gorab, and ISH was also unsuccessful due to low expression level of Gorab. Specific antibody is currently under generation in hope to overcome this obstacle. Nevertheless, the Rosa-LacZ reporter mice provide a good indication on the

spatial-temporal expression pattern of the cre-recombinase and serves as a reference for the tissue and developmental stage in which Gorab was inactivated.

The inactivation of Gorab in the chondrocytes by the Col2a1cre resulted in trabecule loss similar to the Prx1cre and the Dmp1cre was an intriguing finding. These data implied that the chondrocytes contributed, at least partly, to the trabecular phenotype. One possible explanation of how chondrocytes could interfere with a primarily bone phenotype was the transdifferentiation theory.

It was generally believed that chondrocytes underwent hypertrophy to perform the tasks mentioned in the previous section, and then the hypertrophic chondrocytes underwent apoptosis. However, a recent report showed that not all hypertrophic chondrocytes underwent apoptosis. Instead, some of the hypertrophic chondrocytes seem to further differentiate into osteoblasts, contributing to the endosteal pool of osteoblast (Maes et al 2010). Therefore one hypothesis was that inactivation of Gorab in chondrocytes interfered with the transdifferentiation of chondrocytes into osteoblasts, thus resulting in defects in osteoblast function and loss of trabeculae. However, the transdifferentiation of chondrocytes into osteoblasts was only shown at the cartilage-perichondral interface and at the endosteal side of the cortical bone, but not in the metaphyseal region. One possible explanation was that Maes et al 2010 studied transdifferentiation of chondrocytes in the embryonic stage, which could be different from the postnatal bone development. One supporting evident was that the Gorab genetrap mouse showed no significant loss of trabeculae in the embryonic stage, while all three conditional mutants investigated in this study showed postnatal loss of trabeculae. This suggested that the effect of Gorab inactivation in the chondrocytes on trabeculae was likely to be a postnatal effect. To verify this

hypothesis, cell lineage tracing experiment should be conducted to investigate how Gorab interfered with the transdifferentiation process and the effect, if any, on trabecular bone formation in postnatal mutants.

Gorab$^{fl/fl}$;Prx1cre mutant was the only mutant showing consistent decrease in the volume of the cortical bone in the long bones. The other two mutants showed decrease in the volume of femur cortical bone but not in the tibia. The diaphysis of a bone is developed and maintained by osteoblasts differentiated from the perichondrium during embryonic stages and from the periosteum and the bone marrow mesenchymal cells in postnatal stages. The Prx1cre inactivated Gorab in both the perichondrium and the periosteum and hence the osteoblast differentiated from these two tissues. We have shown a decrease in mineral apposition rate in the endosteal surface of the tibia cortical bone of Gorab$^{fl/fl}$;Prx1cre mutants and this was likely to be the reason for thin cortical bone in the mutants.

The transdifferentiation of chondrocytes contributed to the osteoblast pool at the endosteal side of the cortical bone at the cartilage-perichondrium interface (Maes et al 2010). This suggested that chondrocytes may contribute to cortical bone formation adjacent to the metaphysis. In our study, this was the region that has been chosen for measurement of the cortical bone tissue volume. The decrease in cortical thickness in the femur of the Gorab$^{fl/fl}$;Col2a1cre mutants supported that inactivation of Gorab interfered with chondrocyte transdifferentiation and thus thinning of the cortical bone.

The cre recombinase was not expressed in the vertebrae of the Gorabfl/fl;Prx1cre mutant and therefore there was no significant trabecular bone loss found in the lumbar vertebra of the mutant. However, both the Gorab$^{fl/fl}$;Col2a1cre mutant and the

Gorab$^{fl/fl}$;Dmp1cre mutant showed similar level of trabeculae loss in the vertebra. This similarity of the effect of Gorab inactivation on trabeculae loss as in the long bones again argued for a common mechanism influenced in these two mutants. Transdifferentiation of chondrocytes again was a probable hypothesis explaining the phenotype in the Gorab$^{fl/fl}$;Col2a1cre mutant and required further investigation.

Loss of Gorab causes delay in osteoblast differentiation and maturation

In 4weeks old Gorab$^{fl/fl}$;Prx1cre mutant, the osteocytes have a higher expression of late osteoblast markers Osteopontin and Dmp1, but lower expression of osteocyte marker Sclerostin. This implied that there was a delay or defect in osteocyte maturation in the mutants and therefore the 'osteocyte' assumed an expression profile more similar to late osteoblast rather than true osteocytes. Another possible explanation was that inactivation of Gorab specifically induced the expression of Osteopontin and Dmp1 and inhibited the expression of Sclerostin. This explanation was rather unlikely since by 12 weeks of age, the expression of different osteoblast markers were similar to that of the control animals, suggesting that loss of Gorab delayed the maturation of osteoblast rather than disrupted osteoblast maturation or had specific effects on the expression of certain markers. Detailed analysis on the expression of different osteoblast markers in earlier developmental stages would be required to validate this hypothesis. Nevertheless, it clearly showed that there was abnormality in osteoblast differentiation and maturation. How such defect affect osteocyte function remained to be investigated. However the accumulation and change in morphology of the osteocytes suggested that osteocyte function was likely to be compromised.

Another piece of evidence supporting the notion that Gorab inactivation delayed osteoblast differentiation came from the study of the Gorab$^{fl/fl}$;Dmp1 mutant. The Gorab$^{fl/fl}$;Dmp1 mutant didn't show significant thinning in the tibia cortical bone. There was also no accumulation of unmineralized lacunae or enlarged osteocyte in the cortical bone of the mutant. Since, the Dmp1 promoter drove cre expression in late osteoblasts and osteocytes in the cortical bone, it suggested that inactivation of Gorab in these cells has no significant effect in the maturation of osteocytes. In other words, the role of Gorab in osteoblast differentiation was probably in earlier stage of differentiation, that is, the differentiation of mesenchymal cell into osteoblast lineage or the maturation of early osteoblast into late osteoblast. Indeed, preliminary data from mutants in which Gorab was inactivated by the Col1a1cre transgene, which expressed cre recombinase in early osteoblasts, showed accumulation of unmineralized lacunae and enlarged osteocytes in the cortical tibia, although no significant change in cortical thickness was observed (data not shown). This suggested that inactivation of Gorab in early osteoblast impacted on the differentiation of osteoblast into osteocyte, though the effect may not be as significant as inactivation from earlier differentiation stages, i.e. differentiation of mesenchymal cells and osteoblast progenitors into osteoblast as with Prx1cre. Nevertheless, it should not be concluded that inactivation of Gorab in osteocytes (by Dmp1cre) has no effect on osteocytes function and investigation on the function of osteocytes, e.g. as mechanosensor or mediating fracture healing, should be conducted before concluding the role of Gorab on osteocyte function.

On the other hand, it was found that the osteoblast function was impaired as illustrated by decrease in mineral apposition rate and increase in osteoid surface and volume in the mutants. This suggested that defects in osteoblast function participated

in the pathomechanism in osteoporosis in GO patient.

4.2 Cellular senescence in Gerodermia Osteodysplastica

Inactivation of Gorab induced DNA damage and cellular senescence

In this study, it has been shown that the skin fibroblasts from GO patients showed lower proliferation potential, increased senescence associated beta-galactosidase activity and increase in p16/Ink4a expression. The skin fibroblast from Gorab genetrap mouse also showed decrease in proliferation potential. These data showed that inactivation of Gorab resulted in cellular senescence. It has also been shown that there was increase in p21/Cip1 expression in the cortical bone of 4weeks old $Gorab^{fl/fl}$;Prx1cre mutants. This suggested that loss of Gorab induced cellular senescence not only in skin fibroblast culture, but also *in vivo* in the osteoblastic lineage.

Cellular senescence has been defined as irreversible replication arrest in mitotic cells (Campisi et al 2007). The two keywords in this definition are 'irreversible' and 'mitotic cells'. Senescent cells are under irreversible arrest meaning that the cells cannot proliferate again under known physiological stimuli, e.g. the need for tissue repair and regeneration, and this distinguishes senescent cells from quiescent cells. However, under experimental manipulation, e.g. inactivation of cyclin D kinase inhibitors, has been reported to rescue senescent cells and restored their proliferation capability (Su et al 2009). The second keyword 'mitotic cells' includes epithelial cells, fibroblastic cells, stem cells and progenitor cells etc. In contrast, 'postmitotic cells', e.g. differentiated neurons and muscle cell, have lost the ability to proliferate and are not considered as senescent cells.

There are three major causes of cellular senescence: telomere dysfunction, DNA damage and oncogene induced senescence (reviewed in Campisi et al 2007). However, there is one central mechanism involved in the induction of senescence, the DNA damage response (DDR). Fig.4.4 illustrates a simplified scheme of how DNA damage is sensed in a cell and the triggering of DDR. The outcomes of DDR are transient cell cycle arrest, which is reversible and cells resume proliferation after the DNA damage is repaired. DDR may also results in apoptosis when the DNA damage is beyond repair , or cellular senescence. In this study, it has been shown that there was increased in DNA damage upon Gorab inactivation, indicating that the cellular senescence phenotype was due to accumulation of DNA damage. This increase in genome instability was unlikely to be related to telomere dysfunction since siRNA knock down of GORAB in Hela cells and U2OS cells also induced DNA damage in 72 hours.

In order to understand the cause of DNA damage upon Gorab inactivation, the amount of intracellular Reactive Oxygen Species (ROS) in Hela cells upon GORAB knockdown was investigated. It was found that there was no difference in the baseline level of intracellular ROS between control and GORAB knockdown cells. However, when the cells were challenged with CCCP (a mitochondrial uncoupler which disrupts the membrane potential of the mitochondria and thus results in strong ROS generation), knockdown of GORAB resulted in an accumulation of ROS 1.5-2 fold higher than the controls. This indicated that GORAB inactivation resulted in increased sensitivity to CCCP challenge, suggesting that GORAB may play a role in ROS sensing and scavenging. Loss of GORAB thus may increase the cells vulnerability towards ROS and as a result, increase in DNA damage.

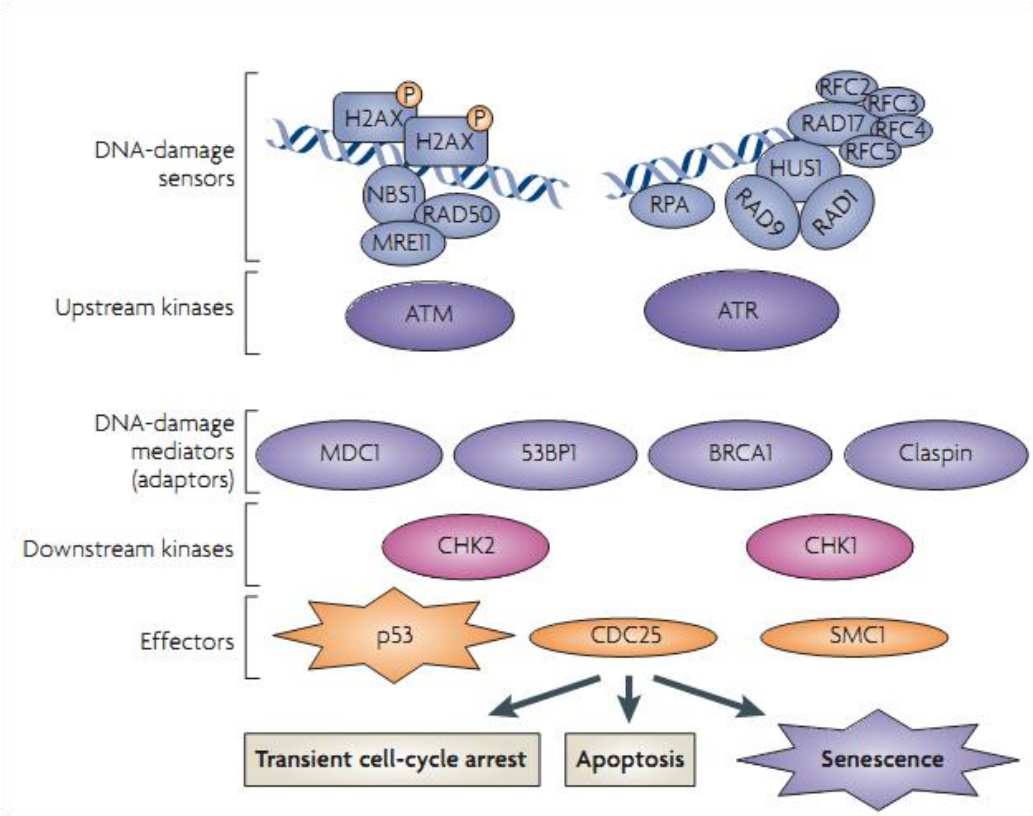

Fig.4.4 Schematic diagram summarizing the DNA damage response. DNA double strand break was suggested to be sensed by the MRN (MREII-RAD50-NBS1) complex or the RPA and RFC complexes. As a result, the upstream kinases ATM and ATR kinases was activated and phosphorylated the histone variant H2AX. phospho-H2AX then recruited mediators such as MDC1, 53BP1, BRCA1 and Claspin which subsequently recruited downstream kinases e.g. CHK1 and CHK2. The downstream kinases mediated the phosphorylation of effector proteins including p53, CDC25 and SMC1. The effector proteins then activated either transient cell cycle arrest, permanent senescence or apoptosis. (Adopted from Campisi et al 2007)

The two major pathways controlling cellular senescence were the p53 and the p16-pRB pathways (Fig.4.4). These two pathways are not independent of each other; instead there are interactions and regulations between the pathways at multiple levels. Nevertheless, the two cyclin dependent kinase (CDK) inhibitors, p16 and p21,

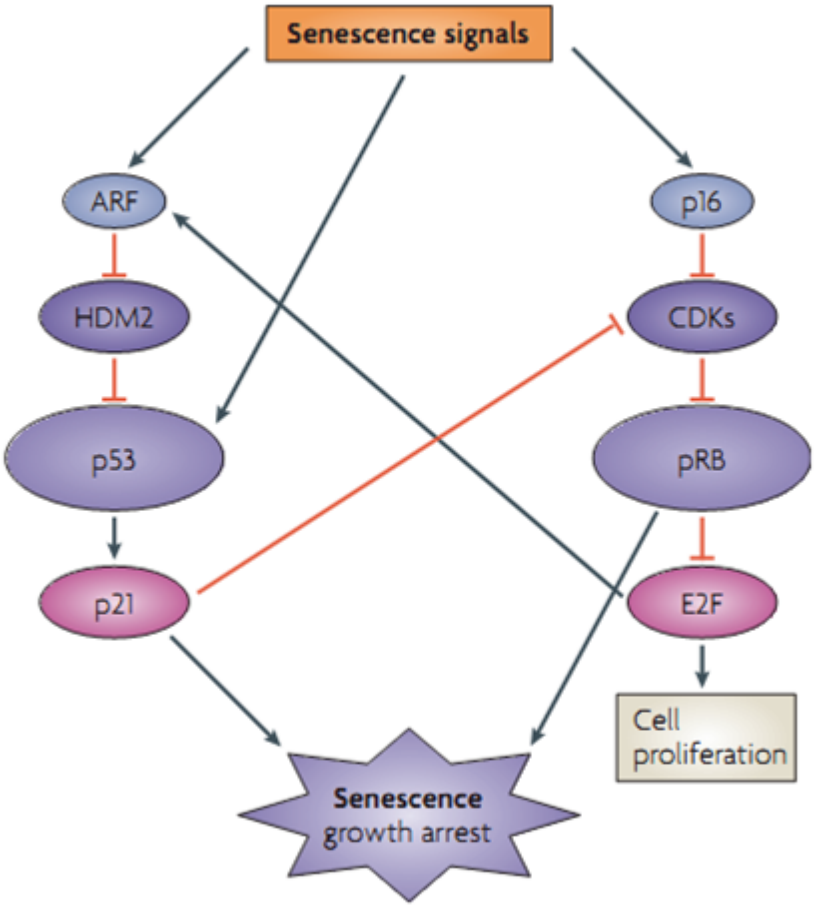

Fig.4.5 Regulation of senescence by the p53 and p16-pRB pathways. Activation of p53 by senescence signal, e.g. DNA damage response, resulted in the activation of p21. p21 suppressed the phosphorylation of pRB protein by CDKs and thus suppressed the proliferation inducing activity of E2F. In contrast, the p16-pRB pathway suppressed the activity of pRB by p16. E2F may also activated the p53 pathway by inducing ARF expression, which inhibited HDM2 (MDM2 in mouse) activity. Adopted from Campisi et al 2007.

---

have been shown to play major role in the initiation and maintenance of senescence. In GO patient fibroblast, it has been shown that there was upregulation in p16 expression, while in the osteocytes of 4weeks old Gorab$^{fl/fl}$;Prx1cre mutants, there was increase in p21 expression. These results supported the idea that Gorab

inactivation induced cellular senescence and suggested that different senescence pathway was undertaken in these two cell types.

Phenotypic comparison of GO with other premature ageing diseases

Ageing is probably the single most significant risk factor for all diseases in organisms. It was a complex process that was influenced by genetic as well as environmental factors. However, there were single gene mutations that caused early onset or accelerated progression of degenerative or proliferative disorders similar to senescent phenotypes. These disorders were considered as premature ageing disorders. Premature ageing disorders have been classified into two major categories, segmental progeroid syndromes, in which multiple organs were affected, and unimodal progeroid syndrome, in which only a single organ was affected (Martin GM 2005).

Werner syndrome and Hutchinson-Gilford Progeria syndrome (HGPS) were two classic examples of segmental progeroid syndromes. The Werner syndrome was caused by null mutations in the *WRN* helicase. Patients of Werner syndrome showed no phenotype until puberty. At adolescence, growth was stopped and thus resulting in short stature of the patient in adulthood. Loss and graying of hair started at early 20s. Other abnormalities included loss of peripheral subcutaneous tissue, type II diabetes, osteoporosis etc (Epstein et al 1996). Fig. 4.5A shows the pictures of a Werner syndrome at different age. The normal appearance during childhood and early aged appearance during adulthood marked Werner syndrome as a classic premature ageing disorder.

HGPS was another classic example of premature ageing disease. In contrast to

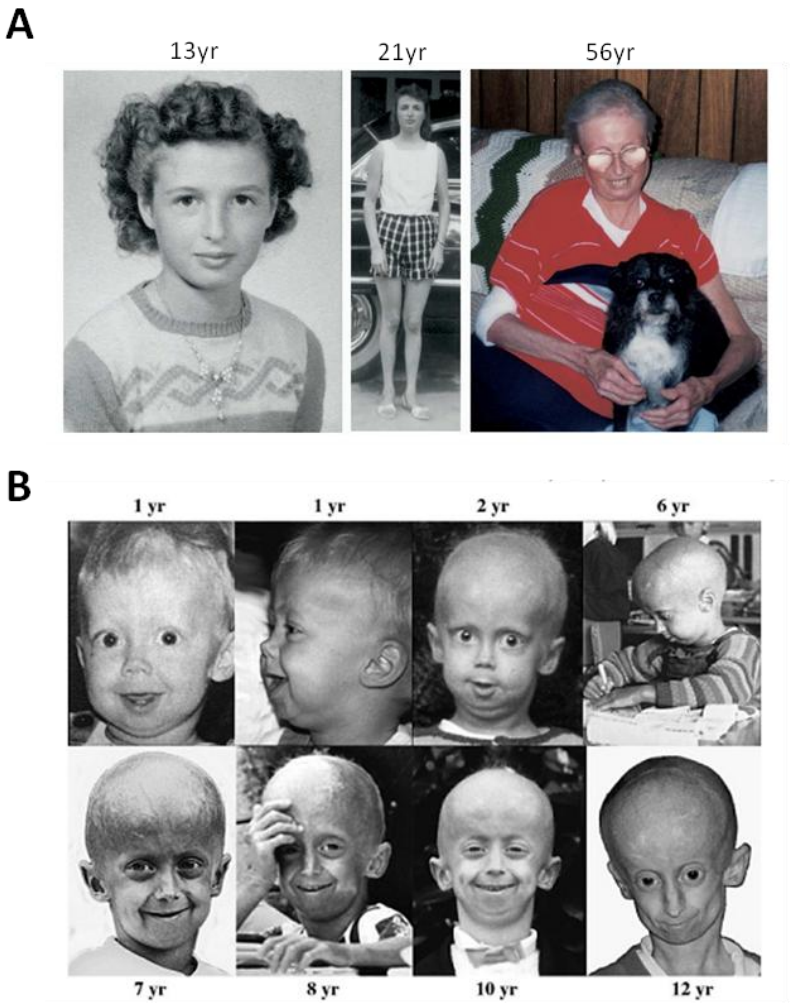

Fig.4.5 (A) Photographs of a female Werner syndrome patient. The patient was normal in appearance at age 13, but rapidly aged afterward. Adopted from Martin GM 2005. (B). Photographs of a HGPS patient at different age. In contrast to the Werner syndrome, the patient had phenotype manifestation early in life. Adopted from Hennekam RCM 2006.

---

the Werner syndrome, HGPS patient showed phenotype manifestation early in life, including short stature, failure to thrive, loss of hair, osteolysis, lipodystrophy etc (Hennekam RCM 2006). HGPS was caused by a splice site mutation in the LaminA/C locus, which resulted in a truncated Lamin A protein product that lacked 50aa at the C-terminal. Fig.4.5B showed pictures of a HGPS patient at different age.

Table 4.1 A summary comparing the three premature ageing disorders, GO, Werner syndrome and HGPS

	GO	Werner Syndrome	HGPS
Skin phenotypes	• Wrinkled skin • Prematurely aged appearance.	• Scleroderma like skin • Loss of subcutaneous fat • Premature graying and loss of hair	• Loss of skin appendages • Loss of subcutaneous fat • Hair loss
Bone phenotypes	• Short stature • Osteoporosis • Maxillary hypoplasia • mandibular prognathism	• Short stature as adult • Osteoporosis	• Short stature • Osteoporosis
Phenotype onset	At birth	Adolescence	At birth
Causative gene	GORAB	WRN helicase	LAMINA/C

Table 4.1 compared the skin and bone phenotypes of GO, Werner syndrome and HGPS. Although all three disorders have been considered as segmental progeroid syndrome, their phenotypes were quite different, especially in the skin phenotype and onset of disease. GO patients had wrinkled skin at birth which was not found in the other two disorders. Werner syndrome and HGPS showed loss of subcutaneous fat which was not found in GO patient. GO patient had characteristic maxillary

malformations not found in the other two disorders. Nevertheless, all three disorders suffered from osteoporosis, genome instability and cellular senescence. The role of genome instability and cellular senescence in the phenotype manifestation of these disorders were not defined and were probably tissue specific. However, in this study, it has been shown that defects in osteoblast differentiation and function were accompanied by an increase in p21 expression. This suggested that cellular senescence may underlie the osteoblast defects in GO and, perhaps, other premature ageing disorders, providing a feasible direction for future investigation.

TGFβ signalling in GO

It was found that there was increase in TGFβ1 and TGFβ2 expression in osteocytes in 4weeks Gorab$^{fl/fl}$;Prx1cre mutant. Apart from the possible implication of TGFβ1-dependent senescence in bone as in the skin fibroblast, the activation of TGFβ signalling may have direct impact on the bone phenotype in the mutant. TGFβ isoforms are stored in the extracellular matrix in their latent form and are released (activated) upon matrix degradation (reviewed by Fox et al 2005). Defects in the extracellular matrix formation, e.g. in the Marfan syndrome, may result in improper activation of TGFβ signalling (Nistala et al 2010). Indeed, upregulation of TGFβ signalling has been reported in a number of cases of autosomal dominant cutis laxa disorder (Renard et al 2010, Callewaert et al 2011). This suggests a link between extracellular matrix integrity and TGFβ activation. Since defects in extracellular matrix is a primary phenotype in GO, it is possible that improper activation of TGFβ signalling plays a key role in GO phenotype manifestations.

TGFβ is essential in the differentiation of monocytes into osteoclasts, the bone

resorping cells. Inactivation of TGFβ, e.g. by overexpression of dominant negative TGFβ receptor II, drives monocytes differentiation into macrophages instead of forming osteoclasts (Erlebacher et al 1998, Fox et al 2005). Improper activation of TGFβ signalling, e.g. in Marfan syndrome, resulted in osteopenia. This phenotype appeared to match that of the bone phenotype in GO. However, recent study on mouse models of Marfan syndrome showed that the osteopenia in Marfan syndrome was due to increase osteoclastogenesis, while osteoblast differentiation and function was normal (Nistala et al 2010). This contradicted the findings in the Gorab$^{fl/fl}$;Prx1cre mutant, in which we showed defects in osteoblast marker expression and decrease in mineral apposition rate. Nevertheless, the effect of TGFβ1 upregulation in the Gorab$^{fl/fl}$;Prx1cre mutant may have secondary effect on osteoclastogenesis and contributes to the osteoporosis phenotype and should also be investigated in the future.

On the other hand, overexpression of TGFβ2 in osteoblast resulted in progressive osteoporosis, thinning of cortical bone, decrease in mineral apposition rate and accumulation of osteocytes (Erlebacher et al 1996, Fig.4.6A and B). These phenotypes in many ways resembled that of the Gorab$^{fl/fl}$;Prx1cre mutant, suggesting that there could be linkage in the phenotype manifestation and TGFβ2 overexpression. Whether this had any interaction with cellular senescence induction, or it was an osteoblastogenesis defect independent of cellular senescence would require further investigation.

4.3 Summary and outlook

In summary, this study has shown that inactivation of Gorab induced cellular senescence in both human and mouse skin fibroblast, which was accompanied by

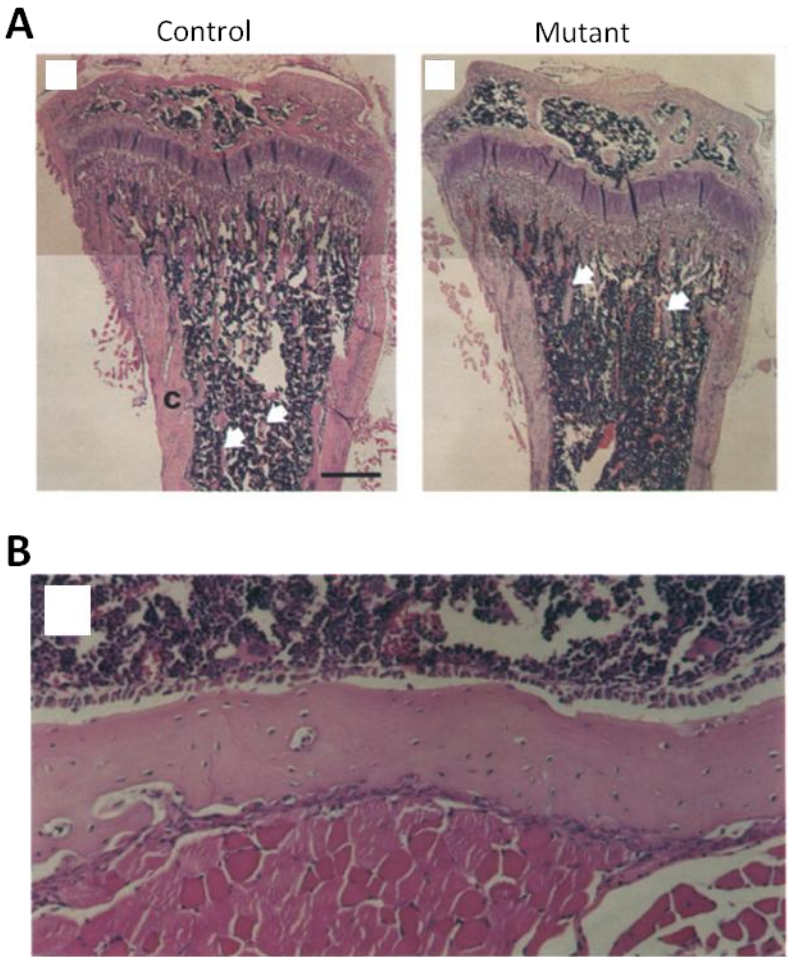

Fig.4.6 Tibia longitudinal section of 35d old Ocn-TGFβ2 transgenic mice. (A) There was marked decrease in trabeculae and thinning of cortical bone comparing to the control animal. (B). Accumulation of round shaped osteocytes in the cortical bone of the mutant. Adopted from Erlebacher et al 1996.

increased in DNA double strand breaks and vulnerability to uncoupler-induced reactive oxygen species accumulation. Inactivation of Gorab in the limb bud mesenchyme resulted in shortening of long bone, loss of trabeculae and thinning of cortical bone. Defects in chondrocytes played a significant part in the manifestation of these phenotypes. Osteoblast function and differentiation was compromised, resulting in decreased mineral apposition rate and accumulation of osteocytes in the cortical bone. These phenotypes were likely to arise during the differentiation of

mesenchymal cells to osteoblast since inactivation of Gorab in late osteoblast and osteocytes did not result in the same phenotype. Inactivation of Gorab has also been shown to activate TGFβ1 expression.

In the future, there are a few key questions that requires further investigation. Firstly, what is the role of Gorab in genome instability and cellular senescence? In this study, it has been shown that inactivation of Gorab induced DNA damage. However it was difficult to link a Golgi protein to genome stability. One possibility was that Gorab may have a role in reactive oxygen species sensing and scavenging. This idea was supported by the increased accumulation of ROS in cells upon CCCP treatment and should be followed in future investigation. Secondly, what is the role of cellular senescence in chondrocyte and osteoblast differentiation? It has been shown that inactivation of Gorab induced cellular senescence. However it is still unclear if cellular senescence also takes place *in vivo* in chondrocytes and osteoblasts, and if yes, how is the differentiation and function of these two cell types affected. Therefore further *in vivo* studies shall be conducted to investigate defects in the differentiation process and if cellular senescence has any part in it. Thirdly, TGFβ signalling pathway was activated upon loss of Gorab. Since the TGFβ signalling pathway is a major participant in cell cycle progression and cellular senescence, further studies shall be conducted to investigate the role of TGFβ signalling in GO pathology. Although there are still many unanswered questions regarding the physiological role of Gorab, this study has laid down the bases and frameworks for future studies. To summarize, this study has provided evidences suggesting cellular senescence as part of the pathomechanism of Gerodermia Osteodysplastica, defined the role of chondrocytes and osteoblast in the bone phenotype of GO and suggested TGFβ signalling pathway as a candidate key pathway involved in GO.

References

Al-Dosari, M., and Alkuraya, F. S. (2009). A novel missense mutation in SCYL1BP1 produces geroderma osteodysplastica phenotype indistinguishable from that caused by nullimorphic mutations. American journal of medical genetics. Part A 149A, 2093-8.

Barnekow, A., Thyrock, A., and Kessler, D. (2009). Rab Proteins and Their Interaction Partners. International Review of Cell and Molecular biology 274, 235-74.

Burman, J. L., Bourbonniere, L., Philie, J., Stroh, T., Dejgaard, S. Y., Presley, J. F., and McPherson, P. S. (2008). Scyl1, mutated in a recessive form of spinocerebellar neurodegeneration, regulates COPI-mediated retrograde traffic. The Journal of biological chemistry 283, 22774-86.

Callewaert, B. et al. (2011). New insights into the pathogenesis of autosomal dominant cutis laxa with report of five ELN mutations. Human mutation.

Campisi, J., and d'Adda di Fagagna, F. (2007). Cellular senescence: when bad things happen to good cells. Nature reviews. Molecular cell biology 8, 729-40.

Debacq-Chainiaux, F., Erusalimsky, J. D., Campisi, J., and Toussaint, O. (2009). Protocols to detect senescence-associated beta-galactosidase (SA-betagal) activity, a biomarker of senescent cells in culture and in vivo. Nature protocols 4, 1798-806.

Di, Y. et al. (2003). Cloning and characterization of a novel gene which encodes a protein interacting with the mitosis-associated kinase-like protein NTKL.

Epstein, C. J., and Motulsky, A. G. (1996). Werner syndrome: entering the helicase era. Bioessays 18, 1025-27.

Erlebacher, a, Filvaroff, E. H., Ye, J. Q., and Derynck, R. (1998). Osteoblastic responses to TGF-beta during bone remodeling. Molecular biology of the cell 9, 1903-18.

Fox, S. W., and Lovibond, A. C. (2005). Current insights into the role of transforming growth factor-beta in bone resorption. Molecular and cellular endocrinology 243, 19-26.

Gong, Y. et al. (2009). Localization of TEIF in the centrosome and its functional association with centrosome amplification in DNA damage, telomere dysfunction and human cancers. Oncogene 28, 1549-60.

He, J. M., and Mcconnell, S. K. (2000). Targeting of cre to the Foxg1 (BF-1) Locus Mediates loxP Recombination in the Telencephalon and Other Developing Head Structures. Developmental Biology 306, 296 -306.

Hennekam, R. C. M. (2006). Hutchinson – Gilford Progeria Syndrome : Review of the Phenotype. American Journal of Medical Genetics 2624, 2603 - 2624.

Hennies, H. C. et al. (2008). Gerodermia osteodysplastica is caused by mutations in interacting golgin. Nature Genetics, 9-11.

Hunter, a G. (1988). Is geroderma osteodysplastica underdiagnosed? Journal of medical genetics 25, 854-7.

Hunter, a G., Martsolf, J. T., Baker, C. G., and Reed, M. H. (1978). Geroderma osteodysplastica. A report of two affected families. Human genetics 40, 311-24.

JM (2003). Pirh2, a p53-induced ubiquitin-protein ligase, promotes p53 degradation. Cell 112, 779-791.

Kato, M., Yano, K.-ichi, Morotomi-Yano, K., Saito, H., and Miki, Y. (2002). Identification and characterization of the human protein kinase-like gene NTKL: mitosis-specific centrosomal localization of an alternatively spliced isoform. Genomics 79, 760-7.

Kornak, Uwe et al. (2008). Impaired glycosylation and cutis laxa caused by mutations in the vesicular H + -ATPase subunit ATP6V0A2. Nature Genetics 40, 2007-2009.

Kramer, I., Halleux, C., Keller, H., Pegurri, M., Gooi, J. H., Weber, P. B., Feng, Jian Q, Bonewald, Lynda F, and Kneissel, M. (2010). Osteocyte Wnt/beta-catenin signaling is required for normal bone homeostasis. Molecular and cellular biology 30, 3071-85.

Kronenberg, H. M. (2003). Developmental regulation of the growth plate. Nature 423, 332-6.

Lewandoski, M., Wassarman, K. M., and Martin, G. R. (1997). Zp3-cre, a transgenic mouse line for the activation or inactivation of loxP-flanked target genes specifically in the female germ line. Current biology : CB 7, 148-51.

Lisker, R., Hernández, a, Martínez-Lavin, M., Mutchinick, O., Armas, C., Reyes, P., and Robles-Gil, J. (1979). Gerodermia osteodysplastica hereditaria: report of

three affected brothers and literature review. American journal of medical genetics 3, 389-95.

Liu, P., Jenkins, N. a, and Copeland, N. G. (2003). A highly efficient recombineering-based method for generating conditional knockout mutations. Genome research 13, 476-84.

Liu, S. C., Lane, W. S., and Lienhard, G. E. (2000). Cloning and preliminary characterization of a 105 kDa protein with an N-terminal kinase-like domain. Biochimica et biophysica acta 1517, 148-52.

Logan, M., Martin, J. F., Nagy, A., Lobe, C., Olson, E. N., and Tabin, C. J. (2002). Expression of Cre Recombinase in the developing mouse limb bud driven by a Prxl enhancer. Genesis (New York, N.Y. : 2000) 33, 77-80.

Lu, Y., Xie, Y., Zhang, S., Dusevich, V., Bonewald, L.F., and Feng, J.Q. (2007). DMP1-targeted Cre Expression in Odontoblasts and Osteocytes. Journal of Dental Research 86, 320-325.

Maes, C., Kobayashi, T., Selig, M. K., Torrekens, S., Roth, S. I., Mackem, S., Carmeliet, G., and Kronenberg, H. M. (2010). Osteoblast precursors, but not mature osteoblasts, move into developing and fractured bones along with invading blood vessels. Developmental cell 19, 329-44.

Marine, J.-c, and Lozano, G. (2009). Mdm2-mediated ubiquitylation : p53 and beyond. Cell Death and Differentiation 17, 93-102.

Martin, G. M. (2005). Genetic modulation of senescent phenotypes in Homo sapiens. Cell 120, 523-32.

Miserey-Lenkei, S. phanie et al. (2006). A role for the Rab6A GTPase in the inactivation of the Mad2-spindle checkpoint. EMBO Journal 25, 278-289.

Morava, E., Wopereis, S., Coucke, P., Gillessen-kaesbach, G., Voit, T., Smeitink, J., Wevers, R., and Gru, S. (2005). Defective protein glycosylation in patients with cutis laxa syndrome. European Journal of Human Genetics, 414-421.

Nistala, H. et al. (2010). Differential effects of alendronate and losartan therapy on osteopenia and aortic aneurysm in mice with severe Marfan syndrome. Human molecular genetics 19, 4790-8.

Opdam, F. J. M., Echard, A., Croes, H. J. E., Hurk, J. A. J. M. V. D., Vorstenbosch, R. A. V. D., Ginsel, L. A., Goud, B., and Fransen, J. A. M. (2000). The small GTPase Rab6B , a novel Rab6 subfamily member , is cell-type specifically expressed and localised to the Golgi apparatus. 2735, 2725-2735.

Ovchinnikov, D. a, Deng, J. M., Ogunrinu, G., and Behringer, R. R. (2000). Col2a1-directed expression of Cre recombinase in differentiating chondrocytes in transgenic mice. Genesis 26, 145-6.

O'Gorman, S., Dagenais, N. a, Qian, M., and Marchuk, Y. (1997). Protamine-Cre recombinase transgenes efficiently recombine target sequences in the male germ line of mice, but not in embryonic stem cells. Proceedings of the National Academy of Sciences of the United States of America 94, 14602-7.

Rajab, A., Kornak, U, Budde, B. S., Hoffmann, K., Jaeken, J., Nürnberg, P., and Mundlos, S. (2008). Geroderma osteodysplasticum hereditaria and wrinkly skin

syndrome in 22 patients from Oman. American journal of medical genetics. Part A 146A, 965-76.

Renard, M. et al. (2010). Altered TGFbeta signaling and cardiovascular manifestations in patients with autosomal recessive cutis laxa type I caused by fibulin-4 deficiency. European journal of human genetics : EJHG 18, 895-901.

Reversade, B. et al. (2009). Mutations in PYCR1 cause cutis laxa with progeroid features. Nature Genetics 41, 1016-21

Schmidt, W. M. et al. (2007). Mutation in the Scyl1 gene encoding amino-terminal kinase-like protein causes a recessive form of spinocerebellar neurodegeneration. EMBO reports 8, 691-7.

Smith, L. (2011). Good planning and serendipity: exploiting the Cre/Lox system in the testis. Reproduction 141, 151-61.

Steiner, C. E., Cintra, M. L., and Marques-de-Faria, A. P. (2005). Cutis laxa with growth and developmental delay, wrinkly skin syndrome and gerodermia osteodysplastica: a report of two unrelated patients and a literature review. Genetics and Molecular Biology 28, 181-190.

Su, X., Cho, M. S., Gi, Y.-J., Ayanga, B. a, Sherr, C. J., and Flores, E. R. (2009). Rescue of key features of the p63-null epithelial phenotype by inactivation of Ink4a and Arf. The EMBO journal 28, 1904-15.

Tang, Z., Zhao, Y., Mei, F., Yang, S., Li, Xuan, Lv, J., Hou, Lin, and Zhang, Bo (2004). Molecular cloning and characterization of a human gene involved in

transcriptional regulation of hTERT. Biochemical and biophysical research communications 324, 1324-32.

Tremain, R., Marko, M., Kinnimulki, V., Ueno, H., Bottinger, E., and Glick, A. (2000). Defects in TGFb signaling overcome senescence of mouse keratinocytes expressing v-ras Ha. Oncogene, 1698-1709.

Yan, J., Di, Y., Shi, H., Rao, H., and Huo, K. (2010). Overexpression of SCYL1-BP1 stabilizes functional p53 by suppressing MDM2-mediated ubiquitination. FEBS Letters 584, 4319-4324.

Yan, J., Zhang, D., Di, Y., Shi, H., Rao, H., and Huo, K. (2010). A newly identified Pirh2 substrate SCYL1-BP1 can bind to MDM2 and accelerate MDM2 self-ubiquitination. FEBS letters 584, 3275-8.

Zhang, L., Li, J., Wang, C., Ma, Y., and Huo, K. (2005). A new human gene hNTKL-BP1 interacts with hPirh2. Biochemical and biophysical research communications 330, 293-7.

Zhao, Y., Zheng, J., Ling, Yun, Hou, Lin, and Zhang, Bo (2005). Transcriptional upregulation of DNA polymerase beta by TEIF. Biochemical and biophysical research communications 333, 908-16.

Appendix: Abbreviations

ARCL	Autosomal recessive cutis laxa
ATP6V0A2	ATPase, H+ transporting, lysosomal V0 subunit a2
BSA	Bovine Serum Albumin
Col1a1	Collagen type 1 alpha1
Col2a1	Collagen type 2 alpha1
DNA	Deoxyribonucleic acid
Dmp1	Dentin matrix acidic phosphoprotein 1
EM	electron microscopy
ER	endoplasmic reticulum
GAPDH	Glycerinaldehyde-3-phosphate Dehydrogenase
GO	Gerodermia Osteodysplastica
GORAB	golgin, RAB6-interacting
HAF	Human Adult Fibroblasts
HGPS	Hutchinson-Gilford Progeria Syndrome
Ocn	Osteocalcin
Opn	Osteopontin

Osx	Osterix
PYCR1/P5CR	Pyrroline-5-carboxylate reductase
qPCR	Quantitative Polymerase Chain Reaction
RNA	Ribonucleic acid
ROS	reactive oxygen species
s.d	standard deviation
Sost	Sclerostin
TGFβ	Transforming growth factor beta
WRN	Werner syndrome